Universidad de Valladolid

Escuela de Doctorado Universidad de Valladolid

PROGRAMA DE DOCTORADO EN INGENIERÍA INDUSTRIAL

TESIS DOCTORAL:

OSMOTIC ENERGY: MODELING, SIMULATION AND OPTIMAL OPERATION

(ENERGÍA OSMÓTICA: MODELADO, SIMULACIÓN Y OPERACIÓN ÓPTIMA)

Presentada por Jacobo Manuel Salamanca Parra. para optar al grado de
Doctor por la Universidad de Valladolid

Dirigida por:
Fernando Tadeo Rico

TABLE OF CONTENTS

OBJECTIVES	1
METHODOLOGY	2
1. Salinity Gradient Energy and Pressure Retarded Osmosis	3
2. Evolution of Salinity Gradient Energy and Pressure Retarded Osmosis	7
3. Thermodynamic aspects of PRO	8
4. PRO in the context of osmotic processes	9
5. PRO and desalination by Reverse Osmosis	12
6. Membranes in Pressure Retarded Osmosis	13
7. Power production and water flux	15
8. Fouling in Pressure Retarded Osmosis	19
9. Pretreatment in Pressure Retarded Osmosis	23
10. Challenges in river-to-sea PRO plants	26
CONCLUSIONS	29
ACKNOWLEDGEMENTS	30
REFERENCES	21
ANNEX: PUBLICATIONS	35
RESUMEN EN CASTELLANO	36

OBJECTIVES

O1) To develop mathematical models for the simulation of Pressure Retarded Osmosis (PRO) processes, with emphasis on the varying salinity gradient throughout the process, in order to reproduce them more accurately, taking draw dilution and reverse salt flux effects into account.

O2) To use real values of river and sea water salinities to determine the attainable electrical power of a PRO power plant and evaluate the actual efficiency of this potential gross power, considering energetic demands inherent to the process.

O3) To provide a sensitivity analysis of the most critical variables of a PRO process and predict the consequent changes in the net power.

O4) To study the viability of stratified river mouths as candidates for PRO power plants, focusing on the locations of the water intakes. Hydrodynamic models that describe the variability of the salinity and temperature profiles along the river mouth are used to evaluate the potential powers; and to search for an optimal set of intake locations to maximize the net power, considering the energy demanded by water transport.

O5) To evaluate recovering osmotic energy from reverse osmosis brines through a PRO process and to study the possible process configurations through simulation, proposing different combinations for the feed and the draw by comparing their performance.

METHODOLOGY

The research from this thesis has been performed according to four guidelines:

Revision of the state of the art: extensive search and analysis of recent investigations on the topic was initially performed. An intense focus was set on recent publications in relevant scientific journals, though conference communications, theses and other works related to the topic at hand were also reviewed. This task was also performed during the whole investigation, periodically updating and expanding the information.

Set of objectives: following the state of the art revision and taking into account the previous experience of the research group, several goals for the investigations were established.

Investigation methods:

Analysis of an experimental case study: The Magdalena river mouth was chosen as the case study. Experimental data were collected and available through collaboration with the OA Silva research group at the Universidad del Norte (Colombia). The results are presented in [P1], [P2].

Adaptation of mathematical PRO models: following the reviewed investigations, a mathematical model was chosen and adapted to the specifics of the investigation, as presented in [P1].

Design proposal and simulation of PRO power plants: the Magdalena river data and mathematical models were used to size a hypothetical PRO power plant and determine its power production. The Matlab® computing software was used in this task [P1]. The possibilities of integrating PRO in seawater desalination were also studied [P3].

Sensitivity analyses: the influence of the variation of several process parameters was studied to extract more information and form conclusions about PRO, [P1], [P2].

Diffusion of results: the research results were presented in high impact scientific journals, at conferences and through cooperation with other research groups. Sharing and discussing the results garnered valuable external input that helped to enrich and improve the investigation. The publications presented throughout this thesis are listed below:

[P1] **Salamanca, J.M.**; Álvarez-Silva, O.; Tadeo, F. Potential and analysis of an osmotic power plant in the Magdalena River using experimental field-data. *Energy* 2019, 180, 548–555 https://doi.org/10.1016/j.energy.2019.05.048

[P2] **Salamanca, J.M.**; Álvarez-Silva, O.; Higgins, A.; Tadeo, F. Analysis of the Intake Locations of Salinity Gradient Plants Using Hydrodynamic and Membrane Models. *Water* 2021, 13, 11-33. https://doi.org/10.3390/w13091133

[P3] Touati, K.; **Salamanca, J.M.**; Tadeo, F.; Elfil, H. Energy recovery from two-stage SWRO plant using PRO without external freshwater feed stream: Theoretical analysis. *Renewable Energy* 2017, 105, 84-95 https://doi.org/10.1016/j.renene.2016.12.030.

1.-Salinity Gradient Energy and Pressure Retarded Osmosis

Since the industrial revolution, modern human activity has been known to cause a rise in the worldwide average temperatures, due to the uncontrolled use of fossil fuels. Developed post-industrial societies consume even more energy [1], which added to the increasing global population, is causing the depletion of natural sources. Global warming has put a strain on the environment and world societies have started to correct this situation. 2016 Paris agreement [2] shaped the path towards a more sustainable development, in which renewable energies take a prominent role [3]. Furthermore, the current geopolitical context demands an acceleration in achieving these goals, focusing on energetic independence [4].

Salinity Gradient Energy (SGE), or blue energy, is the denomination of a group of renewable energies that produces energy from water sources with different salinity. Regarding water use, the majority of electricity generation systems need water, directly or indirectly, and the water system itself consumes energy in extraction, distribution and cleansing. This is sometimes referred as the water-energy nexus, and SGE can be involved in it, since one of the current goals towards sustainable development lies on increasing the efficiency of water and energy systems. Enhanced efficiency in the water system means less energy consumed, whereas efficient energy generation uses less water [5].

SGE exploits the Gibbs free energy of mixing released when two solutions of different salinity are mixed. The actual driving force derives from the difference in chemical potentials. There is a significant worldwide theoretical potential for SGE exploitation in river discharges into oceans of up to 2.6 TW [6]. This figure may be compared with the fact that, in 2020, the global capacity of electricity obtained from renewable sources reached 2.8 TW [7]. Nonetheless, there are some discrepancies regarding the actual potential from river discharge [8] [9]. Silva et al. compiled global data for river discharges to quantify the extractable energy through SGE, considering different practical and realistic scenarios [10] (Figure 1).

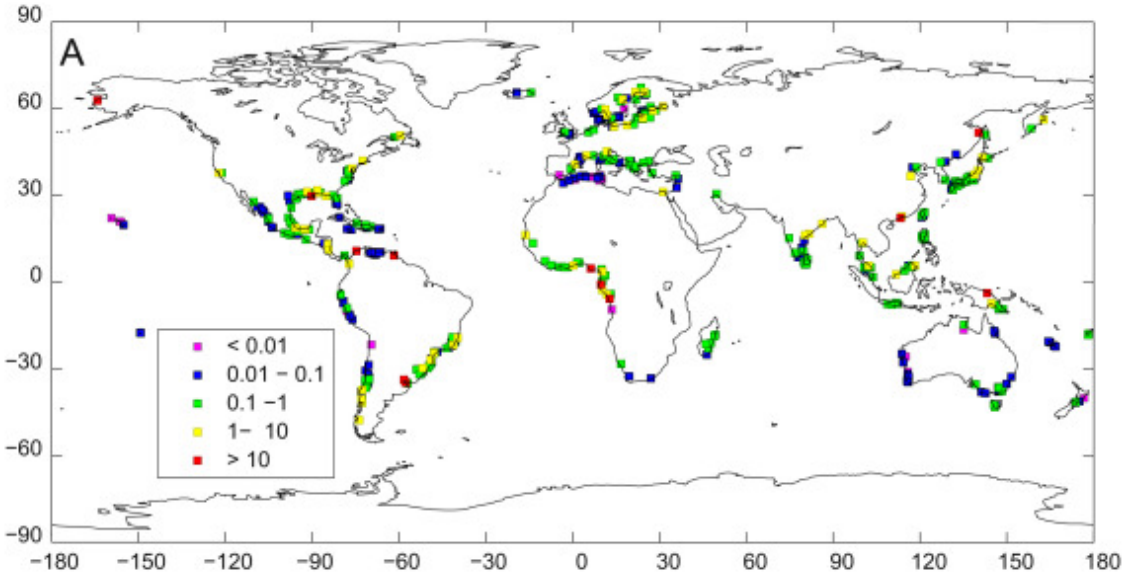

Figure 1: Global map of extractable salinity gradient energy resources: extractable energy (TW·h/a) [10]

There has been recent interest in other sources, aside from rivers and oceans, of natural origin, such as salty lakes (Dead Sea [11], Urmia Lake [12], Great Salt Lake [13], etc) or hypersaline geothermal systems [14]; but also from industrial sources, mainly brines [15], with special focus on the recovery of energy in desalination [16].

SGE comprises several different technologies, foremost among which are Pressure Retarded Osmosis (PRO) [6] and Reverse Electrodialysis (RED) [17]:

1.1-Pressure Retarded Osmosis:

PRO is an osmotic membrane process in which the chemical potential gradient takes the form of an osmotic pressure gradient when two water sources are put in contact through a semipermeable membrane, which allows selective water flow from the low salinity stream (feed stream) towards the high salinity stream (draw stream). In order to generate hydraulic pressure, the high salinity stream is pressurized so the water that crosses the membrane also becomes pressurized. By the action of the external pressurization of the draw stream, and according to osmotic equilibrium laws, the water flow is diminished (when compared to natural osmosis), or retarded, hence the name Pressure Retarded Osmosis. This water transference towards a pressurized stream means that PRO converts the Gibbs free energy of mixing into hydraulic pressure, which is then transformed into electricity by means of a turbine. Figure 2 depicts a schematic of a generic PRO process.

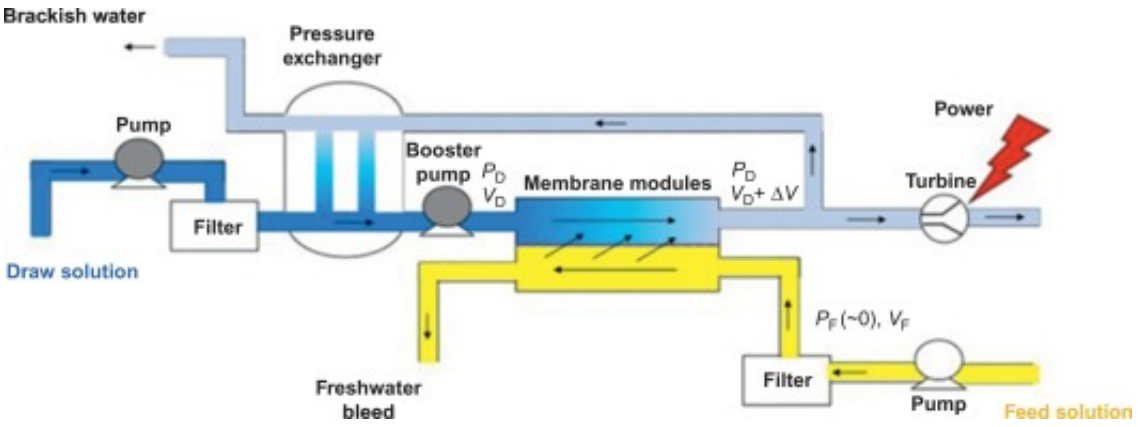

Figure 2: Schematic of a PRO process [18]

Any PRO process should also include a pressure exchanger, in order to keep the high salinity stream pressurized. A fraction of this stream (the portion that crosses the membrane) is delivered to the turbine. Pumping for the transport of the water sources is required; additionally, a booster pump to counter the pressure drop on the draw side circuit is often included [18]. Both inlet streams need to be pre-treated prior to the membrane stage, which notoriously affects the overall net energy gain, as studied in [P1].

1.2-Reverse Electrodialysis:

RED is a membrane process as well, though quite different. A configuration derived from a basic galvanic cell is used, as presented in Figure 3:

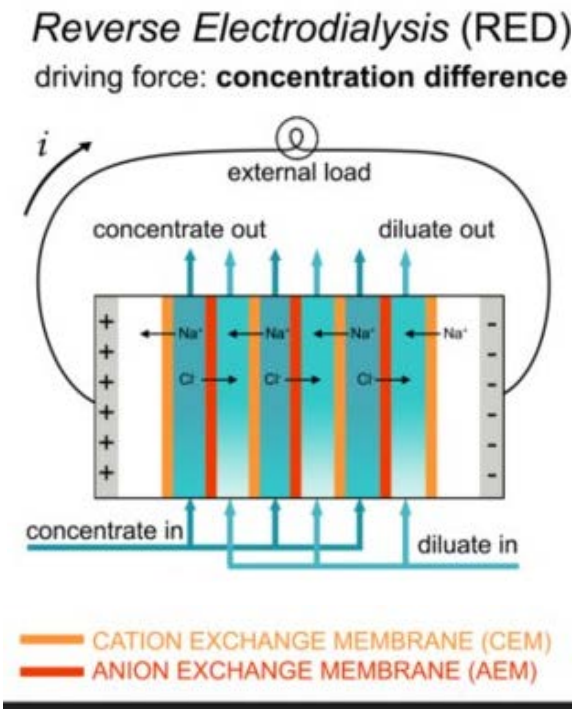

Figure 3: Basic diagram of a RED cell [19]

In RED, several anion exchange membranes and cation exchange membranes are alternately stacked. Concentrated and diluted salt solutions are also placed alternately in the compartments in between. The configuration is completed by one cathode and one anode on opposite ends. This structure results in an electric potential difference. Compared with PRO, the chemical potential is directly converted to electricity [20]. The lack of an external conversion device (turbine) is probably the main advantage of RED versus PRO. Nonetheless, RED presents some disadvantages in performance. Yip et al. compared RED and PRO under different situations, concluding that PRO offers better energy efficiency and considerably higher power density, especially when brines are treated [21]. In addition, RED lacks the extensive industrial experience that reverse osmosis (RO) provides to PRO.

1.3-River-to-sea SGE. Stratified river mouths:

SGE can be applied to varied situations, although its original purpose was intended for the use of river and sea water as energy sources. SGE power plants need to be installed in areas where both types of water source are available at a short distance so as to minimize costs. As shown in Figure 1, not all the river-to-sea systems are equally suitable for SGE generation. There is a type of river-sea system that deserves special attention: stratified river mouths. Stratification appears when the input of freshwater into the saline body of water is strong enough to overcome the saltwater and avoid mixing with it, creating a halocline, that is, an acute vertical salinity gradient [22], as presented in Figure 4:

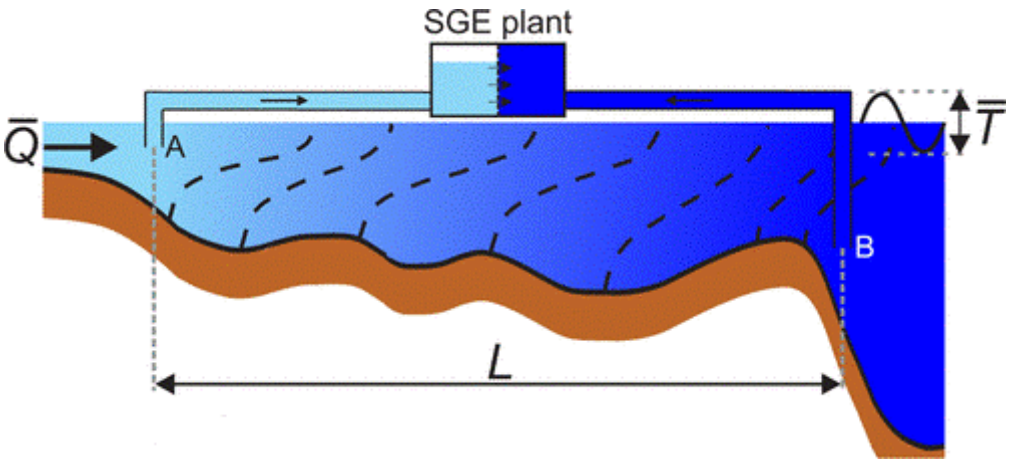

Figure 4: Stratified river mouth with salinity gradients at short distances, dashed lines represent isoclines (same salinity) [23]

These river mouths are generally located in areas with weak tidal ranges, on rivers of medium to high discharge. That the freshwater is warmer than the sea water also facilitates the gradient, while a lower density of the freshwater grants additional buoyancy. They present a salt intrusion on deeper levels, a salt wedge, because water at the surface flows with a higher velocity. These are opposed to well-mixed river mouths, in which river and sea water are gradually mixed through very long stretches of the river mouth, making them poorer candidates for SGE, due to the long distances between the water sources [23]. Highly stratified river mouths are suitable candidates for SGE. For instance, the salinity structure of the Magdalena river mouth in the Caribbean Sea was further studied in [P2].

2.-Evolution of Salinity Gradient Energy and Pressure Retarded Osmosis

The first approach on how to harness energy from the mix of fresh and salt water was presented by Pattle in 1954 [24]. The paper claimed that there is an untapped power in riverwater mixing with seawater equivalent to a 200 m waterfall, and proposed a hydroelectric pile as a sort of RED precursor. Blue energy did not receive much attention until a couple of decades later, when the oil price crisis made the scientific community focus on alternative sources of energy. Norman proposed the first "osmotic salination energy converter", introducing the use of a semipermeable membrane [25], presented in Figure 5:

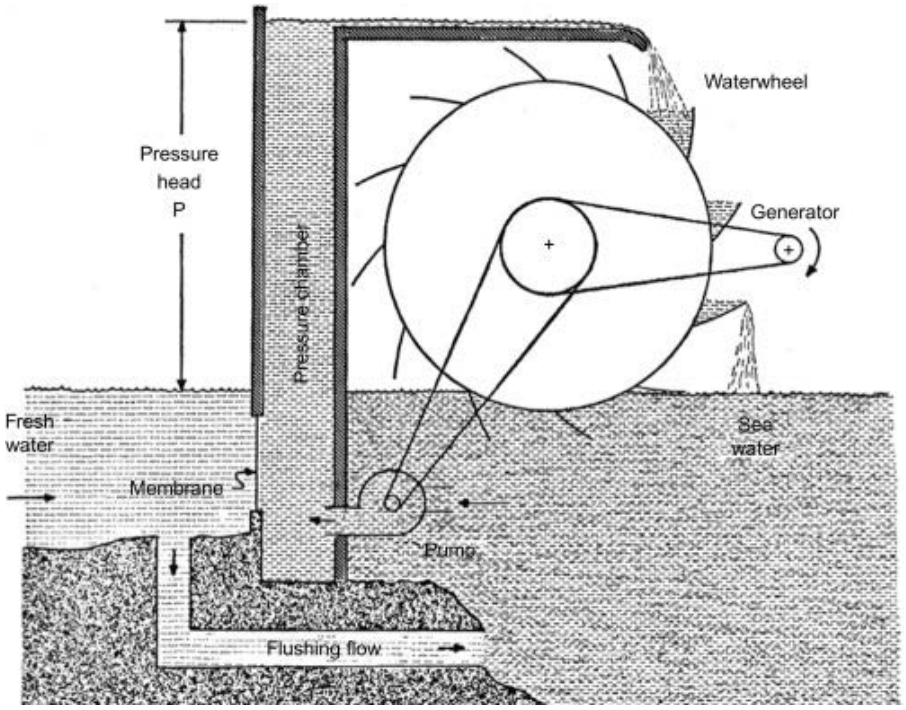

Figure 5: Norman proposal for exploiting osmotic energy [25]

Soon after, pressure retarded osmosis was formally proposed by Norman and Loeb [26], as well the first experimentations using polyamide RO membranes [27]. The results of the power density were very low [28] and PRO did not receive much attention until decades later, when environmental awareness demanded further action in the field of renewable energies. Extended research, experimentation and improvements in membrane technology led to the development of the first osmotic power plant by Statkraft in 2008 in Norway [18]. Unfortunately, the project was discarded a few years later due to insufficient power density (1 W/m^2) with the existing technology. [29]. It was around this time when the goal of 5 W/m^2 was established as rule of thumb [30]. Nowadays, research and improvements in PRO are actively pursued. Proof of this is the Japanese Mega-ton Water system, beginning in 2010, with the goal of operating 1,000,000 m^3/day in seawater reverse osmosis (SWRO) desalination, coupled with PRO, expecting to achieve 4.4 W/m^2 of power density [31]. More recent results tripled the power density (13.3 W/m^2) and allowed a 30% energy reduction in the cost of desalination energy thanks to the hybrid SWRO-PRO system [32]. The 5 W/m^2 requirement for commercial feasibility has been sufficiently surpassed recently [33] [34]; though PRO still faces several challenges that need to be overcome [35] [36] [37]. In parallel, RED technologies continue under development, with the REDstack project in the Netherlands at the forefront [38].

3.-Thermodynamic aspects of PRO

As established in section 1, the goal of PRO, and SGE in general, is to harness the Gibbs free energy released when feed and draw streams are mixed. The Gibbs free energy of mixing ΔG_{mix} is defined by Eq 1 [39]:

$$\Delta G_{mix} = \Delta H_{mix} - T \cdot \Delta S_{mix} \quad (1)$$

where ΔH_{mix} is the enthalpy of mixing, T the temperature and ΔS_{mix} the entropy of mixing.

For instance, the natural mix at river mouths is done irreversibly: no work is produced, since for ideal solutions $\Delta H_{mix} = 0$, so the Gibbs free energy is lost to entropy. However, in a reversible process, since the free Gibbs energy is the maximum thermodynamic work (in an isobaric and isothermal process), the Gibbs free energy of mixing is therefore the maximum theoretical energy that can be produced from that mix. This value is reported to reach 0.7 kw·h/m^3 for seawater and freshwater [40]. A reversible PRO process would indeed obtain this maximum energy by operating at constant pressure with infinite volumes of draw stream, and infinitely slowly, so the whole feed stream would cross the membrane (assumed to be ideally semipermeable) [41]. Obviously, reversible processes cannot be performed in practice, so PRO needs to operate in a practical manner, while aiming to be as close as possible to reversibility in order to make the most of the theoretical potential.

3.1-Chemical potential in PRO:

Chemical potential is involved in PRO and is helpful to interpret the process behaviour, since it is defined as the partial molar Gibbs free energy, and can be estimated easily: assuming ideal conditions, the chemical potential of each component (μ_i), that is, dissolved ions and water, can be calculated as follows [41]:

$$\mu_i = \mu^0 + R \cdot T \cdot \mathrm{Ln}\, a_i \quad (2)$$

where μ^0 is the standard reference chemical potential, R is the universal gas constant, T the temperature and a_i the activity coefficient of substance i.

Pure water has a higher chemical potential than its salt solutions [41]. In other words, the freshwater stream in PRO has a higher chemical potential, and PRO aims to transform this potential into mechanical energy. Thus, the freshwater stream is the source of the energy, so it is called the *feed*. The seawater stream *draws* the solvent, and its osmotic energy, from the feed side, hence its denomination.

4.-PRO in the context of osmotic processes

Osmosis is a natural process that occurs spontaneously when two different solutions with different solute concentrations (that is, different chemical potentials) are put in contact through a semipermeable membrane. The most frequent example found in nature is biological cell membranes, as they act like a semipermeable membrane. The solvent moves from the diluted side towards the concentrated, driven by the difference in chemical potential, trying to reach an equilibrium (Figure 6). It is at this point convenient to introduce the concept of osmotic pressure, which is easier to handle than Gibbs energy or the chemical potential. Osmotic pressure can be calculated as follows [42]:

$$\pi_i = v_H \, C \cdot R \cdot T \tag{3}$$

where v_H is the vant' Hoff factor (for ideal solutions, it is the number of ionic species present, 2 for NaCl), C the molar concentration, R the universal gas constant and T the absolute temperature.

Therefore, the osmotic gradient is easily calculated as the difference of the osmotic pressures on each side of the membrane:

$$\Delta\pi = \pi_a - \pi_b \tag{4}$$

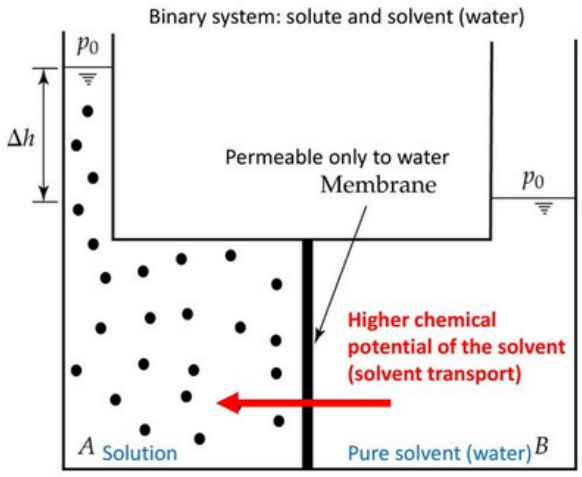

Figure 6: Osmosis and osmotic pressures [43]

The equilibrium in these systems is established when all the pressures intervening in the process are cancelled by those on the opposite side. The application of an external pressure, as is the case of PRO, alters the behaviour of these systems. Based on the applied pressure, several osmotic processes are distinguished:

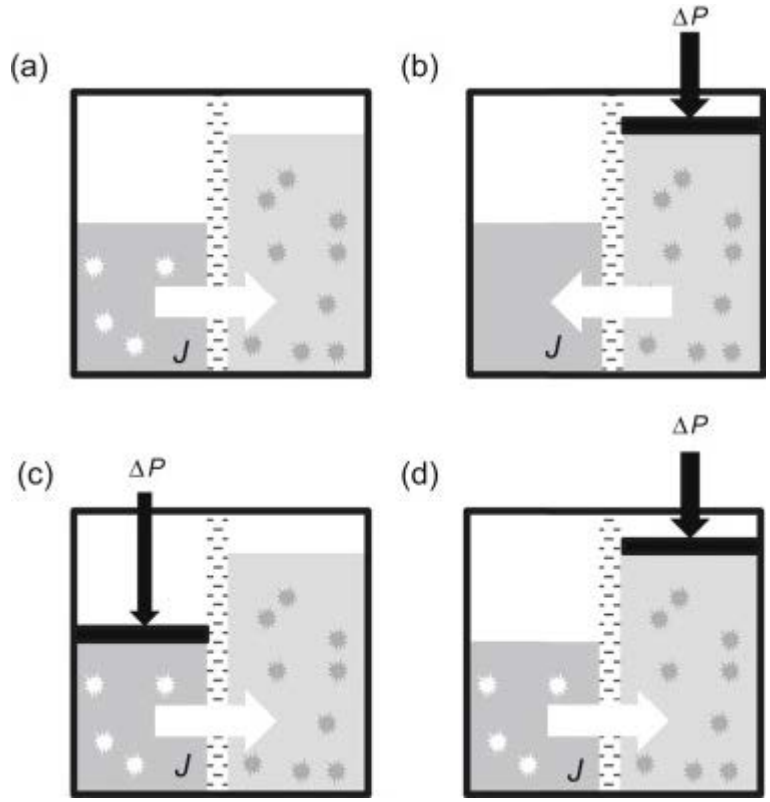

Figure 7: Osmotic processes: a) Forward Osmosis, b) Reverse Osmosis, c) Pressure Assisted Osmosis, d) Pressure Retarded Osmosis [42]

- Reverse Osmosis: when an external pressure is applied on the concentrated stream. The pressure needs to be higher than the osmotic gradient. Under these circumstances, water flows from the concentrated side towards the diluted, *reversing* the natural tendency. RO is mostly employed in water desalination, with more than 13,000 plants operating worldwide producing more than 65 million m^3/day of freshwater [45].
- Forward Osmosis: without any pressure applied, this is the natural osmotic process, and has applications in the food industry, water purification and wastewater treatment [46], [47]. If extra pressure is applied on the dilute side, it is often called Pressure Assisted Osmosis (PAO), and the water flow is higher than in standard FO [48].
- Pressure Retarded Osmosis: when an extra pressure is applied on the concentrated side, but lower than the osmotic pressure gradient [6]. Compared with FO, the water flow is diminished, but it still flows in the same direction and gets pressurized.

Figure 8 presents a graphical description of how the pressure applied is the parameter that defines each process, delimiting one from another, and defining the magnitude and direction of the water flow.

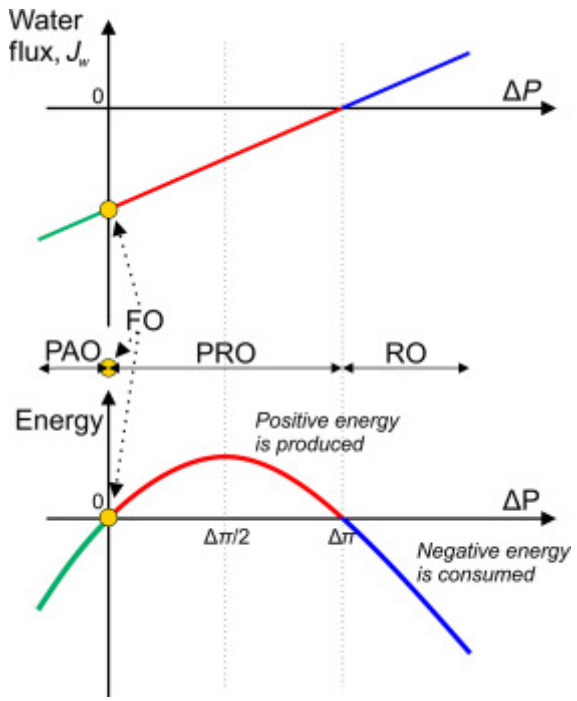

Figure 8: Different osmotic processes and their a) water flow (above) and b) energy (below) depending on the external hydraulic pressure [49]

The highest ΔP interval corresponds to RO, presenting a higher water flow with increasing pressures. If the pressure decreases to the value of the osmotic gradient $\Delta\pi$, the flow is stopped and no water is produced. PRO takes place between this point and $\Delta P = 0$: the water flows in the opposite direction to RO and its rate increases as the ΔP decreases. Zero pressure is the point of operation of FO; if some pressure is applied on the feed side (depicted as negative values of ΔP in the graph), the water flow is increased: PAO.

The pressure applied serves to calculate, in a rough sensibility analysis, the energy demanded (or produced) in the different processes. The interval of PRO has a positive energy in the graph, meaning that energy is produced. It presents a maximum, theoretically corresponding to half the value of the osmotic pressure gradient $\Delta\pi$ [49]. In practice, however, it is higher, so as to compensate for deviations from the ideal at the membrane level. The energy cost of FO is clearly null, as no pressure is applied. RO has a high energy consumption (presented with negative sign in Figure 8 b), increasing in line with the pressure applied.

5.-Pressure Retarded Osmosis and desalination by Reverse Osmosis

PRO development has always been closely linked to RO due to the inherent similarities between both processes. Proof of this is the initial use of RO membranes in PRO [27], or the common challenges shared by both [50], such as membrane fouling (see section 8), concentration polarization (subsection 7.1), or the need for pretreatment (section 9), etc.

However, the PRO/RO relationship extends beyond this. Several studies regarding the integration of PRO in SWRO have been performed [51] [52] [53]. The combination of these two technologies is motivated by two key aspects in which PRO and RO are complementary. The first is the common presence of a high salinity stream, which in RO is the brine, and in PRO is the draw stream. In the former, the high salinity stream is a waste, in the latter it is a source; so the connection is straightforward. The second complementary aspect lies in the nature of the energy of each process; RO demands energy to operate, whereas PRO produces it. Therefore, PRO energy may be used to partially satisfy SWRO energy demands, making it more efficient and less expensive. One of the simplest configurations is depicted in Figure 9, though there are many other options [54]. Some of these other possibilities were studied in [P3].

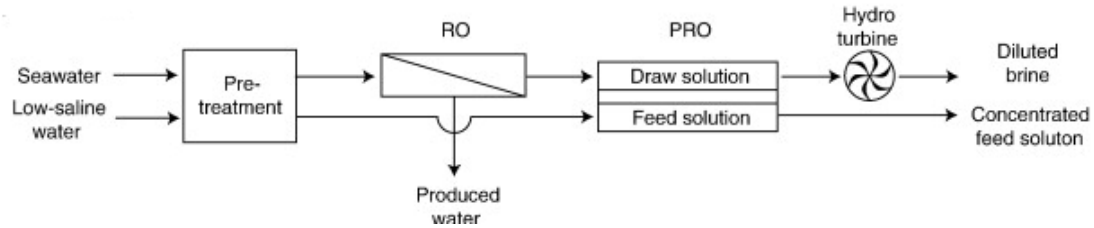

Figure 9: Schematic of a simple RO-PRO hybridization [54]

Moreover, there are other synergies to exploit from this RO-PRO combination. For example, the draw stream in an independent PRO installation needs to be pre-treated, but the brine coming from RO has already been pre-treated prior to the RO process. There is still the need to pre-treat the feed stream, but there may be cost savings from exploiting the conjoint economy scale in the combined pretreatment [52].

Additionally, there is the issue of the production of high salinity brines, which is a substantial problem in seawater desalination. The by-product brines need to be discharged back into the sea, but they have to be treated first or discharged far offshore, in order to reduce their environmental impact [53]. PRO uses this brine, serving as a waste treatment for RO. PRO waste streams have much lower salinity and are more easily disposable [16].

6.-Membranes in Pressure Retarded Osmosis

In the beginnings of PRO, the first membranes tested were the RO membranes available at the time [28], polyamide composite membranes with polysulfone support. However, this first PRO experiment presented very low power density due to low membrane permeability, as expected, because RO membranes only allow for acceptable flow densities at higher pressures. Moreover, in order to withstand the high operation pressure of RO, these membranes have thick support layers with high structural parameter (S) that lead to high ICP (see subsections 6.2 and 7.1). In order to obtain higher flow densities, more permeable membranes were tried later on. Cellulose tri acetate (CTA) FO membranes are more hydrophilic and they have smaller structural parameter, although they allow higher reverse salt flux than RO membranes [55]. FO membranes presented overall better performances than RO membranes, but most experiments did not resist operation at the higher pressures demanded in PRO, presenting severe deformations after short operation time, since they were designed for FO operation.

Currently, PRO membrane research is mostly focused on thin film composite (TFC) membranes and thin film nanocomposite (TFN) membranes. The selective layer most used are polyamides, and some derived polymers from it, such as polyimides, polyamide-imide, polyetherimide, etc [56]. Regarding the support layer, polysulfone (PE) and polyethersulfone (PES) polyacrylonitrile (PAN), polyethylene terephthalate (PET) are often employed. Common goals are improving mechanical stability and durability, permeability and anti-fouling features (see section 8) [57].

6.1-Membrane configurations in PRO:

PRO membranes have an asymmetric structure, an active layer that provides selectivity and permeability, and a support layer in order to withstand operation under pressure. The active layer faces the draw stream while the support layer is put in contact with the feed. Sometimes this disposition is reversed, called FO mode [56]. In addition to this, the membrane can be set up in different configurations (Figure 9). Flat sheet or flat plate membranes is the simplest configuration, only used at laboratory scale. For larger operations the membrane is more efficiently packed on spiral wound, or tubular, though they are still referred as flat sheet membranes. This is the configuration selected for the research presented in [P1].

Another promising possibility are hollow fiber membranes, which are fine capillary tubes (bore generally smaller than 1mm), with the active layer on the inner surface. Their cylindrical geometry and self-supported structure make them able to withstand higher pressure than traditional equivalent flat sheet membranes [57]. In addition, they can be densely packed in modules, offering very high ratios of surface area per module volume.

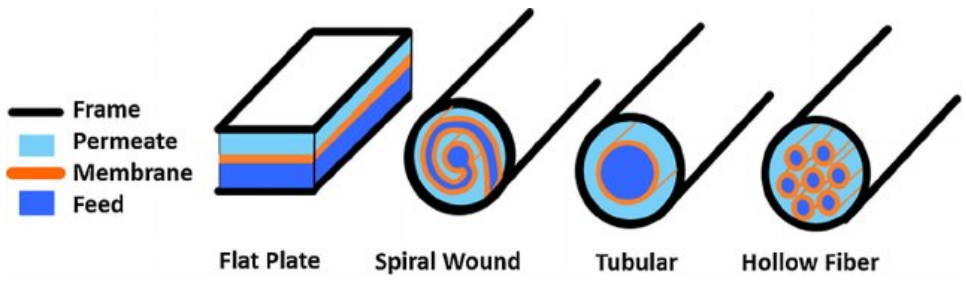

Figure 10: Different membrane configurations [60]

6.2-Membrane properties:

- Permeability, *A*: the most important parameter, the water permeability is the volumetric flow of water able to cross the membrane by unit of surface ($m^3/m^2 \cdot s$, or m/s).
- Solute permeability, *B*: is the quantity of a given solute that is permitted to cross the membrane, salt in the case at hand ($kg/m^2 \cdot s$).
- Selectivity B/A: is the ratio of the salt and water permeabilities.
- Structural parameter, S: is an intrinsic membrane parameter, that, conceptually, gives a measure of how complicated it is for the molecules and ions to move through the membrane. It is defined as the product of the membrane tortuosity (τ) and thickness (x) over the porosity (ϕ) [61]:

$$S = \frac{x \cdot \tau}{\phi} \tag{5}$$

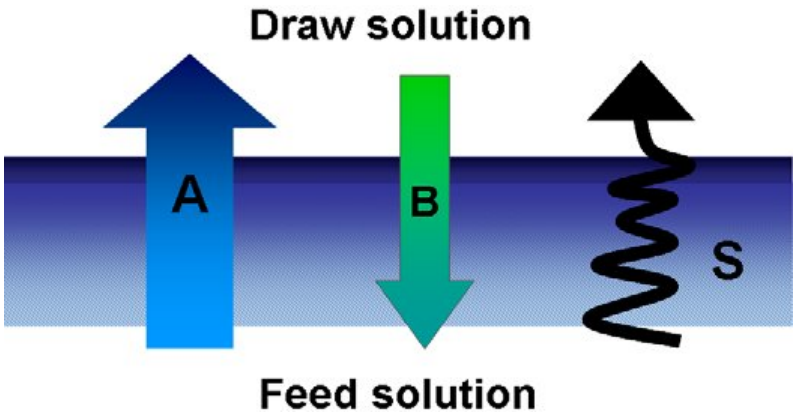

Figure 11: Graphical description of the significance of *A*, *B* and *S* in PRO [62]

At first sight, in order to enhance power production, it is desirable for membranes to have high *A* and low *B*, however; in practice it is difficult to synthesize such membranes, because membranes with high *A* tend to also have high *B*: high permeability is accompanied by low selectivity, whereas when high selectivity is pursued, membranes present lower permeability. Moreover, it has also been demonstrated experimentally that a balance between permeability and selectivity leads to better PRO performance [63].

Membrane properties from a state of the art membrane [64] were used in this work [P1], [P2].

7.-Power production and water flux

PRO goal is to produce energy by making water cross a semipermeable membrane from a diluted stream towards a pressurized salty draw stream. It is clear that the determination of the amount of water able to cross the membrane is of paramount importance. Therefore, the flow density J_w, defined as volumetric flow of permeate per unit of membrane area is established as the variable to observe. The second key variable is the external pressure applied on the draw stream, ΔP. The product of both represents the hydraulic energy in PRO, better named power density W:

$$W = J_w \cdot \Delta P \tag{6}$$

Figure 12 depicts the power density variation with the external pressure:

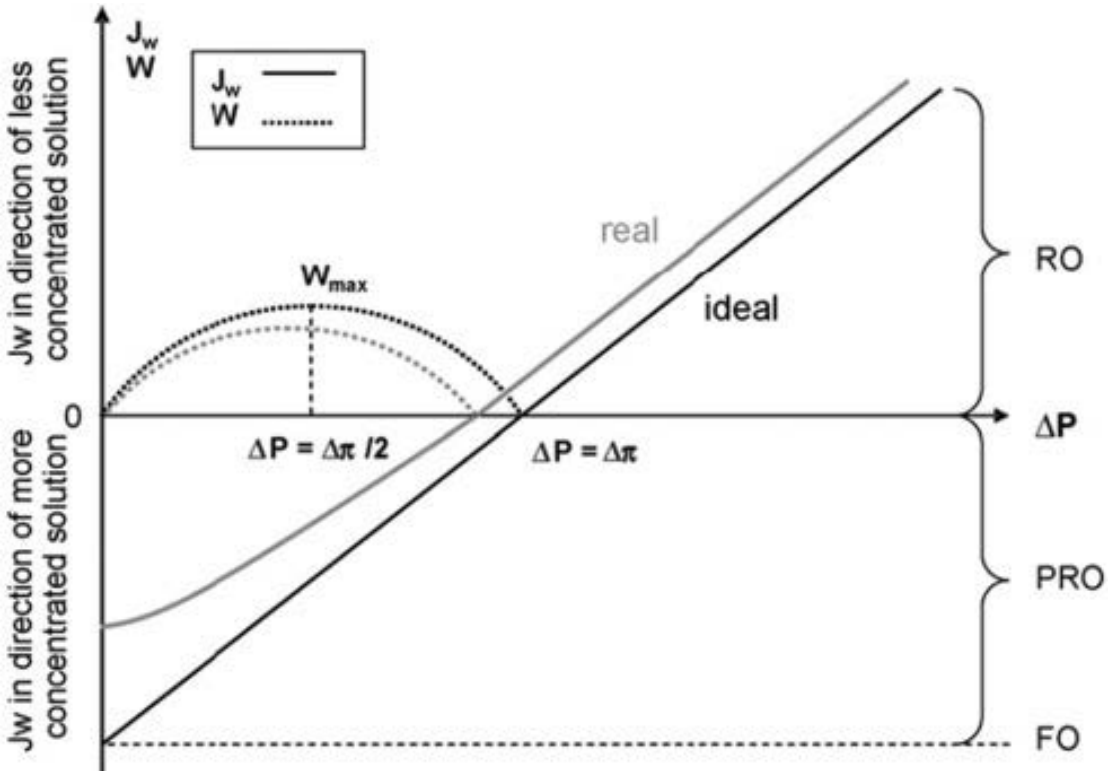

Figure 12: Water flux and power dependence with the external pressure [65]

It is found that the power production presents its maximum when the external pressure equals half the osmotic gradient, for ideal membranes. In real processes, it is slightly displaced to the left, to lower pressures, due to several factors that are detailed in the following subsections 7.1 and 7.3. Sensitivity analysis to the operation pressure and determination of the optimal non-ideal pressure were performed in [P1].

7.1-Concentration Polarization (CP):

In a PRO process using a real membrane, J_W is always considerably lower than ideally expected. The main reason is that PRO membranes are not perfectly selective, so, a reverse salt flux always takes place. This salt flux is not only responsible of the reduction of the transmembrane gradient

(feed concentration increases due to salt leakage, draw decreases because of the salt lost) but also of the concentration polarization (CP) phenomenon that occurs at microscopic level at the membrane interfaces, and inside the porous support.

According to film theory [66], there is a region in close proximity to the membranes, and parallel to it called boundary layer, in which the movement of solvent molecules and ions is hindered, because it lacks the perfect mix conditions of the bulk solution. The same occurs when the solution substances cross the support area: their flows are partially impeded by their interaction with pore walls and affected by the tortuosity.

Consequently, when material transference takes place, concentrations gradients built up in these layers, as a result of the resistance that the substances face to diffuse. This is analogous to heat transfer by conduction on a stack of materials with different conductivity: different resistances to heat transfer lead to different gradients and wall temperatures in between; whereas in PRO there are intermediate gradients and different concentrations at each interface. The concentration polarization phenomena involved in PRO are presented in Figure 13:

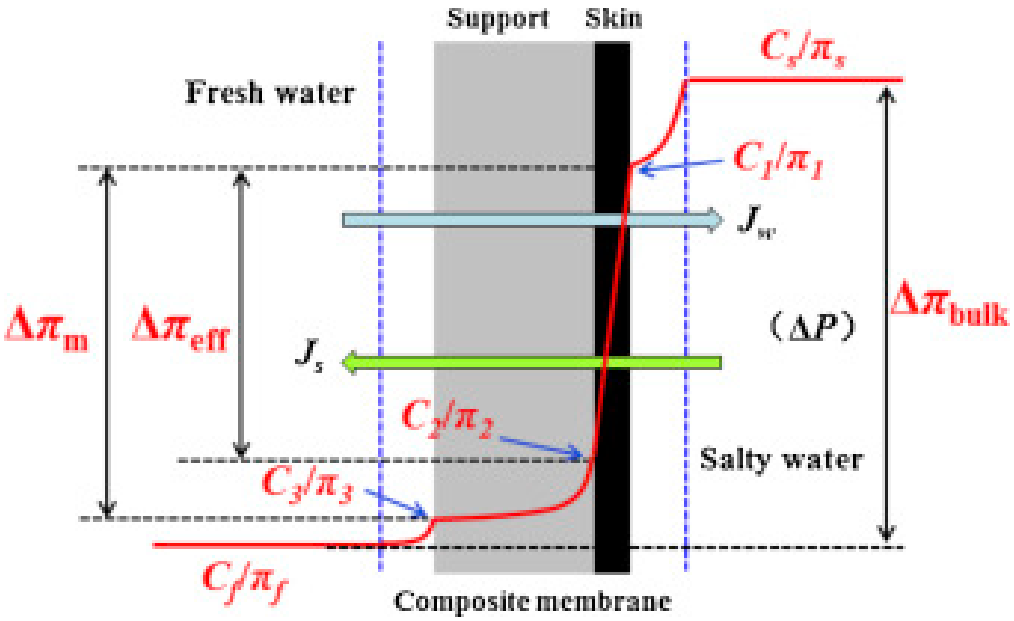

Figure 13: Concentration polarization phenomena in a PRO membrane [65]

Three CP phenomena are considered: looking at the concentration profile in Figure 13, in the draw side, the concentration at the membrane interface C_1 is smaller than in the bulk draw C_s, as the incoming water from the feed side dilutes the salt concentration at the draw interface and salt ions move with more difficulty through the boundary layer. This is called External Concentration polarization (ECP) on the draw side, or dilutive CP. There is also ECP on the feed side, sometimes referred as concentrative CP, generally much smaller [68]. The concentration polarization occurring inside the porous support is called Internal Concentration Polarization (ICP), and is the most severe [37] [69]. Adding the effects of the feed side ECP and the ICP, the interface concentration at the feed side is C_2, which is much smaller than expected. This three concentration polarization effects combined result in a diminished transmembrane effective

gradient $\Delta\pi_{eff}$, meaning that the water flux is also significantly smaller, therefore so is the power production.

Concentration polarization can be mitigated by turbulent regime of flow, membrane spacers are known to increase turbulence and facilitate better mixing to reduce ECP, as has been demonstrated by extensive experience in SWRO industry. This is yet to be fully studied in PRO [70] [71]. ICP is reduced with porous membranes with low structural parameters [57].

7.2-Water flux models:

It is straightforward to assume that J_W is directly proportional to the water permeability *A* of the membrane and to the osmotic gradient $\Delta\pi$. Assuming ideal conditions, J_W is given by the following expression:

$$J_W = A\cdot(\Delta\pi - \Delta P) \tag{7}$$

Polarization concentration phenomena demands more exhaustive models than Eq (7), in order to predict more accurately the water flux. For instance, Lee introduced the effect of ICP on a model for water flux in PRO [72]. Achilli added ECP (draw side, dilutive ECP) [65] and subsequently Yip expanded previous efforts by including the influence of the reverse salt flux [73].

This work ([P1], [P2]) uses a detailed model proposed by Touati [74]. This model is a general mass transport model for the water flux (J_W) accounting all three CP effects, based on the convection-diffusion theory, through the integration of the differential equations that determine the concentration profiles, using mass transfer coefficients:

$$J_W = A\left[\left(\pi_{D,b} + \frac{B}{A}\left(1 + \frac{A\cdot\Delta P}{J_W}\right)\right)\exp\left(-\frac{J_W}{k_D}\right) - \right.$$
$$\left. - \left[\pi_{F,b} + \frac{B}{A}\left(1 + \frac{A\cdot\Delta P}{J_W}\right)\right]\exp(J_W\cdot K)\exp\left(\frac{J_W}{k_F}\right) - \Delta P\right] \tag{8}$$

where *A* and *B* are the water and salt permeabilities of the membrane, $\pi_{F,b}$ and $\pi_{D,b}$ the osmotic pressure at the bulk solutions of feed and draw (determined with Eq. (3)), k_F and k_D the mass transfer coefficients at feed and draw sides [75], ΔP the external pressure on the draw side and *K* the solute resistivity calculated with the structural parameter *S* and the diffusivity (of NaCl in water) *D* [61]:

$$K = S/D \tag{9}$$

Similarly, to Eq (7), J_S is defined as:

$$J_S = B\cdot(\Delta\pi - \Delta P) \tag{10}$$

and can be calculated more accurately once J_W is known:

$$\frac{J_S}{J_W} = \frac{B}{A\cdot\beta\cdot R\cdot T}\left(1 + \frac{A\cdot\Delta P}{J_W}\right) \tag{11}$$

The ratio J_S/J_W represents the amount of salt per unit of permeate and is often used as an expression of the membrane selectivity.

7.3-Draw dilution:

Aside from CP, there is another effect that needs to be considered to avoid overestimation of the salinity gradient and to properly predict the water flux [76]. In a real process, membranes are long and the salinity of both streams varies with the position throughout the membrane length. This occurs because as the feed stream keeps transferring water towards the draw, it becomes progressively diluted. The equivalent happens with the salt flux in the opposite direction (Figure 14).

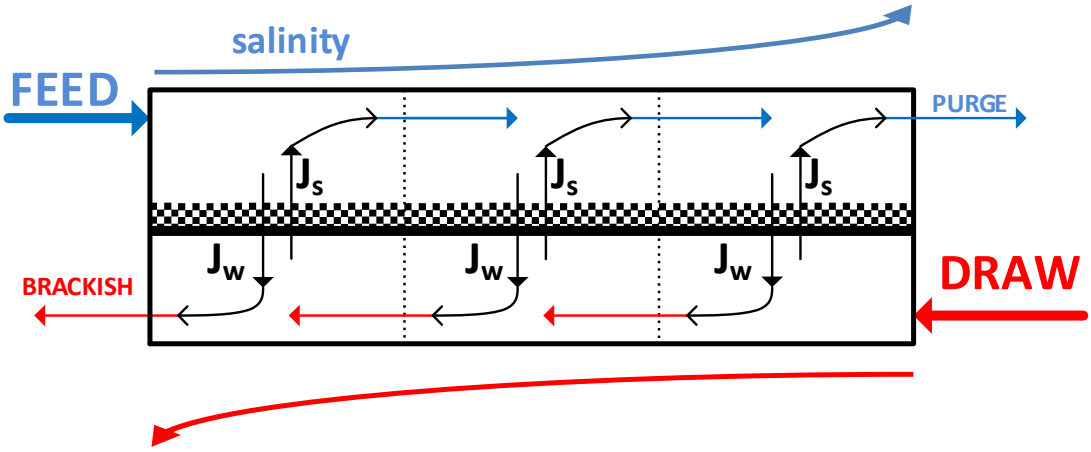

Figure 14: Lengthwise variation of the salinity profiles of feed and draw in PRO

To account for draw dilution, a multi-stage approach was applied in [P1] to determine more accurately the water fluxes in a PRO power plant fed by river and sea water.

8.-Fouling in Pressure Retarded Osmosis

One of the challenges that PRO faces is the decline over time of the permeability and performance of the membranes, as happens in any industrial application of membranes [77]. This behaviour is mostly explained by the presence of impurities in the water sources that slowly but relentlessly obstruct the membrane, when they either have a bigger size than the membrane pore, or they are deposited and adhere to the membrane.

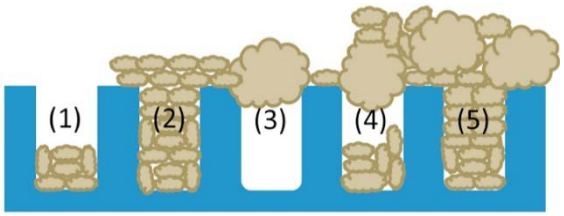

Figure 15: Different fouling situations [77]

These impurities that obstruct the membrane are called foulants, and can be classified depending on their nature [78], as presented in Table 1:

Table 1: Fouling classification and examples

Type of fouling	Foulants
Particle and colloidal fouling	Clay, silt, silica, metal oxides, etc.
Organic fouling	Macromolecular organic compounds: proteins, polysaccharides, fatty acids, etc.
Crystalline fouling or mineral scaling	Low solubility inorganic salts: calcium and magnesium sulphate, phosphate, carbonate, silicate, etc.
Biofouling	Microorganisms

Each type of foulant can cause varying damage, depending on their different affinity to the membrane materials, and their fouling effect can be very different [78]. For instance, mineral scaling is linked to ICP (internal concentration polarization), because the solute concentration increases inside the support layer. Since it has a low solubility, super-saturation may be reached and precipitates can be formed [79]. Anti-foulant membranes are currently being studied and developed [80].

8.1-Fouling models:

Several fouling models have been proposed to describe the mechanisms by which the membrane permeability is affected. The classical models are [81]:

1 *Complete Blocking Model* (CBM): the model considers that each arriving particle seals off pore entrances and completely prevents the flow through that pore. This model is suitable for large fouling particles that can completely block a pore.

2 *Intermediate Blocking Model* (IBM): this is similar to CBM, but only a fraction of the membrane pore gets clogged by foulant particles. Each new particle has a certain chance of being deposited

on an already obstructed pore or on a free pore. Unlike CBM, total flow impediment is not reached, better representing the reality.

3 *Standard Blocking Model* (SBM): this model poses the scenario that the particles accumulate inside the pores, constricting them by adhesion to the pore walls, progressively decreasing the area. This model is mostly adequate for small particles.

4 *Cake Filtration Model* (CFM): unlike the others, this does not consider what happens on the porous internal structure of the membrane, as it assumes that the particles uniformly land on the membrane surface, covering it and providing an additional resistance to the permeate flow, similar to an extra support layer. This cake layer gets thicker over time, progressively increasing its resistance.

Aside from the previous classical models, many other studies have proposed alternative models, considering advection-diffusion, adsorption-desorption equations or interaction among foulants; or a combination of the classical models [82], in order to predict the permeability and power density decline over time due to fouling, [83]. Nonetheless, every fouling situation is unique, dependent on each water source and each membrane. It is generally accepted that membranes with a lower structural parameter S present a lower ICP (see subsections 6.2 and 7.1), and thus a lower fouling predisposition [84].

8.2-Membrane orientation and the effect of ICP:

The classical membrane orientation, often called PRO mode, has the active layer facing the draw solution, so it is denoted as AL-DS. This is the dominant configuration because it presents a lower internal concentration polarization and a higher power density than the alternative with an active layer facing the feed, AL-FS (see Figure 13 in subsection 7.1). It is important to remember that the support layer is wetted by the solution it is facing. This means that the foulants present in this stream will be more responsible for the membrane fouling than those contained in the stream facing the selective active layer. Seawater and brines (draw stream) are expected to contain more scaling precursors than river water. This fact leads us to support this configuration when there is a risk of scaling. However, some authors claim that the FO mode offers lower fouling when treating feed solutions with a high fouling tendency, such as wastewater or river water [85].

It has also been reported that fouling reduces J_S, unexpectedly, to a greater degree than J_W is reduced [$(J_S / J_W)_{fouling} < (J_S / J_W)_{clean}$] in AL/FS, resulting in a decrease in the ICP, making the membrane more selective [84].

Furthermore, it was proposed that, for a low salt permeability membrane, the FO mode after fouling would present a higher power density than the PRO mode [77].

8.3-Pressure loss, the effect on optimal pressure:

A direct consequence of fouling, aside from the reduction in water permeability, is always an increase in pressure loss, which by itself is always an undesirable cause of increased energy costs. However, in addition, it also causes a variation in the optimal operation pressure, as reported by [84]:

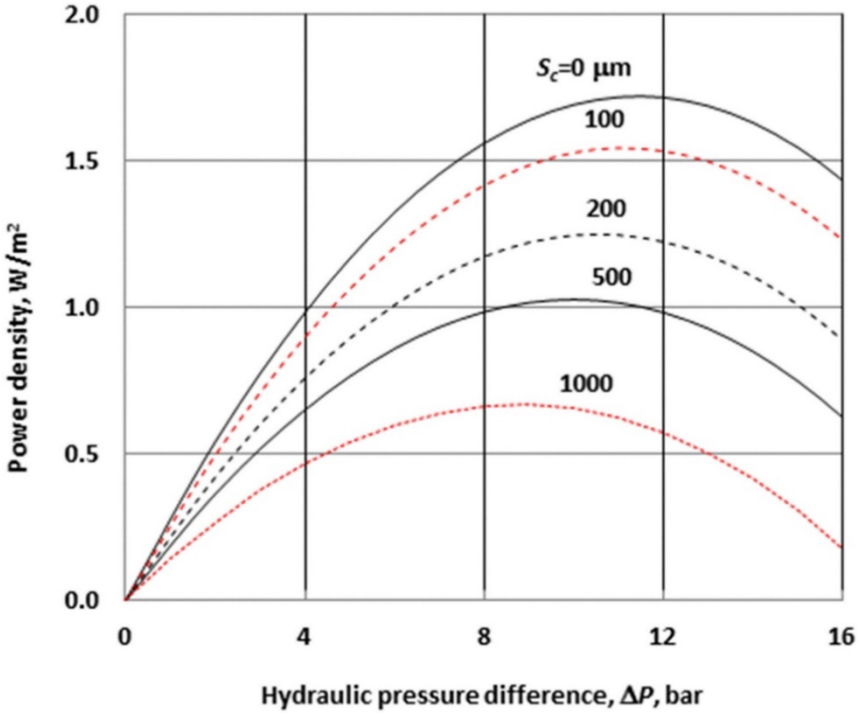

Figure 16: Power density curves for different fouling levels [84]

A higher than optimal operating pressure provokes a diminished water flux and a higher reverse salt flux [75], both of which may aggravate the fouling of the membrane [86].

Thus, if the hydraulic pressure is not carefully controlled in osmotic processes, the fouling reduces the power density, causing the system to operate at a pressure progressively farther from the optimal, leading to a worse performance if the pressure is not adequately controlled.

8.4-Membrane cleaning:

After operation and progressive fouling of the membrane, it is standard practice to clean the membrane. Different procedures have been derived from extensive experience in RO, with the use of such cleaning agents as NaOH or EDTA in aqueous solution [87]. A more environmental-friendly option is osmotic backwash, which consists of briefly switching the feed and draw flows, without external pressure, so the feed water crosses the membrane from the active layer side, sweeping away the foulants deposited on the porous support and/or the cake formed over the membrane [88]. Some authors have reported better results adding air bubbles [89]. However, not all foulant particles are removed and cleaned membranes present lower power densities than new membranes, as depicted in Figure 17 [88]:

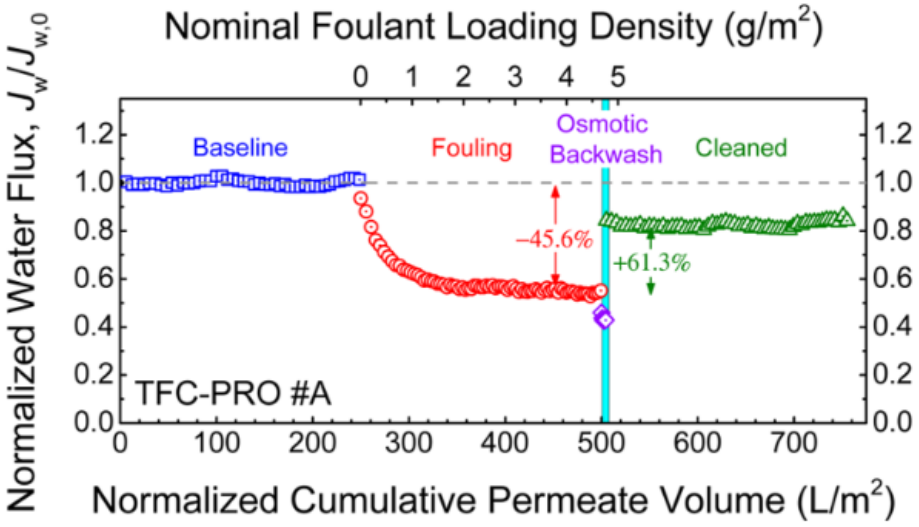

Figure 17: Variation of water flux in PRO after fouling and cleaning by osmotic backwash [88]

Moreover, fouling caused by scaling often damages the membrane structure: the growth of large crystals irreversibly deforms the membrane, and causes the partial loss of selectivity. The scaling caused by gypsum deposition is especially difficult to remove through backwashing [90].

9.-Pretreatment in Pressure Retarded Osmosis

To address the severity of the fouling problem presented in the previous section, there are many possible solutions in the form of pretreatment processes that mitigate the fouling effects to manageable levels, allowing adequate long-term performance of the membrane. Special attention needs to be put on the design of the pretreatment strategy, because its performance will reflect on the global performance [91]. For instance, if not enough foulants are removed, frequent stops for cleaning will be necessary and the membrane lifespan will be reduced. Moreover, pretreatments always represent a sizeable part of both the investment and operational costs (mainly energy consumption). They are also highly space-consuming [92].

Two groups of pretreatments are distinguished: physical and chemical treatments. The former are responsible, in broad terms, of the mechanical filtration of bigger particles of foulants, while the latter deals mostly with dissolved foulants through the addition of chemical components. As it happened in PRO fouling, there are few scientific studies on PRO pretreatments, therefore pretreatment experience from RO is very important as it is easily extensible to PRO [92]. In the recent past, most RO plants used conventional pretreatment, defined as chemical and physical pretreatment without the use of membrane technologies. Experience shows that successful pretreatment designs must combine chemical and physical treatments.

9.1-Chemical treatments [92]:

9.1.1. Chlorination: prevents biological growth. Dechlorination (often with sodium bisulfite) may be needed, excessive chlorine can damage the membrane.
9.1.2. Ozone treatment: to degrade organic matter.
9.1.3. Lime treatment: to remove water hardness. It is also involved in flocculation. Moreover, it may help removing dissolved organic matter and microorganisms.
9.1.4. pH control: the addition of an acid mitigates scaling by increasing calcium solubility.
9.1.5. Addition of antiscalants: organophosphonates, sodium hexametaphosphate or polyacrylate based. However, antiscalants can enhance biofouling if their concentration is not carefully controlled.
9.1.6. Coagulation and flocculation agents: They make colloidal matter to agglomerate, so it t can be physically removed afterwards. Colloidal foulants, especially organic, are well treated by this process. They reduce alkalinity and are very space-consuming. They are traditionally made of iron and aluminium salts, there are also cationic polymers. The coagulant most recommended for treating brines is $FeCl_3$, although there are cheaper options. $AlCl_3$ $NaAlO_2$ are indicated for phosphates, which are one of the most common scalants present in urban wastewater.

9.2-Physical treatments [92]:

9.2.1. Dissolved air flotation: bubbling air helps bringing particles to the surface, where they can be easily removed.
9.2.2. Roughing filters: they eliminate the bigger sized particles, for example sand filters or gravel filters.
9.2.3. Sedimentation: deposition by the action of gravity of particulate matter in suspension to the bottom of big sedimentation tanks.

9.2.4. Adsorption with active carbon: also called filtration with activated media, the use of powdered or granulated activated carbon is used to remove dissolved foulants. Thanks to the large surface area, many organic contaminants are retained.

9.2.5. Membrane filtration, microfiltration (MF), ultrafiltration (MF), nanofiltration (NF): they are a filters that use a membrane with a defined pore size, by which they are classified: MF≈ 1 µm, UF≈ 0.01 -0.1 µm, NF ≈ 1 nm. Each type focuses on eliminating different foulants:

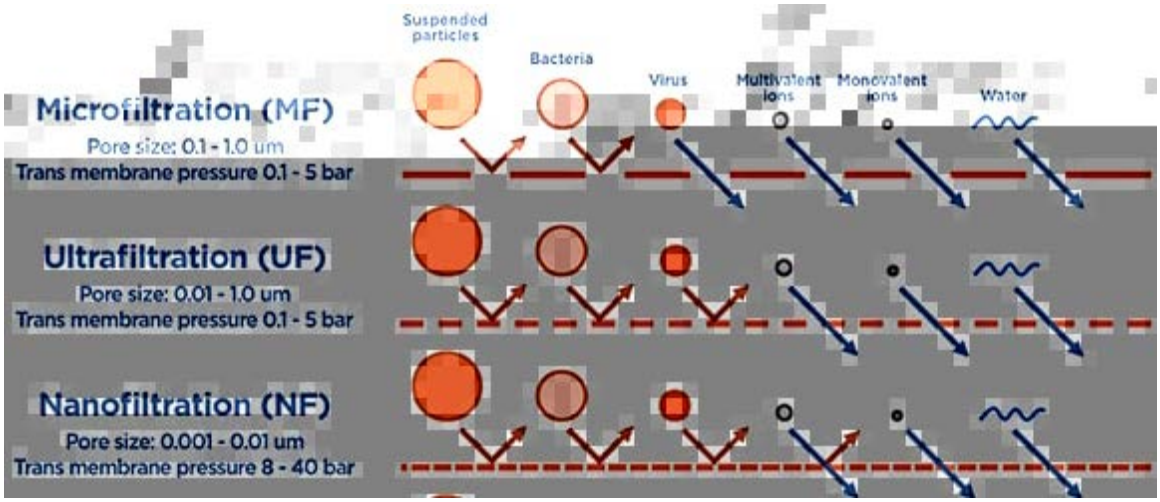

Figure 18: Different type of foulants eliminated through MF UF and NF [93]

All three membranes have different advantageous characteristics; their suitability depends on the specific foulants at hand. For instance, MF is suitable for removal of large particulate matter, while NF membranes are better to remove dissolved contaminants. UF membranes balance contaminant removal and permeate production [94].

It is important to consider that the smaller the pore, the higher the pressure required to make water circulate (see Figure 18). One disadvantage of membrane filtration lays in the inherent nature of the process: the membrane retains the foulants and becomes eventually fouled, with the issues that situation involves (need for cleaning, increased operational costs, etc.).

The traditional conventional pretreatment configuration consists of chemical addition of disinfectants and coagulation-flocculation agents, followed by sedimentation and filtration, without the use of membrane technology. Many variations can be made. Currently UF is very frequently added to the conventional configuration:

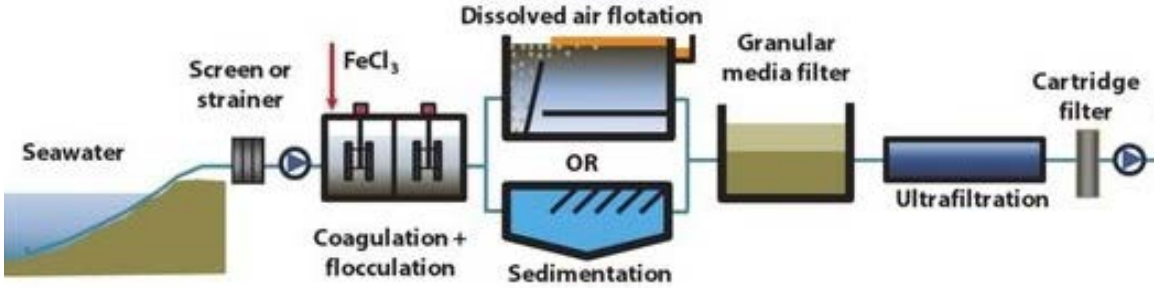

Figure 19: Example of PRO pretreatment configuration [95]

In order to predict the efficiency of a pretreatment method, there are several methods that aim to numerically characterise a water source, in terms of quality and its fouling ability. This characterisation is applied before and after the pretreatment, in order to evaluate the improvement in water quality. The most important characterisation indexes are the Silt Density Index (SDI) and the turbidity. SDI is a standardised method that measures the fouling of a certain filter under fixed conditions [96]. Turbidity is a measurement of the scattering effect on light caused by the particles present in solution.

Commercial membranes often require a maximum SDI in the water to be treated in order to guarantee good performance. However, the presence of scaling and organic foulants are not directly represented by turbidity and SDI. Thus, considering the specific case at hand, it is often necessary to quantify the water hardness and the organic content (for example through determination of Dissolved Organic Carbon, DOC). River water and sea water may need different pretreatments.

10.-Challenges in river-to-sea PRO plants

PRO nowadays still faces several obstacles to overcome before becoming a competitive renewable energy. In addition to the need for improved membranes mentioned earlier, other issues are discussed below.

10.1-Energy efficiency

Starting from the theoretical potential of fresh water of just above 0.7 kw·h/m^3 [40], the efficiency of PRO is diminished by many effects. First of all are the inherent losses derived from proceeding with an actual irreversible non-ideal membrane process: draw dilution and concentration polarization significantly reduce the theoretical potential. This means that the energy generated (or available energy) will drop to almost half the starting value [97]. Figure 19 depicts how the ideal 0.7 kw·h/m^3 potential is distributed:

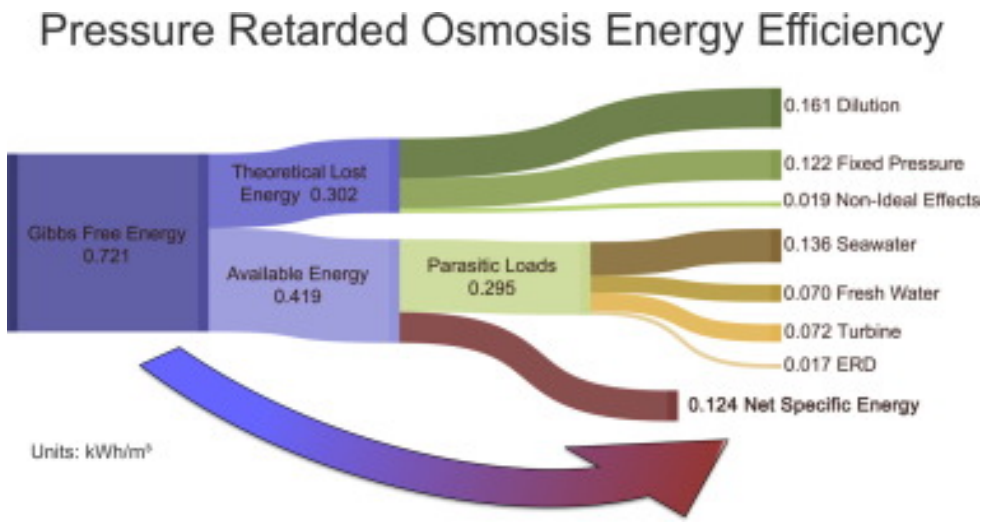

Figure 20: Estimation of PRO net specific energy [97]

Since the goal of PRO is to produce energy, any other relevant energy stages of the process need to be considered to assess the energy efficiency. These are sometimes referred to as parasitic loads [97] [98]. Among these, the most critical are the pretreatments, required to mitigate fouling-driven performance decay. Pretreatments demand a sizeable infrastructure and continuous energy consumption for them to operate; the amount may vary depending on the water quality and the pretreatment technologies selected, but they are roughly estimated to absorb half the energy generated. In addition, each of the mechanical devices involved in the process are expected to have their own inefficiency (see subsection 1.1): the said devices include the pumps, the turbine and the energy recovery device (ERD or pressure exchanger). ERD inefficiencies rarely exceed 3 % [99]. These inefficiencies are resolved by extra energy spent in pumping. Finally, water transport in and out of the plant also needs to be included. The intake and discharge distance is the key variable for that consumption, as further studied in [P2]. O'Toole et al. estimated that all the energy losses and consumptions result in about 15% of the net energy of all the potential remaining [97].

The work presented in [P1] shows a similar distribution for a case study in Colombia, assuming pretreatment with MF [100], and a turbine efficiency of 80% [101].

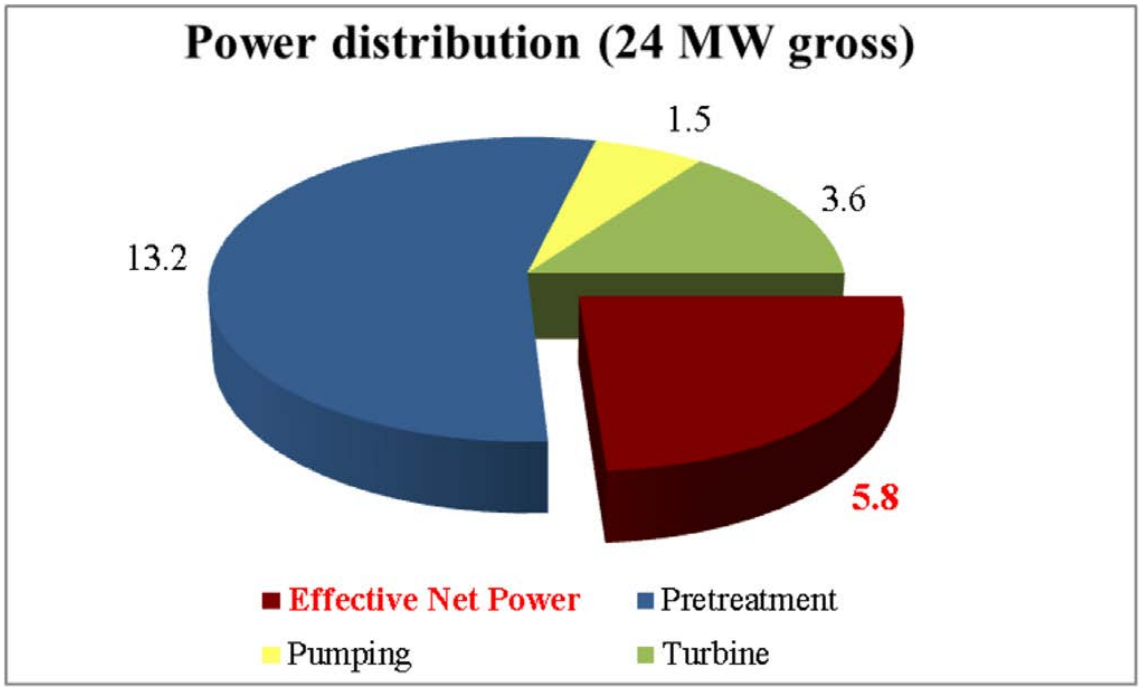

Figure 21: Estimation of the power distribution in parasitic loads [P1]

These results show the need for improvement in these energetic consumptions in order to make PRO more competitive.

10.2-Environmental impact

Due to the lack of direct experience, PRO (and SGE in general) effects on the environment on a large scale can only be inferred from desalination plants. The general damaging effects expected from a river-to-sea SGE power plant are land modification, release of pollutants and disruptions to the habitats of living species [102]. The three main areas to monitor are the influence of the infrastructure of the power plant, of the water intakes and of the effluent discharge [102].

Infrastructure placed in either the marine or fluvial environment undoubtedly creates new surfaces for microorganisms to grow in, as a sort of biofouling. Intake and discharge pipes are often subject to this, sometimes referred to as “artificial reefs”. Excessive growth can interfere with the normal balance between the rest of the local species, maybe even attracting invasive species [104].

Regarding the water intakes, as with desalination, PRO requires the intake of large volumes of sea water, plus similar volumes of fresh water from the river. There is a potential impact on aquatic organisms through impingement and entrainment [102]. The sea water volume intake is not deemed to be of importance, it is the availability of fresh water that is limited. Excessive fresh water intakes could cause severe environmental risks to most of the living organisms by disrupting the water circulation in the river. Álvarez-Silva et al. recommended not exceeding the

environmental flow limit, which should be below 30% of the river discharge, attending to seasonal variations [105].

In contrast, the matter of effluents is fortunately more advantageous. SWRO brine disposal is one of the most potentially environmentally disruptive aspects of the process, but SGE can never produce any stream with such a high salinity. In this area, PRO is deemed to be safer, although brackish effluents will still contain chemical residues from the pretreatment and membrane cleaning that need to be controlled, and possibly diluted [102]. River mouths present areas with different salinities. Effluents can be discharged into river areas with a similar salinity so as to minimize the impacts by changes in salinity. Salinity impacts on the marine environment are of lesser concern [105].

CONCLUSIONS

C1) A modified PRO model has been used to predict the electrical power obtainable from using fresh water and sea water. The modelling paid special attention to not overestimating the available local salinity gradient throughout the process. For this purpose, salinities and flowrates at intermediate points were estimated. Using a state-of-the-art membrane, results show that power densities can exceed 5 W/m^2 [P1], which is the rule of thumb for an economically worthwhile PRO process.

C2) On the basis of the potential gross power calculated through simulation, the net power for a hypothetical PRO power plant has been estimated after the consideration of several factors that reduce the gross power, such as the energy spent in water transport, the pretreatment processes of both water sources and the turbine inefficiency [P1].

C3) The effect of the water intake locations in PRO power plants fed with water from stratified river mouths has been analysed through a multidisciplinary study. For this, hydrodynamic models describing the river mouth salinity and temperature profiles have been used in combination with PRO process models. The conjoined model tool has been proven useful in describing the influence of the distance between intakes in the net power production of a hypothetical PRO process. This procedure has illustrated the need to compromise between the search for the highest salinity gradient available and the minimization of the intake distances [P2].

C4) As a case study, a possible osmotic power plant in the Colombian Magdalena river has been designed and evaluated for treating 30 m^3/s of river water. On-site data of salinity and temperature from the river and the adjacent Caribbean sea were gathered. These experimental data were used to estimate the net power, which was found to be comparable to a small hydropower plant. As the overall efficiency, using state-of-the-art processes, is rather low at about 24%, improvements have been proposed by means of sensitivity analyses. These have shown that a significant gain in the net electrical power production can be achieved if the technologies involved in the process are further developed [P1].Regarding the intake locations from which the power plant is to be fed; it has been demonstrated through this case study that determining these locations is very important: the analysis presented in this investigation shows a potential 14% increase in the net power productivity when optimal intake locations are selected [P2].

C5) Two different SWRO-PRO configurations have been studied to recover energy using brines from different stages in the desalination process. It has been shown that using the brine from the second stage of desalination as feed, together with the brine of the first stage as draw, gives the best overall performance. The addition of pre-treated seawater to the PRO feed has been considered, observing a small improvement in the local performance of the PRO process [P3].

ACKNOWLEDGEMENTS

The author wishes to acknowledge the help provided by the Spanish Ministry of Economy through the project DPI2014-54530-R and the predoctoral grant BES-2015-073871, by the Junta de Castilla y León and European Regional Development Fund, UIC 233, and by the Banco Santander Iberoamérica Research Grants program for international research stays.

REFERENCES

[1] https://www.sciencedirect.com/science/article/pii/S0360544220320508

[2] https://unfccc.int/process-and-meetings/the-paris-agreement/the-paris-agreement

[3] https://www.sciencedirect.com/science/article/pii/S095965262100247X

[4] https://www.mdpi.com/1996-1073/14/17/5396

[5] https://www.sciencedirect.com/science/article/pii/S0304380020300144

[6] https://www.sciencedirect.com/science/article/pii/S0011916420315198

[7] https://www.statista.com/statistics/267358/world-installed-power-capacity

[8] https://www.elsevier.com/books/sustainable-energy-from-salinity-gradients/cipollina/978-0-08-100312-1

[9] https://www.tandfonline.com/doi/full/10.1080/19438151003680850

[10] https://www.sciencedirect.com/science/article/pii/S1364032116002562

[11] https://www.sciencedirect.com/science/article/pii/S0011916498002227

[12] https://www.sciencedirect.com/science/article/pii/S0960148115302159

[13] https://www.sciencedirect.com/science/article/pii/S0360544217303602

[14] https://www.sciencedirect.com/science/article/pii/S0011916416320549

[15] https://www.tandfonline.com/doi/abs/10.5004/dwt.2009.924

[16] https://www.sciencedirect.com/science/article/pii/S0011916420313771

[17] https://www.sciencedirect.com/science/article/pii/S001191641731977X

[18] https://www.sciencedirect.com/science/article/pii/S0011916407006467

[19] https://www.sciencedirect.com/science/article/pii/S0376738816301405

[20] https://www.sciencedirect.com/science/article/pii/S0376738806007575

[21] https://pubs.acs.org/doi/abs/10.1021/es5029316

[22] https://doi.org/10.2112/JCOASTRES-D-17-00144.1

[23] https://pubs.acs.org/doi/abs/10.1021/ez500239n

[24] https://www.nature.com/articles/174660a0

[25] https://www.science.org/doi/10.1126/science.186.4161.350

[26] https://www.science.org/doi/10.1126/science.189.4203.654

[27] https://www.sciencedirect.com/science/article/pii/S037673880083313X

[28] https://www.sciencedirect.com/science/article/pii/S0376738800821833

[29] https://www.statkraft.com/newsroom/news-and-stories/archive/2013/Statkraft-halts-osmotic-power-investments/

[30] https://www.sciencedirect.com/science/article/pii/S0011916410004091

[31] https://www.sciencedirect.com/science/article/pii/S0011916412004213

[32] https://www.mdpi.com/2073-4441/10/1/48

[33] https://www.sciencedirect.com/science/article/pii/S037673881100737X

[34] https://pubs.acs.org/doi/10.1021/acs.iecr.8b03392

[35] https://pubs.acs.org/doi/abs/10.1021/es503790k

[36] https://www.sciencedirect.com/science/article/pii/S2214714421000374

[37] https://pubs.acs.org/doi/abs/10.1021/es203197e

[38] https://redstack.nl/projecten/proefinstallatie-op-de-afsluitdijk/

[39] https://www.sciencedirect.com/science/article/pii/S0011916415001903

[40] https://www.sciencedirect.com/science/article/pii/S0011916401001217

[41] https://pubs.acs.org/doi/abs/10.1021/es300060m

[42] https://link.springer.com/article/10.1007/BF02816331

[43] https://onlinelibrary.wiley.com/doi/10.1002/app.1980.070250301

[44] https://www.sciencedirect.com/science/article/pii/B9781782421214000174

[45] https://www.sciencedirect.com/science/article/pii/S0048969718349167l

[46] https://www.sciencedirect.com/science/article/pii/S0376738806003838

[47] https://www.sciencedirect.com/science/article/pii/S2214714419303551

[48] https://www.sciencedirect.com/science/article/pii/S037673881300495X

[49] https://www.sciencedirect.com/science/article/pii/S001191641731189X

[50] https://www.sciencedirect.com/science/article/pii/S0376738819311391

[51] https://www.sciencedirect.com/science/article/pii/S0376738815302702

[52] https://www.sciencedirect.com/science/article/pii/S1383586617314284

[53] https://www.sciencedirect.com/science/article/pii/S0048969718349167

[54] https://www.sciencedirect.com/science/article/pii/S0376738815001398

[55] https://www.tandfonline.com/doi/abs/10.1080/19443994.2012.672170

[56] https://www.sciencedirect.com/science/article/pii/S004313542031201X

[57] https://www.sciencedirect.com/science/article/pii/S2214714421000374

[58] https://www.sciencedirect.com/science/article/pii/S0011916416300108

[59] https://www.sciencedirect.com/science/article/pii/S0376738815303859

[60] https://www.sciencedirect.com/science/article/pii/S0079670017300102

[61] https://link.springer.com/article/10.1007/s11242-011-9734-9

[62] https://www.mdpi.com/2073-4360/5/1/303

[63] https://pubs.acs.org/doi/full/10.1021/es104325z

[64] https://www.sciencedirect.com/science/article/pii/S0376738818301595

[65] https://www.sciencedirect.com/science/article/pii/S0376738809005134

[66] https://www.sciencedirect.com/science/article/pii/S0011916405006867

[67] https://www.sciencedirect.com/science/article/pii/S0079670015000519

[68] https://www.sciencedirect.com/science/article/pii/S0011916416300522

[69] https://www.sciencedirect.com/science/article/pii/S0011916416300844

[70] https://www.sciencedirect.com/science/article/pii/S0011916415300904

[71] https://pubs.acs.org/doi/10.1021/es3002597

[72] https://www.sciencedirect.com/science/article/pii/S0376738800820888

[73] https://pubs.acs.org/doi/abs/10.1021/es104325z

[74] https://www.sciencedirect.com/science/article/pii/S0011916415001034

[75] https://www.tandfonline.com/doi/abs/10.1080/19443994.2015.1039600

[76] https://www.sciencedirect.com/science/article/pii/S0011916415300588

[77] https://www.sciencedirect.com/science/article/pii/S0376738815302702

[78] https://www.sciencedirect.com/science/article/pii/S0376738815302702

[79] https://www.sciencedirect.com/science/article/pii/S0043135413007604

[80] https://www.sciencedirect.com/science/article/pii/S0079670015000519

[81] https://www.sciencedirect.com/science/article/pii/S0376738807008149

[82] https://www.sciencedirect.com/science/article/pii/S0045653520315216

[83] https://www.sciencedirect.com/science/article/pii/S0376738817317817

[84] https://www.sciencedirect.com/science/article/pii/S0376738818316326

[85] https://www.sciencedirect.com/science/article/pii/S0011916416300108

[86] https://www.sciencedirect.com/science/article/pii/S0376738812007892

[87] https://www.sciencedirect.com/science/article/pii/S0376738811002857

[88] https://pubs.acs.org/doi/abs/10.1021/es403207m

[89] https://www.sciencedirect.com/science/article/pii/S0043135415302736

[90] https://www.sciencedirect.com/science/article/pii/S0011916420313229

[91] https://www.sciencedirect.com/science/article/pii/S0376738815303355

[92] https://www.sciencedirect.com/science/article/pii/S0011916414004925

[93] https://fiizk.com/en/product/membrane-filtration-technology/

[94] https://www.sciencedirect.com/science/article/pii/B9780128134832000022

[95] https://www.sciencedirect.com/science/article/pii/S004313541400284X

[96] https://www.astm.org/d4189-07r14.html

[97] https://www.sciencedirect.com/science/article/pii/S0011916416300091

[98] https://www.sciencedirect.com/science/article/pii/S0960148114006363

[99] https://www.sciencedirect.com/science/article/pii/S0011916406012677

[100] https://www.sciencedirect.com/science/article/pii/S0011916416300091

[101] https://www.sciencedirect.com/science/article/pii/S0360544218309551

[102] https://www.sciencedirect.com/science/article/pii/S1364032118307986

[103] https://www.sciencedirect.com/science/article/pii/B9780081003121000109

[104] https://besjournals.onlinelibrary.wiley.com/doi/10.1111/j.1365-2664.2009.01697.x

[105] https://www.sciencedirect.com/science/article/pii/S1364032116002562

ANNEX: PUBLICATIONS

[P1] **Salamanca, J.M.**; Álvarez-Silva, O.; Tadeo, F. Potential and analysis of an osmotic power plant in the Magdalena River using experimental field-data. *Energy* 2019, 180, 548–555 https://doi.org/10.1016/j.energy.2019.05.048

[P2] **Salamanca, J.M.**; Álvarez-Silva, O.; Higgins, A.; Tadeo, F. Analysis of the Intake Locations of Salinity Gradient Plants Using Hydrodynamic and Membrane Models. *Water* 2021, 13, 11-33. https://doi.org/10.3390/w13091133

[P3] Touati, K.; **Salamanca, J.M.**; Tadeo, F.; Elfil, H. Energy recovery from two-stage SWRO plant using PRO without external freshwater feed stream: Theoretical analysis. *Renewable Energy* 2017, 105, 84-95 https://doi.org/10.1016/j.renene.2016.12.030.

RESUMEN EN CASTELLANO

Objetivos:

O1) Desarrollar modelos matemáticos para la simulación de procesos de Ósmosis Retardada por Presión (PRO), con énfasis en el gradiente de salinidad, a fin de reproducirlos con mayor precisión.

O2) Utilizar los valores reales de las salinidades para determinar la potencia eléctrica alcanzable y evaluar la eficiencia real, teniendo en cuenta las demandas energéticas inherentes al proceso.

O3) Proporcionar un análisis de sensibilidad de algunas variables del proceso PRO y predecir los consiguientes cambios en la potencia neta.

O4) Estudiar la viabilidad de las desembocaduras estratificadas de ríos, centrándose en la ubicación de las tomas de agua. Evaluar las potencias mediante modelos hidrodinámicos, que describirán las variaciones a lo largo de la desembocadura del río, y buscar un conjunto óptimo de puntos de captación para maximizar la potencia neta.

O5) Evaluar la recuperación de energía osmótica a partir de sales de salmueras de desalación, y estudiar posibles configuraciones del proceso, comparando su rendimiento.

Metodología:

M1) Revisión del estado del arte: Inicialmente se realizó una extensa búsqueda y análisis de investigaciones recientes sobre el tema. Se centró intensamente en publicaciones recientes en revistas científicas relevantes, aunque también se revisaron comunicaciones de congresos, tesis y otros trabajos relacionados con el tema en cuestión. Esta tarea también se realizó durante toda la investigación, actualizando y ampliando periódicamente la información al estado actual.

M2) Fijar objetivos: De acuerdo con la revisión del estado del arte y la experiencia previa del grupo de investigación, se establecieron varios objetivos para las investigaciones.

M3) Métodos de Investigación: Análisis de un caso de estudio experimental: Se eligió como caso de estudio la desembocadura del río Magdalena. Los datos experimentales fueron recolectados y disponibles a través de la colaboración con el grupo de investigación OA Silva en la Universidad del Norte (Colombia). Los resultados se presentan en [P1], [P2]. Adaptación de modelos matemáticos PRO: de acuerdo con las investigaciones revisadas, se eligió un modelo matemático y se adaptó a las especificidades de la investigación, como se presenta en [P1]. Propuesta de diseño y simulación de centrales PRO: Se utilizaron datos del río Magdalena y modelos matemáticos para dimensionar una hipotética central PRO y determinar su producción de energía. En esta tarea se utilizó el software informático Matlab® [P1]. También se estudiaron las posibilidades de integración de PRO en la desalinización de agua de mar [P3]. Análisis de sensibilidad: se estudió la influencia de la variación de varios parámetros del proceso, con el fin de extraer más información y sacar conclusiones sobre PRO, [P1], [P2].

M4) Difusión de resultados: los resultados de la investigación se presentaron en revistas científicas de alto impacto, congresos y mediante la cooperación con otros grupos de investigación. Compartir y discutir los resultados obtuvo valiosos aportes externos que ayudaron a enriquecer y mejorar la investigación.

Conclusiones:

C1) Se ha utilizado un modelo PRO modificado para predecir la potencia eléctrica que se puede obtener utilizando agua dulce y agua de mar. Se prestó especial atención a no sobrestimar el gradiente de salinidad, usando salinidades y caudales en puntos intermedios. Utilizando una membrana de última generación, los resultados muestran que las densidades de potencia pueden superar los 5 W/m^2 [P1], que es la regla general para un proceso económicamente viable.

C2) A partir de la potencia bruta potencial calculada mediante simulación, se ha estimado la potencia neta para una hipotética central PRO tras considerar varios factores que reducen la potencia bruta, como la energía gastada en el transporte de agua, los procesos de pretratamiento tanto de las fuentes de agua como de la ineficiencia de la turbina [P1].

C3) Mediante un estudio multidisciplinar se ha analizado el efecto de la localización de tomas de agua en desembocaduras de ríos estratificados. Para ello, se han utilizado modelos hidrodinámicos que describen los perfiles de salinidad y temperatura de la desembocadura del río en combinación con modelos de proceso PRO. Se ha demostrado que esto permite evaluar la influencia de la distancia. Este procedimiento ha ilustrado la necesidad de llegar a un compromiso entre la búsqueda del mayor gradiente de salinidad disponible y la minimización de las distancias de toma [P2].

C4) Como caso de estudio se ha diseñado y evaluado una posible central osmótica en el río Magdalena para tratar 30 m^3/s de agua de río. Se recopilaron datos in situ de salinidad y temperatura del río y del mar Caribe adyacente. Estos datos experimentales se utilizaron para estimar la potencia neta, que resultó ser comparable a una pequeña central hidroeléctrica. Dado que la eficiencia general resultó baja con la tecnología actual, alrededor del 24 %, se han propuesto mejoras mediante análisis de sensibilidad. Se ha demostrado que se puede lograr una ganancia significativa en la producción neta de energía eléctrica desarrollando las tecnologías involucradas en el proceso [P1]. Además, se ha demostrado un aumento potencial del 14 % en la productividad de energía neta cuando se seleccionan las ubicaciones de toma óptimas en este caso de estudio [P2].

C5) Se han estudiado dos configuraciones diferentes de SWRO-PRO para recuperar energía utilizando salmueras de diferentes etapas del proceso de desalinización. Se ha demostrado que el uso de la salmuera de la segunda etapa de desalinización como alimentación, junto con la salmuera de la primera etapa como extracción, proporciona el mejor rendimiento general. Además, se ha evaluado el uso de agua de mar pretratada con la alimentación PRO, observándose una mejora en el rendimiento [P3].

Resultados:

[P1] **Salamanca, J.M.**; Álvarez-Silva, O.; Tadeo, F. Potential and analysis of an osmotic power plant in the Magdalena River using experimental field-data. *Energy* 2019, 180, 548–555 https://doi.org/10.1016/j.energy.2019.05.048

[P2] **Salamanca, J.M.**; Álvarez-Silva, O.; Higgins, A.; Tadeo, F. Analysis of the Intake Locations of Salinity Gradient Plants Using Hydrodynamic and Membrane Models. *Water* 2021, *13*, 11-33. https://doi.org/10.3390/w13091133

[P3] Touati, K.; **Salamanca, J.M.**; Tadeo, F.; Elfil, H. Energy recovery from two-stage SWRO plant using PRO without external freshwater feed stream: Theoretical analysis. *Renewable Energy* 2017, 105, 84-95
https://doi.org/10.1016/j.renene.2016.12.030.

Energy 180 (2019) 548–555

Contents lists available at ScienceDirect

Energy

journal homepage: www.elsevier.com/locate/energy

Potential and analysis of an osmotic power plant in the Magdalena River using experimental field-data

Jacobo M. Salamanca [a, *], Oscar Álvarez-Silva [b], Fernando Tadeo [c]

[a] Department of Systems Engineering and Automation, University of Valladolid, Valladolid, Spain
[b] Department of Physics and Geosciences, Universidad Del Norte, Barranquilla, Colombia
[c] Institute of Sustainable Processes, University of Valladolid, Valladolid, Spain

ARTICLE INFO

Article history:
Received 1 December 2018
Received in revised form
9 April 2019
Accepted 6 May 2019
Available online 7 May 2019

Keywords:
Osmotic energy
Pressure retarded osmosis
River mouths
Renewable energies
Membrane processes

ABSTRACT

The Magdalena River mouth in Colombia is studied as a candidate site for a renewable power plant via osmotic energy technology, using pressure retarded osmosis. This power generation plant would operate through the controlled mix of two flows with different salinities (river water and seawater in this case study). A preliminary design of a pressure retarded osmosis power plant is proposed here by means of experimental data acquisition on-site at the river mouth. The obtained net power production is shown to reach 6 MW, with adequate membrane power densities above 5 W/m^2. These promising results consider energetic losses involved in the process, which have been further analysed to propose improvement targets in pretreatment processes and membrane permeability.

© 2019 Elsevier Ltd. All rights reserved.

1. Introduction

Increasing global population and energy demands in its current trend will inevitably result in global warming and depletion of natural resources [1]. The anthropogenic origin of this global warming and its consequential forthcoming climate change needs to be acknowledged and mitigated [2]. In this context, research for renewable energy techniques is of the utmost importance for a sustainable future [3], in order to reduce the dependency on fossil fuels as the major energy source [4].

Water resources and its availability and uses are slowly becoming a critical issue as well, and are deeply connected to the energy sector [5]. Both water and clean energy are involved in salinity gradient energy (SGE) processes. This relatively new group of technologies (also known as osmotic processes, osmotic energy, blue energy) address the possibility of producing renewable electrical energy through the controlled mix of two water streams with different osmotic pressures, that is, mainly but not only, different salt contents. The availability of two streams with a high salinity gradient across them is found naturally at river mouths [6], though it can appear in other environments, such as hypersaline systems, in which bodies of water with high salinity (e.g. the Dead Sea) are involved [7]. Another natural system gaining scientific attention more recently are geothermal wells. A project combining osmotic and geothermal power is in development in Denmark [8]. Some industrial processes offer this possibility as well, especially in the desalination industry, due to the production of brines as residue, which could instead be regarded as a by-product [9]. This approach could also be extended to other industry sectors if other residual water streams were to be considered, such as treated sewage water [10].

Salinity gradient energy technology has shown much growth since Pattle's approach in 1954 [11], when the idea of the untapped potential of salinity gradients was first considered, although it did not receive much attention until years later. Economic instability and the increase of oil prices drove the scientific community to search for alternative energy sources [12]. In 1974 Loeb presented pressure retarded osmosis (PRO) [13]. Pressure retarded osmosis is a membrane process in which a low salinity water stream (feed) and a pressurized high salinity stream (draw) are made to interact through a semipermeable membrane. Water is selectively allowed to flow from the feed side through the membrane towards the draw side. This results in an increment of the amount of pressurized water, which can be used afterwards in a turbine to produce

* Corresponding author
E-mail addresses: jmsalamanca@autom.uva.es (J.M. Salamanca), oalvarezs@uninorte.edu.co (O. Álvarez-Silva), fernando.tadeo@uva.es (F. Tadeo).

https://doi.org/10.1016/j.energy.2019.05.048
0360-5442/© 2019 Elsevier Ltd. All rights reserved.

electricity.

This paper concentrates on PRO [14], but it is not the only technology that aims to exploit salinity gradients. Reverse electrodialysis (RED) is receiving similar attention. RED is also a membrane process, on which two types of membranes (anion exchange and cation exchange membranes) are placed alternatively forming a stack, with both feed and draw streams flowing in between. This configuration creates a difference of potential over the two types of membranes, which can be connected to provide electricity [15]. It is worth noting that the electrical energy extracted is done directly, whereas PRO needs a converter (e.g. turbine). A third group of technologies is capacitive mixing. This does not employ membranes, but electrodes instead, which are immersed alternatively in the ionic feed and draw solutions following a charge-discharge cycle, which is thermodynamically similar to a heat engine [16].

Real plants have been built using the two main SGE technologies, PRO and RED. In 2009, the first osmotic power plant was started up in Norway by Statkraft, using PRO, followed by the Netherlands' Redstack plant and Japan's MegaTon Water System project [17].

One of the biggest challenges of PRO (and in RED too) is the membrane performance. It is commonly agreed, since the startup and shutdown of the Statkraft power plant, that for a PRO plant to be profitable, the membrane should present a power density above 5 W/m^2 [18]. A lot of effort is being made in that direction: Wan et al. developed membranes with one of the highest power densities [19], Nagy et al. modelled fouling mechanisms and the effects on PRO [20], Long et al. gave indications about energetically optimal operation strategies [21]. Control strategies have also been proposed [22], as well as different process configurations [23], even integration with other processes, such as desalination [9,17]. Taking into account these achievements and the expected solution to the current challenges, PRO is deemed to be a viable option [14] to exploit SGE at the location presented in this research.

Aside from the technical limitations and how to face or mitigate them, it is important to analyse where these technologies could be implemented. If the worldwide riverflow discharge into the oceans is summed up and considered, there is a theoretical potential above 1 TW to be harnessed. However, this global quantification and how to decide whether an actual site is feasible or not, is a matter of disagreement among experts [24]. From a purely energetic point of view, the actual extractable energy will always be considerably smaller than the theoretical potential for all natural systems, due to the inevitability of energy consumption and losses intrinsic to any SGE generation process. The most significant energetic costs are the transportation of the water streams towards the power plant, the water pretreatment to prevent or reduce membrane deterioration and the inefficiencies of the energy conversion system (turbine inefficiencies).

Few investigations have been conducted regarding actual systems and considering their own unique characteristics. Ortega et al. analysed studied the suitability of a Colombian river [25], Sharma et al. evaluated the potential of power production in an estuary in India [26], and in Turkey other evaluations have been performed [27,28]. Experimental data gathering at a real site would provide salinity and temperature data, including their temporal variability, necessary for determining the available salinity gradient and to estimate more accurately the operating pressure, which is one of the most important process variables, and it is key to sizing plant equipment and the behaviour of other variables. More accurate simulations could be performed as well, providing better estimations of the extractable energy and aiding to determine the membrane surface area required to treat a given riverwater stream. Surface area often takes a considerable portion of the economic costs, so it is critical for feasibility [29].

It is also important to have information about the possible impact on the ecosystem [30], the actual water quality, and proximity to the demanding population (connectivity to the electricity grid). Water quality information would provide indications about the potential pretreatments required.

This study is focused on the natural system formed at the Magdalena river mouth in the Caribbean Sea, to evaluate its potential for electrical production via salinity gradient technology, specifically considering pressure retarded osmosis (PRO). Experimental on-site data have been acquired and proved to be useful in the proposal of a preliminary PRO plant design. A realistic approach for power production calculations is considered, taking into account the decrease of the gradient in a continuous flow operation and giving estimations of energetic costs linked to the process.

2. Materials and methods

This section describes the location for the proposed PRO plant and the acquisition of the experimental data. Afterwards, a review of PRO models is presented, in order to establish the calculation procedure to estimate the power production.

2.1. Case study

The Magdalena River mouth (Colombia) presents a very promising chance for SGE production due to its unique morphology, which allows the availability of sea and river water within a short distance. The final stretch of the river before reaching the Caribbean Sea was artificially narrowed in the 1930s in one of the biggest public engineering works of the country. The canalization was built in order to reduce the flux area to cause a rise in the water velocity and enhance the navigability of the Magdalena River. This resulted in the current configuration where the river and sea are separated in the east margin of the river course by a 6 km jetty of only a few meters wide. Fig. 1 shows that the river plume formed in the sea does not interfere with the seawater intake area (white circle). This behaviour is constant throughout the year.

An important feature of the Caribbean Sea is that it is a semi-enclosed sea in a tropical region; these circumstances make it both saltier and warmer than average worldwide ocean water. These characteristics are advantageous to any PRO process [31,32].

2.2. Experimental data

Temperature and salinity data were gathered every 30 min in both river and sea using the conductivity and temperature sensors and loggers described in Ref. [33]. The riverside and seaside sensors present a maximum measurement error of 3% and 5% respectively.

The measurement sites where the sensors were located are shown in Fig. 1. The seaside sensor was placed a few meters away from land. The riverside sensor was placed in a signalling buoy of the navigation channel of the Magdalena river port at 5 m deep, approximately in the middle of the waterflow channel. In order to select representative locations for the deployment of the sensors, preliminary temperature and salinity profiles were measured parallel to the western jetty in both river and sea sides. These measurements showed that the salinity of the river increases closer to the ocean, while the salinity of the sea decreases due to the proximity to the river mouth; therefore, the salinity gradient decreases. In the sector where the sensors were finally installed, the salinity of the river reduces to near zero and remains constant upstream. Thus, it can be assumed that the chosen locations are representative of the best possible conditions achievable on the river mouth.

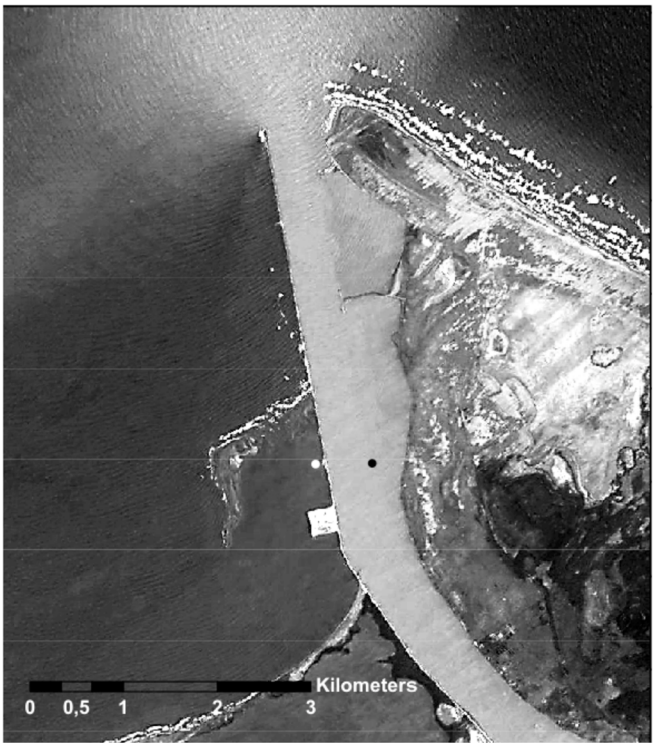

Fig. 1. Magdalena River mouth. Satellite image source: CNES/Astrium 18.03.2016, taken and modified from Google Earth. Black and white circles show the measurement sites in the river and sea sides, respectively.

2.3. Models for pressure retarded osmosis

Different models have been proposed, under different assumptions and different levels of detail. The aim is to determine the water permeation *Jw* and then the power density production *W*:

$$W = J_W \Delta P \tag{1}$$

All these models are based on the fact that water permeation across a semipermeable membrane (J_w) can be expressed in terms of the water permeability coefficient *A*, the transmembrane hydraulic pressure difference ΔP and the osmotic pressures of the feed and draw, π_F and π_D, ideally following the expression:

$$J_W = A(\pi_D - \pi_F - \Delta P) \tag{2}$$

Osmotic pressures are evaluated using Van't Hoff equation:

$$\pi = \beta_{vH} CRT \tag{3}$$

where β_{vH} is the Van't Hoff coefficient, which represents the number of ionic species on the solution coming from the dissociation of the original salt. β_{vH} is close to 2.0, since the majority of sea salt is sodium chloride. *C* depicts the molar concentration of the solution (mol/l), *R* is the universal gas constant and *T* the absolute temperature.

However, this ideal expression (Eq. (2)) is only an approximation because, in practice, membrane selectivity is not perfect: a salt flux always takes place in the opposite direction to the water permeation. This undesired salt flux reduces the effective salinity gradient across the membrane. Another deviation from ideal behaviour is caused by hydrodynamics near the membrane surface, usually presenting concentration polarization [34]. This detrimental phenomenon, in broad terms, consists of the accumulation of solute (feed side of the membrane) or depletion (draw side) near the physical interfaces. This concentration polarization is called external when the active layer of the membrane interface is affected, and internal when it happens on the membrane support layer. It causes a decrease in the actual effective transmembrane salinity gradient. More comprehensive modelling than Eq. (1) is required to include these phenomena in order to describe more realistically this. Thus, several models are now briefly described.

2.3.1. Lee model

The first model to include deviations from ideality due to concentration polarization was Lee's [35], which includes only the effect of internal concentration polarization for a flat sheet membrane:

$$J_W = A\left[\pi_{D,m}\frac{1-\frac{C_{F,b}}{C_{D,m}}\exp(J_W K)}{1+\frac{B}{J_W}\exp(J_W K-1)} - \Delta P\right] \tag{4}$$

where $C_{F,b}$ is the bulk salt concentration at the feed side, $C_{D,m}$ the salinity at the membrane-fluid interface on the draw side, *K* the solute resistivity and *B* the salt permeability of the membrane. From a practical point of view, it is difficult to know concentration values on the active layer ($C_{D,m}$). Moreover, it does not consider the influence of the salinity on the feed side.

2.3.2. Achilli model

Achilli et al. [36] added the effect of external concentration polarization, expressed through a mass transfer coefficient *k*, assumed to be the same on both sides of the membrane:

$$J_W = A\left[\pi_{D,b}\exp\left(-\frac{J_W}{k}\right)\frac{1-\frac{\pi_{F,b}}{\pi_{D,b}}\exp(J_W K)\exp\left(\frac{J_W}{k}\right)}{1+\frac{B}{J_W}\exp(J_W K-1)} - \Delta P\right] \tag{5}$$

This model does not require interfacial concentrations, only bulk osmotic pressures at feed and at draw sides (subindex *b*).

2.3.3. Other models

The contribution of other authors is also noteworthy, like Yip's model [37], similar to previous models, but extending them by implementing the effect of the reverse salt flux, Prante's [38] modification of Achilli's, or Sivertsen's adaptation for hollow fiber membranes [39].

2.3.4. Touati model

In this work, the following model was used because it considers all types of concentration polarization, the reverse salt flux and it describes the PRO process through a general mass transport model [31]:

$$J_W = A\left[\left(\pi_{D,b}+\frac{B}{A}\left(1+\frac{A\Delta P)}{J_W}\right)\right)\exp\left(-\frac{J_W}{k_D}\right) - \left[\pi_{F,b}+\frac{B}{A}\left(1+\frac{A\Delta P}{J_W}\right)\right]\exp(J_W K)\exp\left(\frac{J_W}{k_F}\right) - \Delta P\right] \tag{6}$$

where the mass transfer coefficients differentiated for feed side and draw are represented by k_F and k_D.

Salt permeation can be calculated as follows:

$$J_S = J_W \frac{B}{A\beta\ RT}\left(1+\frac{A\Delta P}{J_W}\right) \tag{7}$$

The equation for Jw (Eq. (6)) is implicit and non-linear, due to

the exponential terms that represent the concentration polarization that correct both osmotic pressures. At first sight, this equation is an adaptation of the ideal model (Eq. (2)). In Touati's model, each osmotic pressure is adjusted by the addition of a term and then multiplying by a gain, representing in a broader sense the effective or practical osmotic pressure on each side of the membrane. Due to the effect of the internal polarization only being present on the feed side (because that is where the actual water transport takes place), the overall osmotic gradient is more sensitive to feed concentration changes than in the draw. This behaviour has been experimentally observed [34] and is adequately represented by this model.

From a calculation point of view, this model is essentially an implicit equation, that must be resolved numerically for each group of three independent variables (the two concentrations and the pressure).

2.4. Simulation and power production calculation for designing a countercurrent flow pressure retarded osmosis process

Countercurrent flow configuration provides a more constant osmotic difference in all the membrane sections compared to a parallel flow system. Thus, the external pressure applied will be near optimal at every point.

In order to prevent an overestimation of the salinity gradients, the aforementioned mathematical model for water permeation in PRO must be used, taking care of two phenomena that happen in any continuous operation. The reverse salt flux is one of the reasons why the effective transmembrane gradient diminishes, the other being the draw dilution. The former increases the salt concentration on the feed side, while the latter decreases the draw salinity, as it can be seen on the schematic in Fig. 2. Both previous undesired effects must be taken into account when simulating the process. Any calculation procedure must consider those concentration variations along the membrane.

In this work, this issue is approached dividing the membrane into different sections (for simplicity, three sections of the same length are considered). A countercurrent flow configuration is selected to maintain a more constant transmembrane salinity gradient and to further exploit the water resources.

Mass balance equations for each section on each side of the membrane are needed in order to determine the intermediate concentrations, these being Q flowrates and C concentrations, subindex F for river feed, D for the draw sea stream, at membrane section i:

$$Q_F(i+1) = Q_F(i) - J_w(i)\cdot Area(i) \tag{8}$$

$$Q_D(i+1) = Q_D(i) + J_w(i)\cdot Area(i) \tag{9}$$

$$C_F(i+1) = [C_F(i)\cdot Q_F(i) + J_s(i)\cdot Area(i)]/Q_F(i+1) \tag{10}$$

$$C_D(i+1) = [C_D(i)\cdot Q_D(i) + J_s(i)\cdot Area(i)]/Q_D(i+1) \tag{11}$$

This countercurrent multiple stage configuration requires iterative calculations to solve its mathematical loop of equations (Eqs. (8)–(11)). The feed (river) and draw (sea) salt concentrations and flowrates serve as boundaries, while the internal intermediate concentrations and flows are updated on each iteration, till the overall mass balance is satisfied.

Once the mathematical system has been solved, it is possible to proceed with the design. One of the most decisive process variables is the external pressure applied to the draw current. It is known that the optimal pressure is approximately half the osmotic gradient between the two water sources at its inlets [14]. However, when considering the gradient variations along the membrane, this assumption is no longer valid. The optimal pressure now will take a different value, significantly smaller, which will have to take place in the range comprised by the osmotic gradients in both ends of the module, $(\pi_{draw} - \pi_{purge})/2$ and $(\pi_{brackish} - \pi_{feed})/2$ for a countercurrent design. A sensitivity analysis has been performed, varying the external pressure and observing its effect on some of the process variables, the power production among them. The optimal pressure determined with this procedure is used in a further analysis (see subsection 3.2.1). The power density in each section is also monitored, since it is highly recommended for it to be above 5 W/m^2 [18].

This general procedure has been applied to the case study. For simplicity, the river and sea intakes are set to 30 m^3/s, which keep the Magdalena River intake flowrate well above its minimum environmental limit of 420 m^3/s [24]. It has been reported [6] that using values of sea to river ratio slightly higher than one lead to higher theoretical potentials. However, higher pumping and pretreatment costs would be associated. In order to simplify, on this analysis the sea to feed ratio is kept at one. The plant sizing is chosen so power production is similar to small hydropower plants, common in Colombia [40,41].

The physical properties of the membrane are a critical aspect of PRO processes, mainly its salt and water permeabilities B and A, respectively. These permeabilities have been chosen according to experimental results provided by other authors [19]. Physical properties have been previously determined experimentally [34].

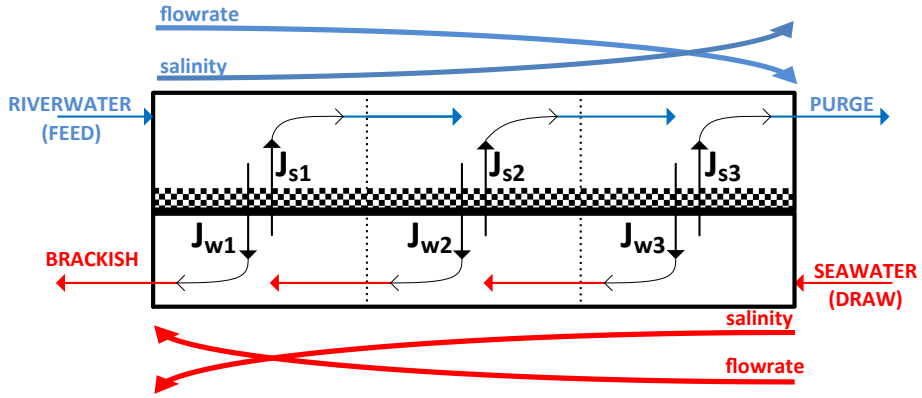

Fig. 2. Flow distribution on the system.

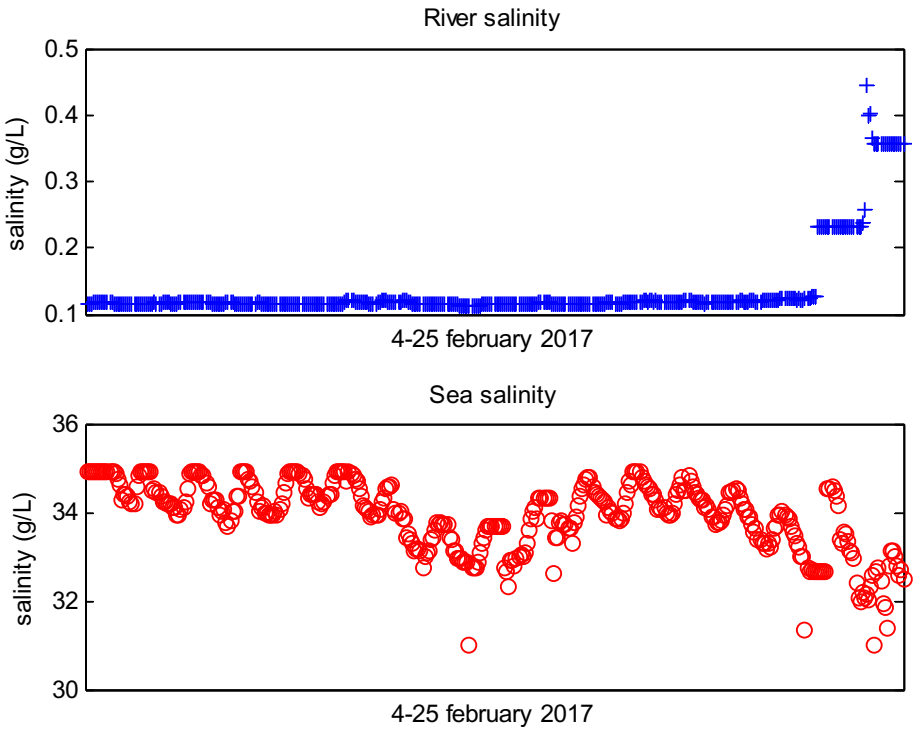

Fig. 3. Magdalena River and Caribbean Sea measured salinities for the selected period.

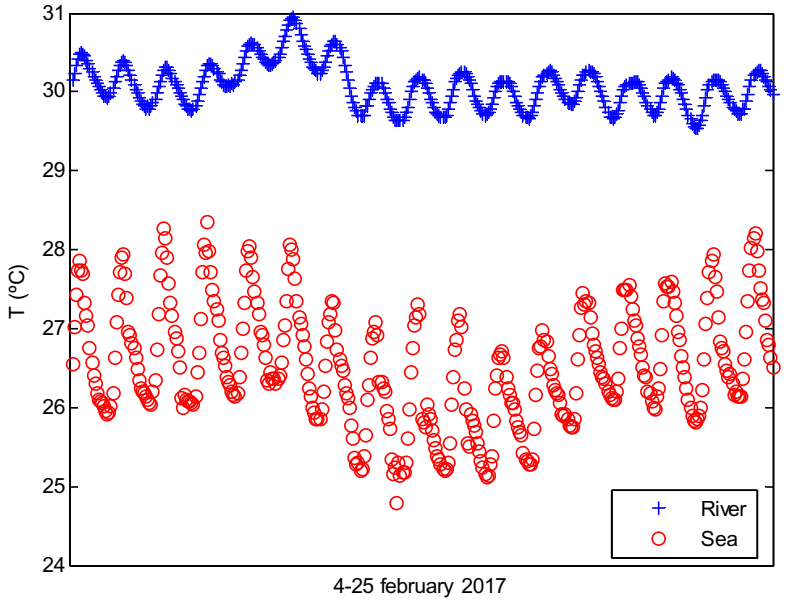

Fig. 4. Magdalena River and Caribbean Sea measured temperatures for the selected period.

2.5. Estimation of the potential net power production

The raw power production estimated for the case study is considerably diminished when deducting from it the pumping and pretreatment energetic costs and taking into account the turbine efficiency. Pumping costs, considering distances (200 m) and height differences (2 m) from the intake points, have been calculated following Darcy's law. Pretreatment costs and turbine efficiency are accounted following these works [42,43], microfiltration or ultrafiltration pretreatments are selected, since they demand much less energy than other conventional treatments, 0.2 MJ/m^3 vs 0.9 MJ/m^3, for both river and sea water.

3. Results and discussion

The experimental data and calculations derived from the previously described model show the following results.

3.1. Experimental field data

Salt concentration and temperature data gathered during the three-week registered period are presented on Figs. 3 and 4, respectively. Their variability has been shown, on both sides of the jetty. The magnitudes of both variables oscillate on a daily period, with the exception of the salinity at the riverside. The daily average of all variables remains moderately stable throughout the days. The salinity of the river is very low and only started to take higher values at the end of the registration period. This increase in the river salinity is due to the reduction of the river discharge during the dry season and the consequent salt wedge intrusion by seawater [8]. This seawater penetration in the channel, which varies throughout the yearly seasons, means that the river water intake should be placed either further inland or closer to the water surface at that time of the year. Further data collection is being performed at different river locations to solve this issue.

The average salinity is 0.21 g/l (river) and 33.7 g/l (sea) with maximum and minimum of 0.11 g/l and 0.46 g/l for the river, 30.1 g/l and 34.9 g/l, a standard deviation of 0.02 g/l and 0.66 g/l.

3.2. Simulation of the process in a countercurrent flow design

As discussed in 2.4, the mathematical model is simulated, carefully choosing the optimal external pressure, and followed by the preliminary design.

3.2.1. Determination of the optimal pressure

A central aspect for the design, analysis and operation of PRO plants is the selection of the external applied pressure ΔP. This pressure is the one that would lead to the maximum power production. Under several assumptions [18], it is half the osmotic pressure difference across the membrane. In practice, this optimal pressure is always less than half the osmotic gradient, because the gradient progressively diminishes as the process goes by (draw dilution, reverse salt flux towards the feed), as explained in subsection 2.4. Using the detailed models (Eqs (4)–(6)), it is difficult to determine this optimal pressure in an analytical manner, even when considering only three sections. Consequently, in this work, the optimal pressure was tracked through simulation of the model, following the idea presented in 2.4.

A sensitivity analysis on the influence of the external pressure has been performed, and its results are shown in Fig. 5. Here the focus is on the power production, although the purge stream characteristics are also shown, because they affect the analysis of the overall plant flows. The maximum simulated pressure is selected to be half the osmotic difference between the river and sea water at their inlets (which corresponds to an ideal one-stage PRO process), and then decreasing it until the maximum power production is found.

The results show that the optimal operating pressure for this configuration is 11.5 bar. Purge characteristics (flow rate and salinity) are shown for each pressure in Fig. 5. The purge salinity is a good indicator to predict the levels of fouling that would be present in a real process. It is shown that operating with slightly higher pressures than the optimal (up to 12 or 12.5) does not incur a big loss of power production, but can decrease significantly the purge salinity and avoid scaling of the membrane [44]. The purge flow rate varies inversely, increasing while the salinity decreases. In general, for better functioning of the process, it might be convenient to operate with higher purge flow rates, to avoid blockage, pumping issues, and having the purge drag impurities.

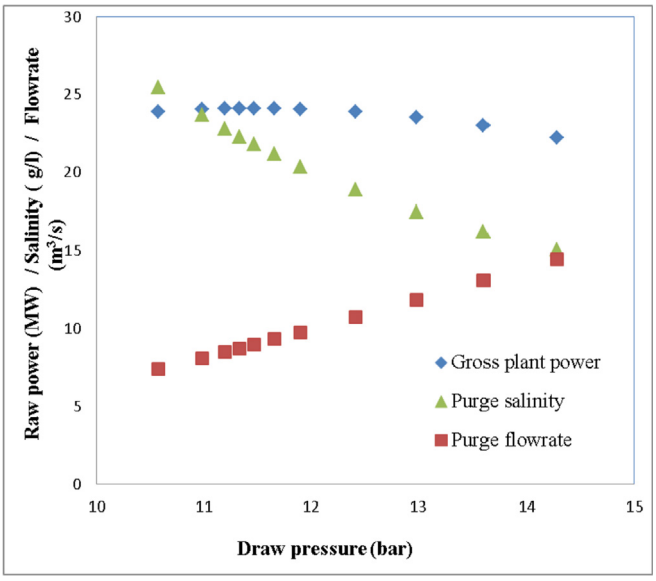

Fig. 5. Power production and purge characteristics dependance on the external pressure applied to the draw stream.

3.2.2. Simulation results and overall preliminary design

Once the optimal external pressure to be applied is determined, the strategy proposed in section 2.4 leads to the following results when introducing the experimental data. The schematic presented on Fig. 6 shows the flowrates and salinities corresponding to the optimal pressure, different for each section.

For a facility with the capacity to treat 30 m^3/s of river water, some of the parameters are listed below in Table 1:

3.3. Power capacity and process energetic costs

The total gross energy produced reaches 24 MW. Common turbine efficiency in energy recovery ratios is usually around 80%, though in some applications can reach up to 92% [45]. A conservative value of 80% has been taken for this work. To the resulting power produced from the turbine, other energetic costs must be deducted, their distribution is shown in Fig. 7. The advantageous geography of the river mouth is demonstrated when observing the transport costs required. Pumping costs would amount to only 6%, including both intakes and discharges. The process responsible for the biggest energetic consumption is the pretreatment.

3.4. Potential power production: analysis and improvement targets

Several more simulations have been performed and are presented in Fig. 8, focusing on how much the power production would increase if membranes with higher permeability and more energetically efficient pretreatment processes were to be used.

As shown before (Fig. 7), the pretreatments take the biggest share of the energy losses and it is here where most efforts should be made to improve the feasibility of the process. 25% lower pretreatment costs (from 0.22 to 0.16 MJ/m3) would lead to 50% higher power production, or almost three times more for a 75% pretreatment cost reduction.

A hypothetical membrane with double water permeability, A, would lead to values near double the original power production (from 5.7 to 9.9 MW). A simultaneous increase of 25% in both water and salt permeabilities would show very similar results, though in

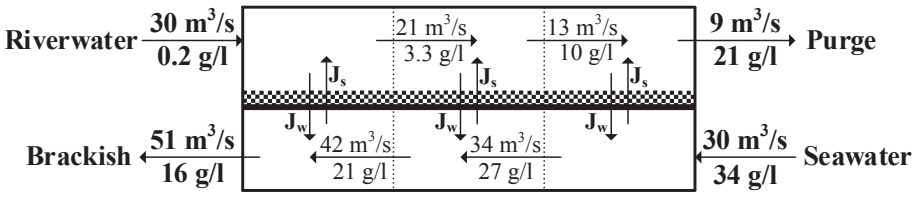

Fig. 6. Preliminary design results of the flowrates and salinities along the three sections of the membrane.

Table 1
Membrane parameters, operation variables and performance results.

Water permeability A	1.06×10^{-11} m³/m²·s·Pa
Salt permeability B	1.22×10^{-7} m³/m²·s
Hydraulic external pressure	11.47 bar
Average osmotic gradient	19.7 bar
Membrane area	5×10^{6} m²
Average power density	6.45 W/m²

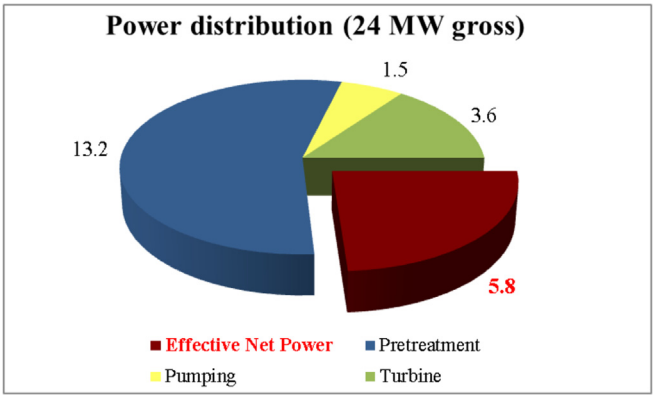

Fig. 7. Power distribution (MW).

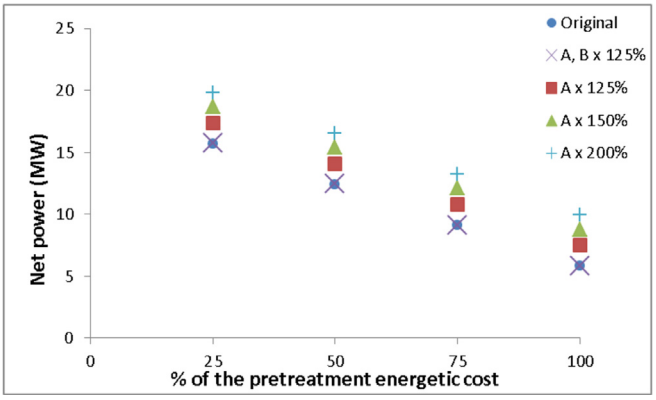

Fig. 8. Net power estimations for more efficient pretreatments and higher permeability membranes.

practice it would result in the reduction of the membrane area required. The combined situation, double permeability and 75% reduction on pretreatment would lead to a power production of more than triple, i.e. 19 MW.

3.5. Expected uncertainty

Due to the sensor measurement potential errors and the data variability, an uncertainty in the power capacity is to be expected. The design capacity of 5.8 MW could be reduced to 5.3 MW or increased to 6.3 MW (9% each) only considering the sensor errors, worst and best case scenario.

The work presented here has been carried out for average values of the experimental data for the gathering period. In order to take into account the influence of the variability of the data, simulations have been repeated for the maximum and minimum values of the salinities. The temperature variation was also considered, but it only showed negligible repercussions. The expected variation due to the salinity variability amounts to 4.66 MW (−20%) and 6.2 MW (7%) when the sea and river salinity reached minimum and maximum values respectively, and vice versa, that is, best and worst situation possible. Both effects combined would incur a variability of −24% and +17% in the power capacity.

It is important to notice the greater negative effect caused by higher river salinity than the positive one due to higher sea salinity, even though the sensor is more precise when measuring river water. This observation is to be expected, due to the non-linear nature of the model (as described in section 2.3), in which fresh water with higher salinity leads to a harder penalization in the resulting water flux, and consequently in the power density.

4. Conclusions

In this work, the potential development of an osmotic power plant in the Colombian Caribbean region is proposed. On-site data of both Magdalena River and Caribbean Sea have been acquired. The potential capacity for a power plant facility has been estimated by modelling and simulation of the process, with special focus on not overestimating the salinity gradients and getting a more practical sense of the hypothetical process performance. A state-of-the-art membrane has been used in the simulations, showing that power densities could surpass the limit of 5 W/m², which is commonly accepted as the minimal value for an economically feasible design. The net power potentially achievable for a power plant treating 30 m³/s amounts to almost 6 MW and fits within the range of small hydropower plants. The overall efficiency is low, 24%, due to the energetic costs associated to the process. Design indications and improvement targets have been given, showing that if a more energetically efficient pretreatment process and higher permeability membranes were available, the net electrical production could be more than three times higher.

Acknowledgements

The authors wish to acknowledge the help provided by the Spanish Ministry of Economy through the project DPI2014-54530-R and the predoctoral grant BES-2015-073871, by the Junta de Castilla y León and European Regional Development Fund, UIC 233, and by the Banco Santander Iberoamérica Research Grants program. Field data acquisition was funded by COLCIENCIAS -Department of Science, Technology and Innovation of Colombia- by the project: 121571451074, resolution 881 − 2015.

References

[1] Zidanšek A, Blinc R, Jeglič A, Kabashi S, Bkteshi S, Šlaus I. Climate changes, biofuels and the sustainable future. International Journal of Hydrogen 2009;34(No. 16):6980–3.
[2] Riti JS, Shu Y, Song D, Kamah M. The Contribution of energy use and financial development by source in climate change mitigation process: a global empirical perspective. J Clean Prod 2017;148:882–94.
[3] Akorede MF, Hizam H, Ab Kadir MZA, Aris I, Buba SD. Mitigating the anthropogenic global warming in the electric power industry. Renew Sustain Energy Rev 2012;16(No. 5):2747–61.
[4] Wang L, Wei Y-M, Brown MA. Global transition to low-carbon electricity: a bibliometric analysis. Appl Energy 2017;205:57–68.
[5] Wakeel M, Chen B, Hayat T, Alsaedi A, Ahmad B. Energy consumption for water use cycles in different countries: a review. Appl Energy 2016;178:868–85.
[6] Álvarez-Silva O, Winter C, Osorio AF. Salinity gradient energy at river mouths. Environ Sci Technol Lett 2014;1(10):410–5.
[7] Bajraktari, N., Hélix-Nielsen, C., Madsen, H.T., Pressure retarded osmosis from hypersaline sources – a review, Desalination, Vol. 413, pp 65-85, 2017
[8] Nissen, S.S., Clausen, J.M., (2015). Electricity Generation Process, US Patent US20180135604A1, retrieved from https://patents.google.com/patent/US20180135604A1/en.
[9] Touati K, Salamanca JM, Tadeo F, Elfil H. Energy recovery from two-stage SWRO plant using PRO without external freshwater feed stream: theoretical analysis. Renew Energy 2017;105:84–95.
[10] Saito K, Irie M, Zaitsu S, Sakai H, Hayashi H, Tanioka A. Power generation with salinity gradient by pressure retarded osmosis using concentrated brine from SWRO system and treated sewage as pure water. Desalination and Water Treatment 2012;41:114–21.
[11] Pattle RE. Production of electric power by mixing fresh and salt water in the hydroelectric pile. Nature 1954;174:660.
[12] Sørensen B. Energy and Resources, *Science* 1975;189:255–60.
[13] Loeb S. Osmotic power plants. Science 1975;189:654–5.
[14] Touati K, Tadeo F, Chae SH, Kim JH, Álvarez-Silva OA. Pressure retarded osmosis. Renewable energy generation and recovery. Academic Press; 2017.
[15] Mei Y, Tang CY. Recent Developments and future perspectives of reverse electrodialysis technology: a review. Desalination 2018;425:156–74.
[16] Rica RA, Ziano R, Salerno D, Mantegazza F, van Roji R, Brogioli D. Capacitive mixing for harvesting the free energy of solutions at different concentrations. Entropy 2014;15:1388–407.
[17] Kurihara M, Sakai H, Tanioka A, Tomioka H. Role of pressur-retarded osmosis (PRO) in the mega-ton wáter project. Desalination and Water Treatment 2016;57:26518–28.
[18] Helfer F, Lemckert C, Anissimov YG. Osmotic power with pressure retarded osmosis: theory, performance and trends – a review. J Membr Sci 2014;453:337–58.
[19] Wan, C.F., Yang, T., Gai, W., De Lee, Y., Chung, T.S., Thin-film composite hollow fiber membrane with inorganic salt additives for high mechanical strength and high power density for pressure retarded osmosis, J Membr Sci, Vol. 555, pp 388-387, 2018.
[20] Nagy E, Hegedüs I, Tow EW, Lienhard JH. Effect of fouling on performance of pressure retarded osmosis (PRO) and forward osmosis (FO). J Membr Sci 2018;565:450–62.
[21] Long R, Lai X, Liu Z, Liu W. Pressure retarded osmosis: operating in a compromise between power density and energy efficiency. Energy 2019;172:592–8.
[22] Maisonneuve J, Chintalacheruvu S. Increasing osmotic power and energy with maximum power point tracking. Appl Energy 2019;238:683–95.
[23] Soltani R, Struchtrup H. Modeling and simulation of the dual stage pressure retarded osmosis systems. Desalination 2019;460:28–40.
[24] Álvarez-Silva O, Osorio AF, Winter C. Practical global salinity gradient energy potential. Renew Sustain Energy Rev 2016;60:1387–95.
[25] Ortega S, Stenzel P, Alvarez-Silva O, Osorio AF. Site-specific potential analysis for pressure retarded osmosis (PRO) power plants: the León River example. Renew Energy 2014;68:466–74.
[26] Sharma M, Chakraborty A, Kuttippurath J. The potential of power production using salinity gradient at the Hooghly estuary system. In: International conference on 21st century energy needs – materials. Systems and Applications; 2016.
[27] Pasaoglu ME, Koyuncu I, Sengur-Tasdemir R, Guclu S, Turken T, Budeyri B, Baykan O, Daskiran F, Tezcan E. Applicability of pressure retarded osmosis power generation technology in Istanbul. Period Eng Nat Sci 2018;6:141–7.
[28] Saki S, Uzal N, Gökçek M, Ates N. Predicting potential of pressure retarded osmosis power for different estuaries in Turkey. Environ Prog Sustain Energy 2018. https://doi.org/10.1002/ep.13085.
[29] Chung HW, Swaminathan J, Banchik LD, Lienhard JH. Economic framework for net power density and levelized cost of electricity in pressure-retarded osmosis. Desalination 2018;448:13–20.
[30] Seyfried C, Palko H, Dubbs L. Potential local environmental impacts of salinity gradient energy: a review. Renew Sustain Energy Rev 2019;102:111–20.
[31] Touati K, Hänel C, Tadeo F, Schiestel T. Effect of the feed and draw solution temperatures on PRO performance: theoretical and experimental study. Desalination 2015;365:182–95.
[32] Touati, K., Tadeo, F., Hänel, C., Schiestel, T., Effect of the operating temperature on hydrodynamics and membrane parameters in pressure retarded osmosis, Desalination and Water Treatment, Vol. 23, pp 10477-10489, 2015.
[33] HOBO Salt Water Conductivity/Salinity Data Logger http://www.onsetcomp.com/products/data-loggers/u24-002-c. Last accessed February 6, 2019.
[34] Touati, K., Tadeo, F. (2016), Study of the reverse salt diffusion on pressure retarded osmosis: influence on concentration polarization and effect of the operating conditions, Desalination, Vol. 389, pp 171-186, 2016.
[35] Lee KL, Baker RW, Lonsdale HK. Membranes for power generation by pressure-retarded osmosis. J Membr Sci 1981;8:141–71.
[36] Achilli A, Tzahi YC, Childress AE. Power generation with pressure retarded osmosis: an experimental and theoretical investigation. J Membr Sci 2009;343:42–52.
[37] Yip NY, Tiraferri A, Phillip WA, Schiffman JD, Hoover LA, Chang Kim Y, Elimelech M. Thin-film composite pressure retarded osmosis membranes for sustainable power generation from salinity gradients. Environ Sci Technol 2011;45:4360–9.
[38] Prante JL, Ruskowitz JA, Childress AE, Achilli A. RO-PRO desalination: an integrated low-energy approach to seawater desalination. Appl Energy 2014;120:104–14.
[39] Sivertsen EH, Thelin TW, Brekke G. Modeling mass transport in hollow fiber membranes used for pressure retarded osmosis. J Membr Sci 2012;417–418:69–79.
[40] Duque EA, González JD, Restrepo JC. Developing sustainable infrastructure for small hydro power plants through clean development mechanisms in Colombia. Procedia Engineering 2016;145:224–33.
[41] Zapata S, Castaneda M, Garces E, Franco CJ, Dyner I. Assessing security of supply in a largely hydroelectricity-based system: the Colombian case. Energy 2018;156:444–57.
[42] O'Toole G, Jones L, Coutinho C, Hayes C, Napoles M, Achilli A. River-to-sea pressure retarded osmosis: resource utilization in a full-scale facility. Desalination 2016;389:39–51.
[43] Pearce GK. UF/MF pre-treatment to RO in seawater and wastewater reuse applications: a comparison of energy costs. Desalination 2008;222:66–73.
[44] Zhang M, Hou D, She Q, Tang CY. Gypsum scaling in pressure retarded osmosis: experiments, mechanisms and implications. Water Res 2014;48:387–95.
[45] Seme S, Sredensk K, Praunseis Z, Stumberger B, Hadziselimovic M. Optimal price of electricity of solar power plants and small hydro power plants – technical and economical part of investments. Energy 2018;157:87–95.

water

MDPI

Case Report

Analysis of the Intake Locations of Salinity Gradient Plants Using Hydrodynamic and Membrane Models

Jacobo M. Salamanca [1], Oscar Álvarez-Silva [2], Aldemar Higgins [2] and Fernando Tadeo [1,*]

[1] Institute of Sustainable Processes, University of Valladolid, 47002 Valladolid, Spain; jmsalamanca@autom.uva.es
[2] Department of Physics and Geosciences, Universidad del Norte, 081007 Barranquilla, Colombia; oalvarezs@uninorte.edu.co (O.Á.-S.); higginsa@uninorte.edu.co (A.H.)
* Correspondence: Fernando.Tadeo@uva.es

Abstract: The gain in net power produced by Salinity Gradient plants in river mouths due to the optimal location of water intakes is analysed in this paper. More precisely, this work focuses on stratified river mouths and the membrane-based technology of Pressure-Retarded Osmosis. A methodology for this analysis is proposed and then applied to a case study in Colombia. Temperature, salinity and water discharge data were gathered at the Magdalena river mouth to develop a hydrodynamic model that represents the salinity profile along the river channel. The net power production of a pressure-retarded osmosis plant is then estimated based on the power produced at membrane level, considering different locations for the saltwater and freshwater intakes. The most adequate locations for the intakes are then deduced by balancing higher power production (due to higher salinity differences between the water intakes) with lower pumping costs (due to shorter pumping distances from the intakes). For the case study analysed, a gain of 14% can be achieved by carefully selecting the water intakes.

Keywords: osmotic energy; pressure retarded osmosis; river mouths; renewable energies; estuarine dynamics

check for updates

Citation: Salamanca, J.M.; Álvarez-Silva, O.; Higgins, A.; Tadeo, F. Analysis of the Intake Locations of Salinity Gradient Plants Using Hydrodynamic and Membrane Models. *Water* **2021**, *13*, 1133. https://doi.org/10.3390/w13091133

Academic Editor: Alberto Figoli

Received: 26 February 2021
Accepted: 14 April 2021
Published: 21 April 2021

Publisher's Note: MDPI stays neutral with regard to jurisdictional claims in published maps and institutional affiliations.

Copyright: © 2021 by the authors. Licensee MDPI, Basel, Switzerland. This article is an open access article distributed under the terms and conditions of the Creative Commons Attribution (CC BY) license (https://creativecommons.org/licenses/by/4.0/).

1. Introduction

In the current context of global warming and increasing worldwide energy demands, the development of renewable energies is essential to reduce carbon emissions to the atmosphere. It is now generally accepted that sustainable and prosperous societies require a major use of clean energies [1,2]. Throughout the world, wind and solar energies are now being extensively implemented for power generation, but these renewable energies are limited by the inherent variability of wind and solar radiation, respectively [3]. Thus, there is a demand for controllable power sources that could complement wind and solar sources to ensure that renewable power is available when needed, and at reasonable costs [4].

This need is pushing the development of emerging renewable energy sources that would complement existing renewable energies [5]. One of these emerging energy sources is salinity gradient energy (SGE), also known as blue energy or osmotic energy [6]. SGE technologies are based on the exploitation of the chemical potential difference of water sources with different salinity. This potential energy is then transformed into electricity. In order to do this, several strategies are being developed. The most studied technologies are the reverse electrodialysis (RED), which uses a configuration similar to galvanic and fuel cells to generate electricity from the salinity gradient, and pressure-retarded osmosis (PRO), which pursues the conversion of the salinity gradient into hydraulic work, with the help of a semipermeable membrane [7]. A schematic of a generic PRO process is presented in Figure 1. One of the main advantages of these emerging technologies is that the power produced could be available throughout the day or the seasons, unlike solar and wind energy, which are time- and season-dependent.

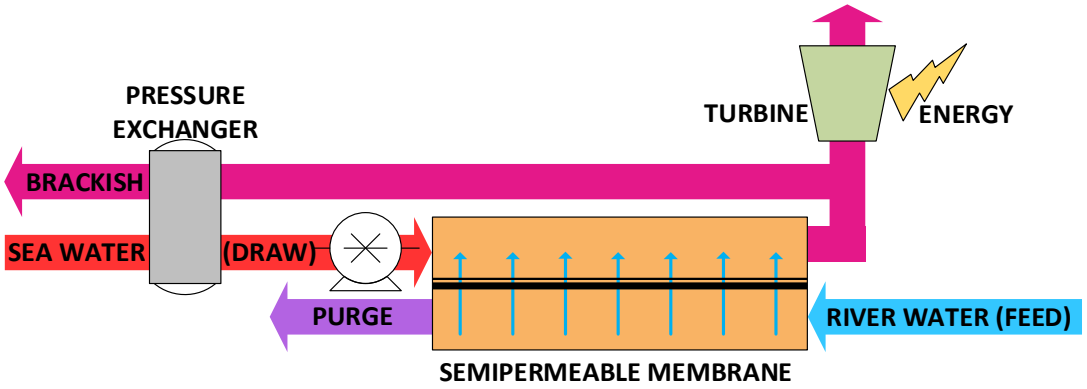

Figure 1. Block diagram of a standard PRO process.

In this context of Salinity Gradient Energy, river mouths are one of the main possibilities for exploiting this resource, since salinity gradients are found naturally at river mouths. However, not every river mouth is suitable for an SGE facility [8], as river water and seawater should be available at a short distance, in order to reduce water transport requirements and its associated costs. Thus, the best river mouths are stratified river mouths, in which there are significant salinity gradients in the vertical direction thanks to seawater intrusion close to the bottom in the estuarine zone. This intrusion generates a two-layered flow with different densities that remain unmixed in regions where the tidal range is small (less than 2 m). Therefore, if freshwater and saltwater intakes are placed in the area of highest stratification of the estuary, the freshwater could be extracted close to the surface while the seawater would be taken at a nearby coordinate, near the bottom of the river. This configuration significantly reduces the distance between both intake points and, consequently, the energy required for water transport towards the power plant. However, establishing the location in this zone of maximum stratification is not straightforward due to the inherent variability of the flows in the river mouth. It is at this point when a hydrodynamic model of the river mouth is useful to understand the salinity gradients and their temporal variability at specific river mouths [9,10].

A methodology is then developed to analyse the effect of intake locations in the power produced by Pressure-Retarded Osmosis in stratified river mouths. This methodology can then be used to select the intake locations that maximize net power. It is illustrated with a case study of the Magdalena river mouth in Colombia. This estuary is selected as it is in the top-ten river mouths with the highest SGE potential worldwide [8], it is also highly stratified and presents salt wedge intrusion into the river channel during low freshwater discharges and migration of the stratification towards the sea during high discharges [11]. Experimental data acquired at different locations and depths through the length of the river channel, combined with comprehensive information of river flow rates and climatic conditions, are then used to elaborate a detailed model able to estimate the salinity structure of the river mouth, following the proposed methodology. This model is then used to predict the salinity along the estuary, and, based on this, to assess the potential power production of a hypothetical PRO plant fed from different locations, in order to select the most adequate location for the intakes.

2. Methods

The methodology proposed to evaluate the optimum location of the water intakes to maximize the energy yield is given by the following steps.

2.1. Development of a Hydrodynamic Model of the River Mouth

In order to analyse the thermohaline field in the estuary, the numerical model MOHID 3D [12] can be employed. MOHID 3D solves the Navier–Stokes equations for incompressible fluids, assuming hydrostatic equilibrium and employing the Boussinesq and Reynolds

approaches [13]. In this model, the transport equations are discretized numerically using the finite volume method through the Arakawa-C stepped grid.

For the Magdalena River, a configuration nested on two levels was implemented. On the first level, the fluid was assumed to be barotropic, considering tidal forcing in the open boundary with the ocean, using data from the global tidal model FES2012 [14] and daily-averaged river discharges. Salinity at the ocean and river boundaries was assumed constant and equal to 37 g/kg and 0.1 g/kg, respectively. The calculation domain was represented by a regular rectangular mesh with $\Delta x = \Delta y = 160$ m covering a simulation domain of 851.35 km^2, including 22 km of river channel, as shown in Figure 2A and using a time step $\Delta t = 8$ s (see Table 1 for the list of symbols). A more detailed second mesh was nested. In this mesh, the fluid was treated as baroclinic, also using a regular rectangular mesh with $\Delta x = \Delta y = 80$ m and vertical discretization on 37 z-coordinate layers, covering the simulation domain of 390.76 km^2 shown in Figure 2B, and using a step $\Delta t = 4$ s. The boundary conditions of velocity, water level and salinity for the nested mesh are obtained from the results of the first general mesh. Wind forcing at the surface for both meshes was obtained from the Global Forecast System model (GFS) [15]. Winds were considered constant in space and variable in time with temporal resolution $\Delta t = 3$ h.

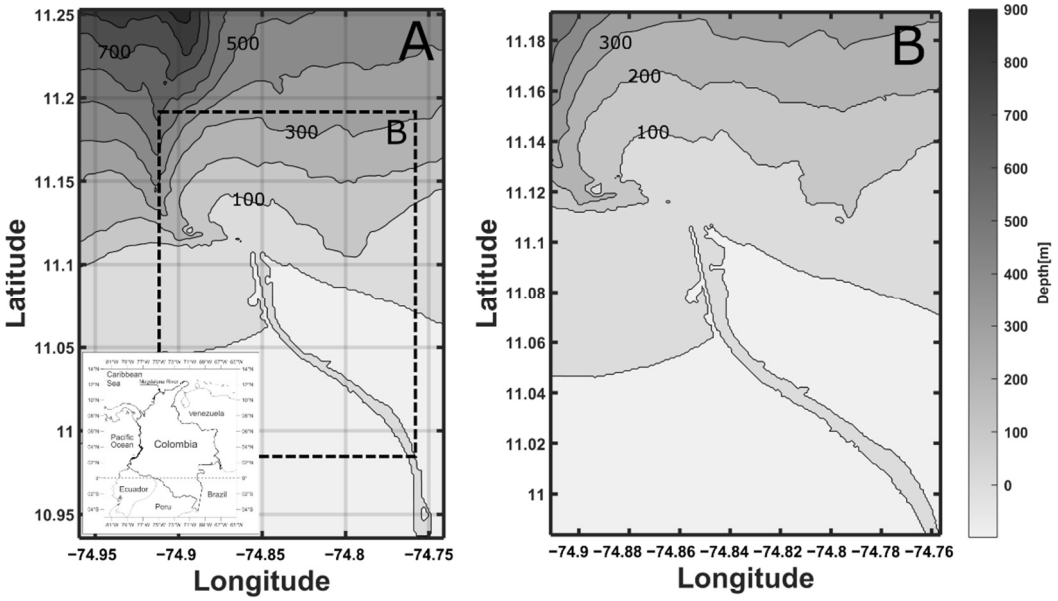

Figure 2. (**A**) Location of the study zone and domain of the first mesh of the model. The dashed square shows the simulation domain of the nested and more refined model. (**B**) Details of the covered area and bathymetry of the nested model.

Table 1. List of symbols.

Symbol	Variable	Units
A	Water permeability	m/s·Pa
B	Salt permeability	m/s
C_D	Salinity in draw stream	mol/m^3
C_F	Salinity in feed stream	mol/m^3
J_W	Transmembrane flow density	m/s
J_s	Transmembrane salt flow density	mol/m^2·s
K	Solute resistivity	s/m
k_D	Mass transfer coefficient (membrane draw side)	m/s
k_F	Mass transfer coefficient (membrane feed side)	m/s
R	Universal ideal gas constant	J/mol·K

Table 1. *Cont.*

Symbol	Variable	Units
T_D	Draw temperature	K
T_F	Feed temperature	K
W_{PRO}	Power density from pressure retarded osmosis	W/m^2
β_{vH}	van't Hoff coefficient	-
Δx	Hydrodynamic model mesh width	m
Δy	Hydrodynamic model mesh length	m
ΔP	Draw external pressure	Pa
Δt	Hydrodynamic model time step	s
π_D	Osmotic pressure of draw stream	Pa
π_F	Osmotic pressure of feed stream	Pa

Vertical turbulence followed the General Ocean Turbulent Model (GOTM) with a k-ε closure model and Canuto's stability function [16,17], whereas horizontal turbulence was described by Smagorinsky's parameterisation. The model was calibrated and validated comparing modelling results with field measurements during low and high freshwater discharges. Calibration and validation revealed an optimal performance of the model with a horizontal eddy viscosity of 8 m^2/s, a horizontal turbulent parameter of 0.4, a bottom roughness of 0.0025 m, and a wind drag coefficient of 0.001.

2.2. Evaluation of Power Consumed and Power Produced

For each possible combination of intake locations, it is necessary to evaluate the associated pumping requirements in terms of power, and the produced PRO power can be estimated based on the characteristics of the available flows. This is to be done as follows:

In a PRO process, freshwater (feed solution) and seawater (draw solution) are separated by a semi-permeable membrane that allows water flow from the feed side towards the draw side. This water flow (expressed per unit of surface) J_W multiplied by the transmembrane pressure gradient ΔP gives the power produced W_{PRO}

$$W_{PRO} = J_W \cdot \Delta P \tag{1}$$

In order to determine the water flux through the membrane, Touati's general mass transport model can be employed, as it considers the concentration polarization on both sides of the membrane, internal and external [18]. Regarding the membrane, this model assumes that the active layer is on the draw side, and that its porous support is isotropic. Local thermal equilibrium and negligible thermal dispersion are assumed as well. As for the hydrodynamic conditions, the flow regime is turbulent and the process isobaric. The necessary parameters to apply this model are the membrane water permeability A, the salt permeability B, the transfer coefficients on the feed side k_F and on the draw side k_D (taken from [18], assuming negligible variation with temperature and viscosity in the operating range of values and hydrodynamic conditions), the solute resistivity K, and the osmotic pressures on the feed and draw sides π_D and π_F, respectively (see Equations (4) and (5)). A and B are chosen according to recent research results [19], considering average values of those obtained under similar conditions to the ones in this research.

$$J_W = A\left[\left(\pi_D + \frac{B}{A}\left(1 + \frac{A\Delta P}{J_W}\right)\right)\cdot \exp\left(-\frac{J_W}{k_D}\right) - \left(\pi_F + \frac{B}{A}\left(1 + \frac{A\Delta P}{J_W}\right)\right)\exp(J_W \cdot K)\cdot \exp\left(\frac{J_W}{k_F}\right) - \Delta P\right] \tag{2}$$

The salt flux J_s can be calculated as follows:

$$J_s = J_W \frac{B}{A \cdot \beta_{vH} \cdot R \cdot T_D}\left(1 + \frac{A\Delta P}{J_W}\right) \tag{3}$$

Moreover, π_D and π_F are calculated through the van't Hoff equation (that is, ideal solutions are assumed):

$$\pi_F = \beta_{vH} \cdot C_F \cdot R \cdot T_F \quad (4)$$

$$\pi_D = \beta_{vH} \cdot C_D \cdot R \cdot T_D \quad (5)$$

where β_{vH} is the van't Hoff coefficient, which represents the number of ionic species in the solution dissociated from the original salt, β_{vH} is approximated to 2.0, since most of the sea salt is sodium chloride, C depicts the molar concentration of each flow (mol/L), R is the universal gas constant and T the absolute temperature.

Osmotic pressures are dependent on the salinity; however, the salinities, and therefore π_D and π_F, do not remain constant throughout the process, they vary along the membrane, because a mass exchange is taking place. To correct this situation, several stages are considered using concentrations at intermediate locations of the membrane, estimating these concentrations at each of these intervals of the membrane [20]. Since the process is configured in countercurrent flow, iterative calculations are required to solve a loop of equations. A simple algorithm summarises the procedure: firstly, initial concentrations are estimated, and with them the salinity gradients at individual intervals can be calculated. Secondly, Touati's model (Equation (2)) is applied to calculate J_W in each stage, followed by the solution of mass balances at each section, obtaining newly calculated intermediate concentrations. Finally, the initial estimations and the calculated concentrations are compared: if the deviation does not satisfy a given tolerance, the procedure is repeated.

The salinity values of the feed and draw sides at the inlet can be taken from the salinity profile obtained with the hydrodynamic model described in Section 2.1. The temperature of both streams is also estimated with the model and used in the calculations.

The energy required for pumping water from the intake locations to the power plant is estimated considering friction losses, due to pumping from long distances, and the height difference (estimated at 2 m). Friction losses are estimated using Darcy's equation, the most important variable being the distance. Pumping efficiency is also considered. The pressure drop of the draw circuit (Figure 1) is roughly estimated to be 0.5 bar, covered by a support pump; with a 99% efficiency of the pressure exchange system. Turbine efficiency is also considered when evaluating the net power, it is assumed to equal 85% [21]. Pretreatment power costs should also be considered; however, given the lack of state-of-the-art widely agreed-upon pretreatment technologies, and that these pretreatment costs would be similar in nearby locations, this energetic cost had to be excluded from the net power calculation in this case study [22–24]. Table 2 summarises some of the characteristics of the possible PRO power plant.

Table 2. Membrane parameters, operation variables and performance results.

Water permeability A	1.1×10^{-11} $m^3/m^2 \cdot s \cdot Pa$
Salt permeability B	1.2×10^{-7} $m^3/m^2 \cdot s$
Average osmotic gradient	19.7 bar
Membrane area requirement	1.5×10^5 $m^2/m^3_{feed}/s$
Average power density	Up to 6.4 W/m^2

2.3. Selection of the Intakes Location

Once the power produced and consumed at different locations has been analysed, it is possible to deduce the most adequate location, based on the final power produced when subtracting the pumping power. There is a clear trade-off between the higher power production when the intakes are more separated, and the higher power costs associated to this distance. A compromise must be reached to optimize the net power production that can be achieved by comparing the results at different intake locations throughout the year.

3. Results and Discussion

The procedures described previously render the results presented in this section when applied to the case study of the Magdalena River.

3.1. Hydrodynamic Model

Figure 3 shows some results of the proposed hydrodynamic model: the mean salinity along the estuary during the dry season of an average climatic year is presented near the surface and at 10 m depth. In can be seen that near the surface the salinity remains close to zero until the end of the river mouth, where salinity increases rapidly as fresh water mixes with the ocean, reaching ocean salinities about 2 km seaward. On the other hand, at 10 m depth the water retains oceanic salinities up to 300 m inside the river channel, showing salt wedge intrusion and stratification. Further inside the river, close to the bottom, seawater starts mixing until reaching uniform freshwater conditions in the vertical profile about 4 km inside the river.

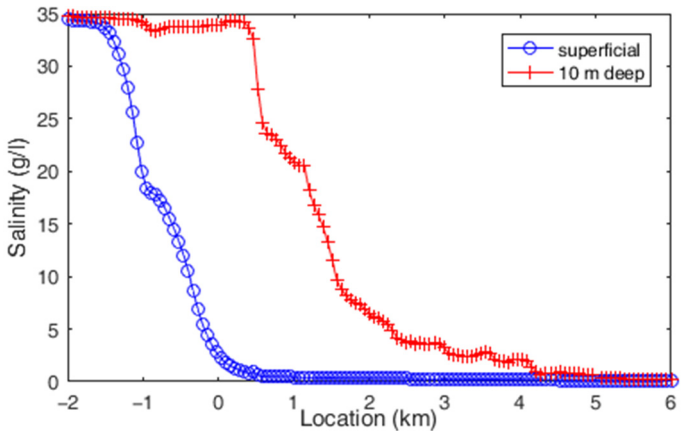

Figure 3. Salinity profile estimated by the hydrodynamic model for the final stretch of the Magdalena river. The horizontal axis indicates distance in km from the end of the river's channel, with positive distances upstream of the river and negative distances seaward.

Based on Figure 3, the potential for a PRO plant can be seen, with extensive possibilities for combinations of feed and draw locations: draw water can be obtained at 10 m depth up to 1 km upriver; feed can be directly obtained from the surface from approximately 0.2 km.

Given that a map of concentrations has been provided by the model, another utility for it can be found when addressing the issue of outflows discharge. Suitable locations for outlet streams can be determined by an examination of their salinity and looking for a location with similar concentrations, so as not to disturb the salinity structure and the ecosystems at the estuary [25]. In this way, the incorporation of these streams should not affect the salinity profile significantly, neither should the intake streams at the Magdalena's mouth because the river flow is much higher (7000 m^3/s on average) [26]. However, this will vary in each case depending on the sizing of the power plant and the freshwater discharge of the river. This issue can be studied with the same hydrodynamic model, and is considered as future work.

Another important issue that has not been discussed yet is membrane fouling. At this point, it is assumed that the biological content in the water is constant in the riverbed, although higher organic content closer to the banks was observed. It would be possible to further analyse the presence of fouling materials in order to study membrane performance decay, and include this information in the hydrodynamic model.

3.2. PRO Power Production and Pumping Costs

The calculation method described in Section 2 was applied to different combinations of water intakes. For instance, considering the superficial data at different distances as

the feed, and the data close to the bottom at different distances as the draw, curves can be obtained to represent the different possible outcomes for the power production and to evaluate their potential. An example of what these curves look like is considered in a particular case: using a preliminary feed location fixed at 1.8 km, all possible intake points are used to calculate the power that a PRO plant would provide if draw water was taken from all these locations. Figure 4 is obtained based on Equations (1) and (2). For each of these locations, the pumping energy required can be evaluated using Darcy's equation, as proposed. These pumping costs are presented in Figure 5.

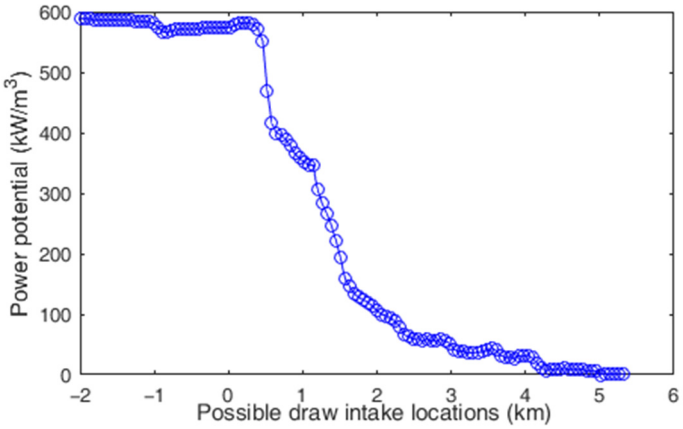

Figure 4. Power production dependence with the location of the draw water for a given feed location at 1.8 km.

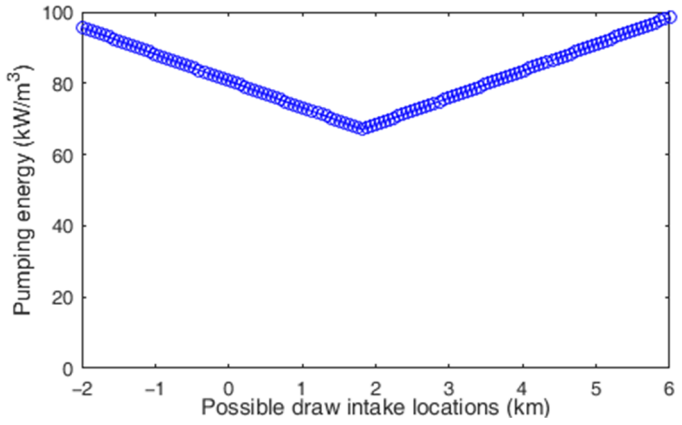

Figure 5. Pumping energy required for draw water taken from different locations for a given feed intake point at 1.8 km (horizontal axis: distance from the end of the river's channel, with positive distances upstream).

Comparing Figures 4 and 5, the clear trade-off between the higher power production can be seen when the intakes are more separated, and the power costs associated to this distance. The net power productivity (Figure 6) can be calculated by subtracting Figure 5 values from Figure 4, after the turbine efficiency deduction. This net variable is much more useful and is the one that should guide any design decisions, because it shows where the potential can be best exploited.

This procedure has been repeated for the set of feasible intake locations (for this, the estuary length was partitioned into 131 intervals). The numerical results make it possible to find some combinations of locations that lead to an increased overall efficiency, that is, the highest power after deducting pumping costs. Figure 7 shows a 3D representation of the available power for every combination of possible draw and intake location,

after eliminating non-feasible pairs of data (those presenting a very large negative net power generation).

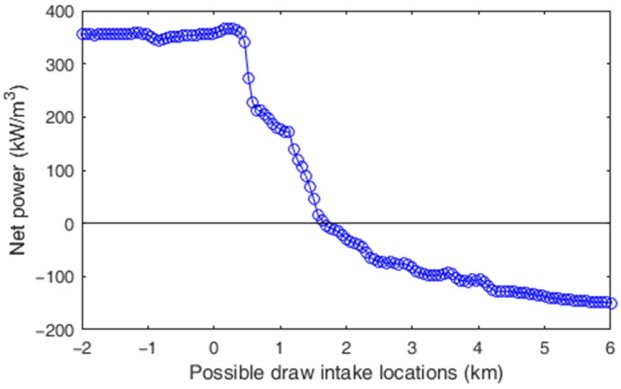

Figure 6. Pumping energy required for draw water taken from different locations (horizontal axis: distance from the end of the river's channel, with positive distances upstream).

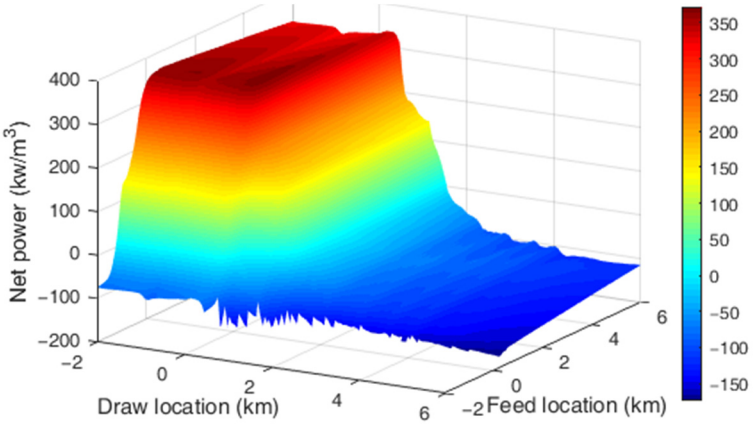

Figure 7. Available net power after subtracting pumping energy for each combination of pairs of data (feed intake distance-draw intake distance).

Figure 7 depicts the value of all the possible combinations of pairs of feed-draw locations. It presents a high net power region, identifiable by the red plateau, and a non-feasibility region presented in different shades of blue. The transition between both regions is abrupt due to the highly stratified conditions that take place in the Magdalena river mouth, where strong salinity gradients take place in short distances. The pattern of these results was expected, since Figure 3 already showed a limited interval of locations with high salinity gradient available.

The presence of this high net power delimited region, which overlaps with the high concentration gradient interval shown in Figure 3, suggests that the main driver for the feasibility of SGE generation at a given river mouth is precisely the salinity gradient. However, the optimum net SGE potential has been shown to be determined instead by the pumping distance, which is the decisive factor. This is because, at any river mouth, two locations can be found where salinity of the feed solution is close to zero, while the salinity of the draw solution is oceanic, but if both locations are too far from each other, the pumping energy will be higher than the power potential, which is limited.

After analysing all the data represented in Figure 7, Table 3 summarises some of the most relevant scenarios: first (A), the combination which leads to the highest potential power; second (B), the highest power exploitable among all the locations with the lowest pumping demand (feed and draw intake in the same place); and third and most important, (C), the pair of feed and draw locations that presents the best efficiency.

Table 3. Comparison between relevant combinations of feed and draw locations.

	A: Highest Power	B: Lowest Pumping	C: Best Efficiency
Feed intake (km)	6.0	0.03	0.58
Draw intake (km)	−2.0	0.03	0.15
Relative Distance (km)	8.0	0	0.43
Feed mean salinity (g/L)	0.11	1.9	0.28
Draw mean salinity (g/L)	34.8	33.9	34.3
Gross power potential (kW/m^3)	593	546	579
Pumping power (kW/m^3)	166	106	109
Net power (kW/m^3)	**327**	**347**	**373**

Figure 8 shows a detail of the high net power data region from Figure 7, containing combinations A, B and C. The apparent red plateau from Figure 7 is not so smooth when looked at in more detail. A variability of up to 20% in the net power is shown in this representation.

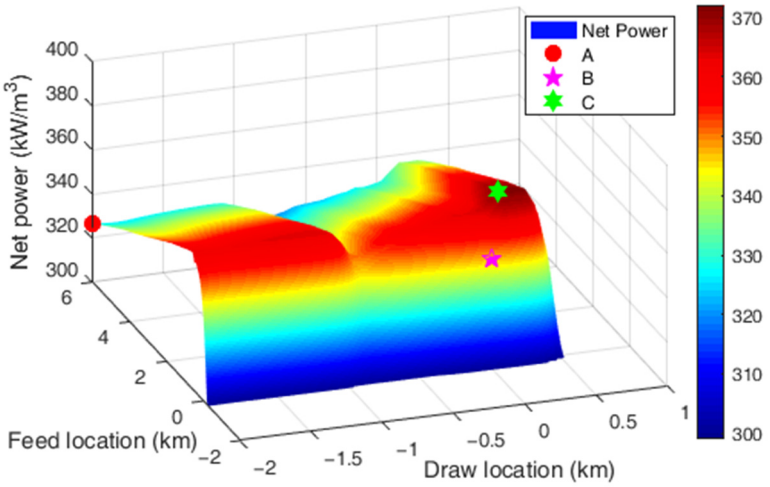

Figure 8. Detail of the highest net power data region from Figure 7, with relevant scenarios A, B and C from Table 3.

Examination of Table 3 and Figure 8 shows that an improvement of up to 14% in the net power can be reached by choosing a location with a slightly lower potential. Additionally, it can be seen that the pumping distance is an important factor, but not the only one, hence scenario C provides an efficiency 7% higher than B.

The data region of high net power shown in Figure 7 is expected to vary with several factors. Variations in the river flowrate may alter the stratification and salinity profile, this would translate into a shrinking (higher flow rate) or widening (lower flow rate) of the plateau, along with a shift of its location within the distance locations map, because the length of the salinity intrusion in strongly stratified estuaries is very sensitive to the river discharge [27]. However, due to the stratification, water close to the surface will remain fresh while water close to the bottom will still be oceanic, even with very large discharge increments [28]. Salinity variations are expected in that situation, causing the high net power plateau to rise with increments of the salinity in the deeper layer, or fall with increments of the salinity in the superficial water, and vice versa.

A sensitivity analysis for the net power has been performed, considering variations in temperature and in salinity from the conditions obtained at best efficiency (case C in Table 3 and Figure 8). Five different scenarios have been considered: D, an increase of 1 °C of feed and draw temperature; E, a decrease of 1 °C in both temperatures; F, an increase of 1 g/L in the feed salinity; G, an increase of 1 g/L in the draw salinity; H, a decrease of

1 g/L in the draw salinity. Results from these disturbances are reflected in the net power, shown in Table 4.

Table 4. Sensitivity analysis for the net power.

Scenario	Base Case	D: +1 °C	E: −1 °C	F: +1 g/L Feed	G: +1 g/L Draw	H: −1 g/L Draw
Net power (kW/m^3)	373	375	371	314	388	353
% variation		+0.6%	−0.6%	−15.8%	+3.9%	−5.3%

These results show a small but substantial variation with temperature which responds in the same proportion to equal negative and positive variations, as expected from the linear dependence presented in Equations (4) and (5). A stronger dependence on salinity has been reported, especially in feed. Unlike the behaviour with temperature, salinity variation is highly non-linear: two perturbations of 1 g/L, positive in G and negative in H, lead to different percentage variations. The sensitivity to the feed salinity is more pronounced. This non-linear behaviour is expected from Touati's model (Equation (2)).

4. Conclusions

A methodology has been presented in order to analyse the effect of intake locations in power produced by the membrane-based technology of Pressure-Retarded Osmosis in stratified river mouths. The methodology is based on the development of a multidisciplinary procedure that combines hydrodynamic models of the river mouth with models of the PRO process. This combination of models is then an effective way to predict the salinity structure of the river mouth, and as a result, to determine the net power production of the PRO as a function of the possible locations of the two water intakes. The results show the compromise between the desired lower intake distances and higher salinity gradient, for achieving higher power production. Here, we showed how important it is to find optimal locations in the planning and design of a potential power plant. The analysis proposed here found that the optimal locations provide 14% higher net power productivity, when comparing the set of optimal locations with the ones that give the maximum power.

Author Contributions: Methodology, J.M.S., O.Á.-S. and F.T.; software, J.M.S. and A.H.; validation, J.M.S., O.Á.-S. and A.H.; investigation, J.M.S.; resources, O.Á.-S. and F.T.; writing—original draft preparation, J.M.S.; writing—review and editing, J.M.S., O.Á.-S., A.H. and F.T.; visualization, J.M.S.; supervision, O.Á.-S. and F.T.; funding acquisition, J.M.S. and F.T. All authors have read and agreed to the published version of the manuscript.

Funding: Funded by Junta de Castilla y León with EU-FEDER funds (CLU-2017-09, VA232P18, UIC 225), and by Ministry of Science, Technology, and Innovation of Colombia (MINCIENCIAS, contract 145-2019).

Institutional Review Board Statement: Not applicable.

Data Availability Statement: Data supporting the reported results can be found publicly in https://www.researchgate.net/publication/350975902_Supporting_data_from_Analysis_of_the_intake_locations_of_Salinity_Gradient_plants_using_hydrodynamic_and_membrane_models_Water, accessed on 13 April 2021.

Conflicts of Interest: The authors declare no conflict of interest. The funders had no role in the design of the study; in the collection, analyses, or interpretation of data; in the writing of the manuscript, or in the decision to publish the results.

References

1. Gross, M.; Rüdiger, M. *Renewable Energies*; Routledge: London, UK, 2014.
2. Østergaard, P.A.; Duic, N.; Noorollahi, Y.; Mikulcic, H.; Kalogirou, S. Sustainable development using renewable energy technology. *Renew. Energy* **2020**, *146*, 2430–2437. [CrossRef]
3. Twidell, J. Tony Weir. In *Renewable Energy Resources*; Routledge: London, UK, 2015.

4. Halkos, G.E.; Eleni-Christina, G. Reviewing Usage, Potentials, and Limitations of Renewable Energy Sources. *Energies* **2020**, *13*, 2906. [CrossRef]
5. Hussain, A.; Syed, M.A.; Muhammad, A. Emerging renewable and sustainable energy technologies: State of the art. *Renew. Sustain. Energy Rev.* **2017**, *71*, 12–28. [CrossRef]
6. Micale, G.; Cipollina, A.; Tamburini, A. Salinity gradient energy. In *Sustainable Energy from Salinity Gradients*; Woodhead Publishing: Sawston, UK, 2016; pp. 1–17.
7. Touati, K.; Tadeo, F.; Kim, J.H.; Silva, O.A.A.; Chae, S.H. *Pressure Retarded Osmosis: Renewable Energy Generation and Recovery*; Academic Press: Cambridge, MA, USA, 2017.
8. Alvarez-Silva, A.; Osorio, A.F.; Winter, C. Practical global salinity gradient energy potential. *Renew. Sustain. Energy Rev.* **2016**, *60*, 1387–1395. [CrossRef]
9. Sandbach, S.D.; Nicholas, A.P.; Ashworth, P.J.; Best, J.L.; Keevil, C.E.; Parsons, D.R.; Simpson, C.J. Hydrodynamic modelling of tidal-fluvial flows in a large river estuary. *Estuar. Coast. Shelf Sci.* **2018**, *212*, 176–188. [CrossRef]
10. Panchenko, E.; Max, L.; Serafima, L. Hydrodynamic modelling of the Onega River tidal estuary. *E3S Web Conf.* **2020**, *163*, 01-008. [CrossRef]
11. Restrepo, J.C.; Ortiz, J.C.; Pierini, J. Freshwater discharge into the Caribbean Sea from the rivers of Northwestern South America (Colombia): Magnitude, variability and recent changes. *J. Hydrol.* **2014**, *509*, 266–281. [CrossRef]
12. Leitao, P.; Mateus, M.; Braunschweig, L.; Fernandes, L.; Neves, R. *Modelling Coastal Systems: The MOHID Water Numerical Lab, Perspectives on Integrated Coastal Zone Management in South America*; IST Press: Lisboa, Portugal, 2008.
13. Martins, F.; Leitao, P.; Silva, A.; Neves, R. 3D modelling in the Sado estuary using a new generic vertical discretization approach. *Oceanol. Acta* **2001**, *24*, 51–62. [CrossRef]
14. Available online: https://www.aviso.altimetry.fr/en/data/products/auxiliary-products/global-tide-fes/description-fes2012.html (accessed on 16 April 2021).
15. Available online: https://www.ncdc.noaa.gov/data-access/model-data/model-datasets/global-forcast-system-gfs (accessed on 16 April 2021).
16. Skote, M. *Studies of Turbulent Boundary Layer Flow through Direct Numerical Simulation*; Technical Report; Royal Institute of Technology, Department of Mechanics: Stockholm, Sweden, 2001.
17. Canuto, V.M.; Howard, A.; Cheng, Y.; Dubovikov, M.S. Ocean Turbulence. Part I: One-point closure model momentum and heat vertical diffusivities. *J. Phys. Oceanogr.* **2001**, *31*, 1413–1426. [CrossRef]
18. Touati, K.; Hänel, C.; Tadeo, F.; Schiestel, T. Effect of the feed and draw solution temperatures on PRO performance: Theoretical and experimental study. *Desalination* **2015**, *365*, 182–195. [CrossRef]
19. Gonzales, R.R.; Abdel-Wahab, A.; Adham, S.; Dong, S.H.; Phuntsho, S.; Suwaileh, W.; Hilalf, N.; Shon, H.K. Salinity gradient energy generation by pressure retarded osmosis: A review. *Desalination* **2021**, *500*, 114841. [CrossRef]
20. Salamanca, J.M.; Álvarez-Silva, O.; Tadeo, F. Potential and analysis of an osmotic power plant in the Magdalena River using experimental field-data. *Energy* **2019**, *180*, 548–555. [CrossRef]
21. Seme, S.; Sredensk, K.; Praunseis, Z.; Stumberger, B.; Hadziselimovic, M. Optimal price of electricity of solar power plants and small hydro power plants–Technical and economical part of investments. *Energy* **2018**, *157*, 87–95. [CrossRef]
22. Abbasi-Garravand, E.; Catherine, N.; Mulligan, C.B.; Laflamme, G.C. Role of two different pretreatment methods in osmotic power (salinity gradient energy) generation. *Renew. Energy* **2016**, *96*, 98–119. [CrossRef]
23. Roldan-Carvajal, M.; Vallejo-Castaño, S.; Álvarez-Silva, O.; Bernal-García, S.; Arango-Aramburo, S.; Sánchez-Sáenz, C.I.; Osorio, A.F. Salinity gradient power by reverse electrodialysis: A multidisciplinary assessment in the Colombian context. *Desalination* **2021**, *503*, 114933. [CrossRef]
24. Alvarez-Silva, O.; Maturana, A.Y.; Pacheco-Bustos, C.A.; Osorio, A.F. Effects of water pretreatment on the extractable salinity gradient energy at river mouths: The case of Magdalena River, Caribbean Sea. *J. Ocean Eng. Marine Energy* **2019**, *5*, 227–240. [CrossRef]
25. Ortega, S.; Stenzel, P.; Alvarez-Silva, O.; Osorio, A.F. Site-specific potential analysis for pressure retarded osmosis (PRO) power plants–The León River example. *Renew. Energy* **2014**, *68*, 466–474. [CrossRef]
26. Alvarez-Silva, A.; Winter, C.; Osorio, A.F. Salinity gradient energy at river mouths. *Environ. Sci. J. Technol. Lett.* **2014**, *1*, 410–415. [CrossRef]
27. Geyer, W.R.; Ralston, D.K. The dynamics of strongly stratified estuaries. In *Treatise on Estuarine and Coastal Science*; Elsevier: Amsterdam, The Netherlands, 2011; pp. 37–52.
28. Ospino, S.; Restrepo, J.C.; Otero, L.; Pierini, J.; Alvarez-Silva, O. Saltwater Intrusion into a River with High Fluvial Discharge: A Microtidal Estuary of the Magdalena River, Colombia. *J. Coast. Res.* **2018**, *34*, 1273–1288.

Renewable Energy 105 (2017) 84–95

Contents lists available at ScienceDirect

Renewable Energy

journal homepage: www.elsevier.com/locate/renene

Energy recovery from two-stage SWRO plant using PRO without external freshwater feed stream: Theoretical analysis

Khaled Touati [a, b, *], Jacobo Salamanca [a], Fernando Tadeo [a], Hamza Elfil [b]

[a] Department of Systems Engineering and Automatic Control, University of Valladolid, 47011, Valladolid, Spain
[b] Laboratory of Natural Water Treatment- Water Researches and Technologies Center, Technopark Borj Cedria, BP 273, 8020, Soliman, Tunisia

ARTICLE INFO

Article history:
Received 11 July 2016
Received in revised form
12 November 2016
Accepted 13 December 2016
Available online 20 December 2016

Keywords:
Pressure retarded osmosis
Seawater reverse osmosis
Energy recovery
Modeling
Dilution factor

ABSTRACT

Research into pressure retarded osmosis (PRO) as a method to extract energy from salinity gradients is on the rise. Seawater Reverse Osmosis (SWRO) is now a leading technology in the desalination industry worldwide, in both small and large scale applications, due to the remarkable improvements in membrane performance and associated energy efficiency. Nonetheless, SWRO desalination is inherently more energy intensive when compared to conventional fresh water treatment. The integration of PRO with SWRO systems is studied in terms of energy consumption and effluent changes. For this, two novel integration designs are evaluated, with SWRO-PRO specific energy consumption being modeled using SWRO conditions at the thermodynamic restriction, and a developed PRO model. The results show lower SWRO energy consumption for both configurations, with a reduction in consumption of 12%–18%, depending on the RO recovery ratios. Lastly, the effect of the initial flow ratio on the dilution factor has been studied. To do so, the dilution was modeled and studied for different operating conditions. It was found that detrimental effects severely reduce the dilution, especially the internal concentration polarization, which induces a decrease of energy recovery when using the PRO process.

© 2016 Elsevier Ltd. All rights reserved.

1. Introduction

Desalination technologies are quickly growing, combining engineering and science to develop innovative means for drinkable water production [1]. In fact, several countries, especially in the Middle East, already depend on seawater desalination as the main source of drinking water [2,3], so desalination plants have seen considerable expansion over the past decade: the desalination capacity is expected to reach about 100 million cubic meters per day at the end of 2016 [2]. The main challenge in desalination is the use of energy: As a drinking water treatment technology, seawater desalination requires more energy than conventional fresh water treatment methods [3]. However, the power consumption is frequently inaccurately represented when compared to other treatment technologies that provide safe and reliable public water supply [4,5]. Typically, the energy consumption represents 44% of the total water cost of a SWRO plant [6]. Another challenge in the desalination industry is the handling of reject brine, which is the highly concentrated by-product of the desalination process [7,8]. Osmotic Energy systems were proposed as a solution due to the fact that it has been found to be very promising, with the potential of reducing the cost of seawater desalination as well as the environmental impact from brine discharge [9–11]. In other words, as a SWRO system produces high water concentration (brine) and PRO uses solutions with high concentrations, it would be beneficial to hybridize the two processes due to the reliance of the two membrane processes on the concentration of solutions. In addition, The SWRO-PRO system has several advantages. Compared to an optimized stand-alone SWRO system (SWRO with a recovery energy device), SWRO energy consumption is reduced by energy production using PRO [12]. Another advantage of this system is that the brine generated during the SWRO process is diluted back to seawater concentration, thus minimizing the adverse environmental impact that seawater RO brine disposal can have on marine ecology/habitats. Furthermore, the impaired water and SWRO product water are in separate circuits, so there is no contact between impaired water and drinking water. Compared to a stand-

* Corresponding author. Department of Systems Engineering and Automatic Control, University of Valladolid, 47011, Valladolid, Spain. Laboratory of Natural Water Treatment- Water Researches and Technologies Center, Technopark Borj Cedria, BP 273, 8020, Soliman, Tunisia.
E-mail addresses: kha.touati@gmail.com (K. Touati), jmsalamanca@autom.uva.es (J. Salamanca), fernando@autom.uva.es (F. Tadeo), elfilhamza@gmail.com (H. Elfil).

http://dx.doi.org/10.1016/j.renene.2016.12.030
0960-1481/© 2016 Elsevier Ltd. All rights reserved.

alone PRO system (i.e., river-to-sea PRO), PRO energy production in the SWRO-PRO system is augmented by the higher concentration of the draw solution (SWRO brine). Another key advantage of the SWRO-PRO system is that the influent draw solution is pre-treated by the RO pre-treatment system. Thus, the brine entering the PRO sub-system is relatively free of foulants. This draw solution pre-treatment in the SWRO-PRO system avoids additional energy expenditure that would be necessary in a stand-alone PRO system. As the energy and chemical costs of pre-treating seawater is a substantial operating expenditure in SWRO desalination [13], the fact that SWRO-PRO capitalizes on the pre-treated brine reduces some pre-treatment concerns, which can be significant in the PRO process. As a consequence of these encouraging advantages, the integration of PRO into SWRO has attracted the attention of many researchers and several studies are currently involved in investigating the feasibility of SWRO-PRO systems [14–18]. In 2010, Japan launched the Megaton water system. As part of the project, a prototype SWRO-PRO hybrid plant was built and operated. Recycled water was supplied from a regional sewage treatment facility and concentrated brine from a SWRO plant, using PRO hollow fiber modules. The prototype PRO plant got the maximum output power density of 13.8 W/m^2 at 30 bars of hydraulic pressure difference, corresponding to 38% permeation of pure water into the brine [14]. Another study was carried out using an experimental pilot system, designed and constructed to investigate the reduced SWRO energy consumption by its integration with PRO [15,16]. The experiments showed that the enhanced power densities for the RO-PRO system ranged from 1.1 to 2.3 W/m^2 and indicated that future RO-PRO systems may reduce the specific energy consumption requirements for desalination by 1 kWh/m^3 [16]. Another work investigated the feasibility of a RO desalination system powered by a stand-alone PRO unit [17]. Unfortunately, the study did not take into consideration the effect of the concentration polarization and the salt reverse flux on the performance of the SWRO-PRO system, which would affect the results. Seawater brine from the TuaSpring desalination plant and wastewater retentate from the NEWater plant were used in Ref. [18] for energy recovery. Experiments gave a power density of 4.6 W/m^2 at 20 bar obtained with seawater brine as the draw solution and waste water as the feed solution. A recent paper investigated two SWRO-PRO designs based on the positions of the pressure exchangers and the pump, then studied as a function of SWRO recovery [19].

However, most of the previously studied SWRO-PRO cases deal with conventional integration design, where one-stage SWRO brine is the PRO draw solution and a river water/wastewater effluent is the PRO feed solution. This integration methodology reveals that the amount of energy produced is relatively low and requires a feed solution from a low salinity water source, which increases the energy cost (pre-treatment, installations, etc …). Moreover, previous studies have been based on supplying the PRO with external freshwater sources. However, it is well known that the world is facing a serious fresh water scarcity problem [20]. Then, the use of fresh water for energy recovery should be avoided. Furthermore, the use of wastewater effluents shows low energy recovery performance, due to the severe membrane fouling and the necessity for pre-treatment, which increases the energy consumption [18]. In this study, for the first time, an operational two-stage SWRO unit is integrated with PRO to reduce its energy consumption. Herein, the use of an external feed water source is avoided, and an alternative location of the PRO inside the process is proposed. To do so, two novel SWRO-PRO designs have been proposed in terms of the PRO location and the nature of the feed solution. To accomplish this objective, a model for the PRO system has been developed, taking into consideration the membrane characteristics, reverse salt flux, concentration polarization, and pressure drop in the membrane module. The SWRO specific energy consumption is calculated by considering the SWRO at its thermodynamic limit, using models from the literature [21]. Then, the SWRO-PRO model was developed by combining the SWRO and PRO models. In addition, the results of the model were presented for both configurations considered and compared to the ideal case. Lastly, the dilution factor of the draw solution was modeled and investigated as a function of PRO detrimental effects.

2. Material and method

2.1. Description of the SWRO desalination plant

To investigate the feasibility of PRO integration with the SWRO unit, a case study is considered here. A Reverse-Osmosis based desalination unit is used, intended for producing water for the electrolyzation process, and which is composed of the elements presented in Fig. 1. This plant was developed by SETA S-L as a part of the H2OCEANproject [22]. The desalination unit is based on two independent lines, divided into two stages, which can be connected or disconnected, as required for maintenance or operational requirements. In order to reduce the number of spare parts required, both lines have the same components. The procedure is started by a pre-treatment composed of three steps: chlorination to avoid organic matter, ultra-filtration to block metals and particles in suspension, and finally, a backwash to eliminate foulants accumulated on the membrane surfaces during the process.

The first pass of the SWRO unit consists of a chemical treatment applied to remove the residual chlorine from the pre-treatment, then bisulphite is used (to remove the oxidants dissolved in the water and provide a bacteriostatic effect) and, finally, antifouling is

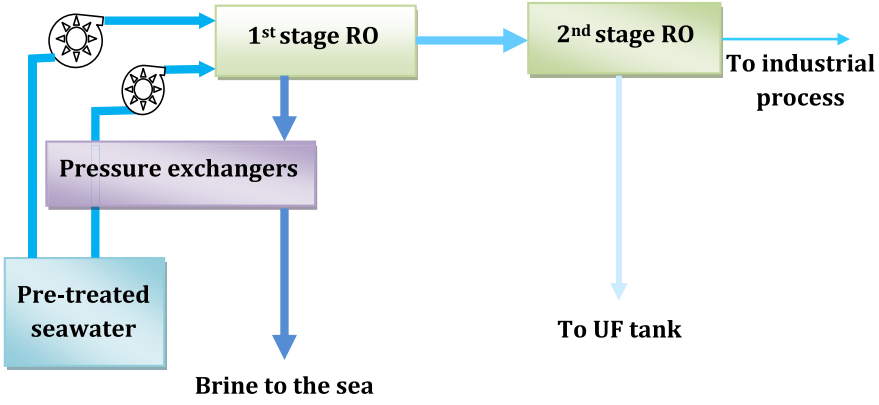

Fig. 1. Two-stage Reverse Osmosis desalination unit.

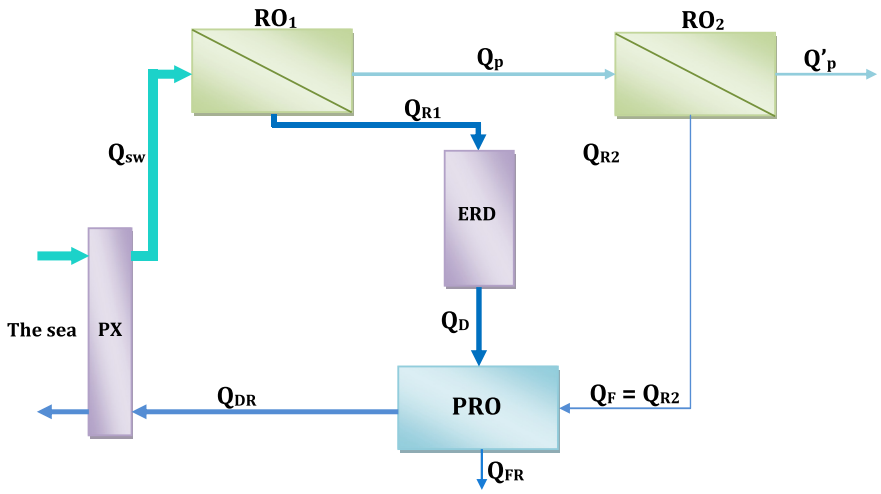

Fig. 2. First configuration SWRO-PRO integration: Standard with brine mixture. Darker colors correspond to more concentrated solutions and the thickness of each arrow denotes the approximate flow rate. (For interpretation of the references to colour in this figure legend, the reader is referred to the web version of this article.)

used to mitigate salt precipitation on the membrane surfaces to avoid the increase in energy consumption. As a safety system to avoid damaging the membrane, a micro filter is installed just before the High Pressure Pump (HP) with a degree of 5 μm of filtration. To feed the first-pass membranes, an HP is required; the water produced is stored in a water tank, whereas the brine goes to an Energy Recovery system (Pressure exchanger PX). In routine operational conditions, the recovery factor is arbitrarily selected to be 45%.

The Second RO Pass consists of two phases, it is first dosed with an antifouler designed to avoid salt precipitation and a micro filter is installed with a degree of 5 μm of filtration, as a safety system to avoid membrane fouling. Second, to feed the second-pass, the RO requires an HP to pressurize the water before it enters the membrane. The reverse osmosis recovery is around 70%. The water produced is stored in a DEMI water tank, whereas the brine goes to an energy recovery system before being reused in the proposed osmotic energy recovery system or being returned to the Ultra-Filtration Tank.

2.2. SWRO-PRO configurations and integration methodologies

2.2.1. First SWRO-PRO configuration

A simplified presentation of the first SWRO-PRO configuration is illustrated in Fig. 2: the seawater feed solution (Q_{sw}) is first pre-pressurized in the pressure exchanger PX prior to entering the desalination process. Exiting the first stage SWRO sub-system (RO_1) are two streams: a freshwater permeate stream (Q_p) and a concentrated brine stream (Q_{R1}). Q_{SR1} is then depressurized to approximately half its pressure to reach an adequate condition for the PRO process [7]. The permeate of the RO_1 feeds the second stage RO sub-system (RO_2). To recover the brine energy, an isobaric or turbocharged device could be used; alternatively, a turbine could be employed to convert it into electrical energy. Following this depressurization, the brine stream enters the PRO sub-system as a high salinity (draw) solution ($Q_{R1} = Q_D$). The feed solution for the PRO sub-system ($Q_F = Q_{R2}$) is the retentate of the second stage. Through osmosis, the pressurized draw solution extracts water from the impaired water source under isobaric conditions, resulting in a diluted draw solution (Q_{DR}). The energy stored in the diluted draw solution is then exchanged with the seawater RO feed prior to discharge in order to recover its potential energy and increase the energy savings of the SWRO-PRO system. The PRO feed solution bleed Q_{FR} is rejected to the sea.

2.2.2. Second SWRO-PRO configuration

In the second configuration, the feed solution entering the PRO sub-system was changed. The retentate of the second stage (Q_{R2}) was mixed with an additive pre-treated seawater flow (Q_{ad}); the sum embodies the PRO feed solution. The amount of seawater flow is chosen to guarantee the condition that the feed and draw solution flows are equal ($Q_F = Q_{ad} + Q_{R2} = Q_D$). For this, a controllable valve (V) is placed to provide the desired amount of Q_{ad}. The draw solution of the PRO is the brine of the first RO stage; this brine passes through the energy recovery device (ERD) to adjust its pressure, when necessary, to a suitable applied pressure value (which is theoretically the optimum pressure value to be applied to the draw solution in the PRO process). It should be noted that the functioning of the ERD in this configuration is studied later, in Section 2.4.3. The exiting PRO draw solution flow is then conducted to the PX to recover the pressure to the feed SWRO flow (Q_{sw}). The PRO feed solution bleed Q_{FR} is rejected to the sea. Fig. 3 illustrates the second SWRO-PRO configuration. It should be pointed out that the choice of seawater as an added flow to the entering PRO feed solution is based on the fact that the SWRO plant is placed near the sea, and no river water is close to the SWRO facility.

2.3. Modeling the ideal energy consumption of the SWRO-PRO system

2.3.1. Two-stage reverse osmosis (SWRO)

The theoretical energy consumption is the minimum amount of energy required to produce a desired volume of permeate. More precisely, the theoretical Specific Energy Consumption (SEC) gives, for a given recovery rate, the absolute minimum amount of energy by assuming that the efficiency of every component (pumps, motors, Energy Recovery Devices, etc.) is 100%. At the theoretical limit of constant-pressure operation, the one-stage reverse osmosis (RO) system will operate with an applied hydraulic pressure equal to the final osmotic pressure of the brine exiting the RO module. Thus, the minimum specific energy of desalination for a one-stage RO

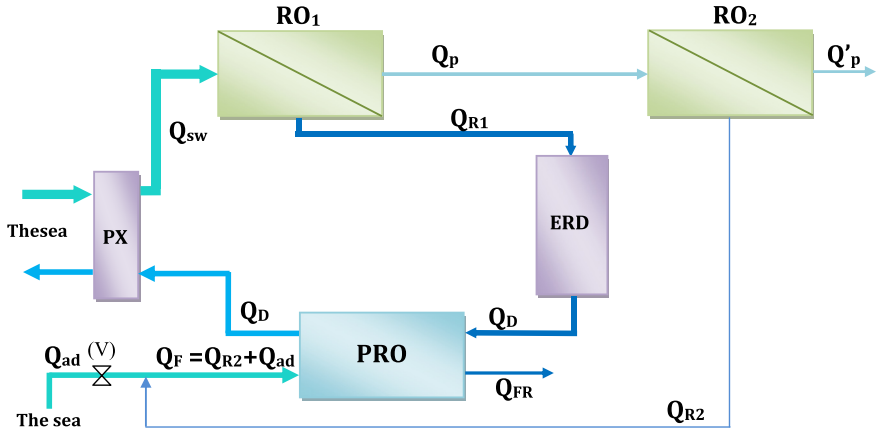

Fig. 3. Second configuration SWRO-PRO integration: standard with second brine-seawater mixture. Darker colors correspond to more concentrated solutions and the thickness of each arrow denotes the approximate flow rate. (For interpretation of the references to colour in this figure legend, the reader is referred to the web version of this article.)

process, $SE_{RO,desal}$, is equal to the final brine osmotic pressure [21,30]:In our case, considering two RO stages, the total theoretical energy consumption of the two-stage RO system ($SEC_{RO_1-RO_2,theo}$)is the sum of the energy consumption of each stage:

$$SEC_{RO_1-RO_2,theo} = \pi_{sw}\left(\frac{1}{1-Y_1}+\frac{Y_1}{1-Y_2}\right) \quad (1)$$

where Y_1 and Y_2 are the recoveries of RO_1 and RO_2, respectively. The salt rejection coefficient R_s for both RO stages is defined as:

$$R_{s1} = 1-\frac{C_p}{C_{sw}} \quad (2)$$

$$R_{s2} = 1-\frac{C_{p'}}{C_p} \quad (3)$$

where C_p and $C_{p'}$ are the salt concentration in the permeate solutions of the first and second stages, respectively. For simplicity, the salt rejection coefficients are considered equal ($R_{s1} = R_{s2} = R_s$). Throughout the study, a linear relation between salt concentration and osmotic pressure, based on the van't Hoff equation, is assumed ($\pi = \beta RTC$). This assumption makes the development of simple analytical expressions easy, without a significant compromise in accuracy, because a concentration relevant to seawater ($C_{sw} = 35$ g/L) is low enough for the van't Hoff equation to be reasonably accurate. Fig. S1 (Supplementary material) describes the minimum separation energy for a two-stage SWRO as a function of Y_1 according to Eq. (1), which is achievable only in an ideal, reversible, thermodynamic process. In this case, since the majority of the energy is consumed by the first stage, the recovery of the second stage is maintained equal to 70% throughout the study. It should be pointed out that the minimum specific energy does not include the energy required to generate excess pressure in the module, or the energy spent on pre-treatment or post-treatment. As can be seen in Fig. S1, the minimum work needed theoretically would be 0.81 kWh/m^3 of fresh water. This lower limit corresponds to a rate of production that is nearly zero. It can also be seen that, when the recovery rate increases, the specific energy consumption also increases. For the one-stage SWRO system, it has been shown in the literature that the optimal recovery rate for a one-stage SWRO unit is around 40%–50% [13]. For these recovery rates, the $SEC_{RO,theo}$ would be between 1.24 and 1.49 kWh/m^3, which clearly differs from real values [18,24,25].

2.3.2. Pressure retarded osmosis (PRO)

In the PRO system, the difference in osmotic pressure between the feed and draw solutions is a key parameter for increasing the energy production. Also, the harvested energy is proportional to the mixing volume. These two parameters should be optimized to guarantee sufficient energy production. Clearly, the energy consumption of the SWRO plant is manifested in the increase of the brine concentration. In other words, it is the minimum energy that should be consumed to extract freshwater from the seawater, which is the theoretical, minimum thermodynamic energy for desalination (i.e. the separation energy equal in magnitude but opposite in sign to the free energy of mixing). In fact, the PRO process is, in practice, acting inversely to the RO process: the feed solution concentrated to brine during the RO process is now diluted under the PRO process. Thus, an equation similar to Eq. (1) can be developed for the PRO process. A recent investigation has introduced the theoretical energy production for the PRO process integrated with SWRO [16], when the brine of the RO unit was used against freshwater from river. Unfortunately, this relation is only valid for a PRO feed solution assumed to be zero. Based on an analogy between RO and PRO, a generalized expression of $SE_{PRO,theo}$ is introduced, taking into account the concentration of the PRO feed solution concentration. Assuming finite dilution in an ideal mixing process, the Specific Energy production, $SE_{PRO,theo}$, can be calculated as follows:

$$SE_{PRO}^{Theo} = r\left(\frac{\pi_{Draw}-\pi_{Feed}}{\pi_{Draw}}\right)\left(\frac{\pi_{sw}-\pi_{Draw}}{1-DF}\right) \quad (4)$$

where π_{Draw} and π_{Feed} are the osmotic pressures of the PRO feed and draw solutions, respectively. DF and r are, respectively, the dilution factor of the draw solution in the PRO system and the PRO entering flow ratio. Based on the analogy between RO and PRO, DF and r are defined as follows:

$$DF = \frac{\Delta Q}{Q_D} \quad (5)$$

$$r = \frac{Q_F}{Q_D} \quad (6)$$

where ΔQ, Q_D, Q_F are the PRO permeate, the draw solution and the feed solution flow rates. The boundaries of the permeate flowing across the PRO membrane is $0 \le \Delta Q \le Q_F$. In other words, the maximum dilution that can be reached with a perfect semi-

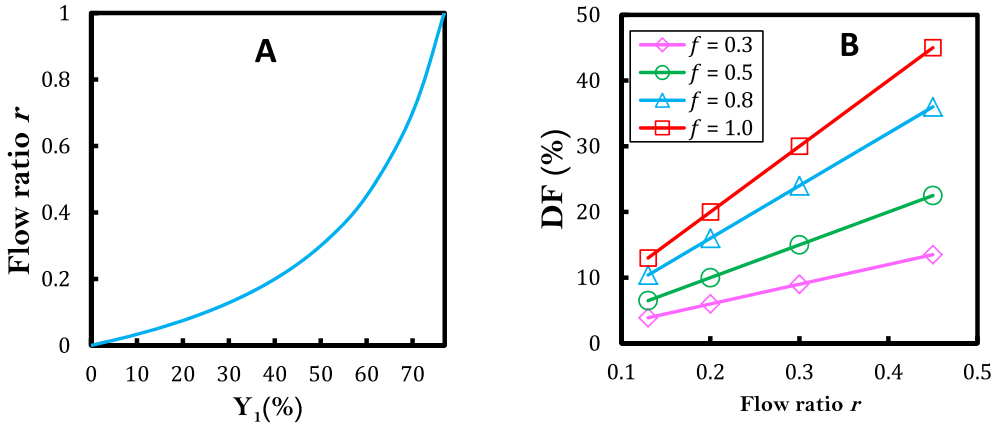

Fig. 4. Variation of the dilution factor. (A) represents the variation of r with the recovery of the first stage. (B) shows the variation of the dilution with the feed and draw flow ratio for different feed flow fractions f.

permeable membrane with no detrimental effects is reached when $\Delta Q = Q_F$. The dilution factor, DF, can be described as follows by rearranging Eq. (5):

$$DF = f \times r \tag{7}$$

where

$$f = \frac{\Delta Q}{Q_F} \tag{8}$$

The parameter $f(0 \le f \le 1)$ reflects the fraction of PRO feed flow that crosses the membrane to be mixed with the draw solution. The ratio r is not equal to unity and varies with the recoveries. Then, the dilution factor should be determined based on the fraction f and the recoveries. Using Eqs. (7) and (8) for arbitrary values of f, the variation of the dilution with r is presented in Fig. 4. As the volume of brine is proportional to the recovery of the first stage, r increases with Y_1 to reach the unity at $Y_1 = 77\%$. It is clear that the increases in r and f lead to the increase in the dilution factor. The maximum dilution that can be achieved when $f = 1$, is equal to r. Theoretically, operating at high recoveries optimizes the performance of PRO in terms of energy production thanks to the optimized feed flow ratio r. In realistic conditions, high recoveries for seawater desalination are not achievable. Therefore, the choice of input parameters should be studied in detail to guarantee high water production and considerable energy recovery using PRO.

2.3.2.1. First configuration. For the first configuration, Eq. (4)of the Specific Energy production can be written using the operational parameters of the SWRO as follows:

$$SE^1_{PRO,\ ideal} = R_s \pi_{sw} \left(\frac{Y_1}{1-Y_1}\right)\left(\frac{r}{1-DF}\right) \left\{1-(1-R_s)\left(\frac{Y_1}{r}\right)\left[\frac{1-Y_2(1-R_s)}{1-Y_1(1-R_s)}\right]\right\} \tag{9}$$

The results of the PRO energy production connected to the SWRO, as described for the first configuration, are shown in Fig. 5. In this case, two fractions f were adopted to calculate the energy recovery. As mentioned previously, the increase in the recoveries induces the increase in the dilution. This is justified by the increase of the feed water stream provided by the second RO stage. It can be seen that increasing the dilution factor leads to an increase in the amount of energy produced. This behavior is directly related to the performance of the PRO membrane. Otherwise, the energy produced depends on the operational parameters of the SWRO (recoveries, feed solution concentration, and RO membrane performance). Logically, at high DF, the PRO performance is much better due to the increase of the first stage brine concentration (draw solution of the PRO) and the increase in the amount of feed water that crosses the membrane to the draw water side. It is also clear that the increase in f enhances the energy recovery. Theoretically, at maximum dilutions (DF = 45% when $f = 1$, DF = 22% when $f = 0.5$), PRO produces around 1.01 kWh/m^3 and 0.72 kWh/m^3, respectively. These values mean that the energy consumption is reduced by 28% and 20%, respectively.

2.3.2.2. Second configuration. Clearly, the PRO feed flow is lower than the PRO draw flow for a wide range of Y_1 in the first configuration. During the second SWRO-PRO processing, the entering flows of the PRO sub-system (Q_F and Q_D) are maintained equal, thanks to the added pre-treated seawater flow Q_{ad}, as shown in Fig. 3. The amount of added seawater flow respects the following relation:

$$Q_{ad} = Q_{sw}(1 + Y_1 Y_2 - 2Y_1) \tag{10}$$

where Q_{sw} is the initial seawater flow that enters the first SWRO stage. Consequently, the osmotic pressure of the PRO feed flow, Q_F, depends on the recovery of the first stage. Fig. S2 (Supplementary material) shows the variation of Q_{ad} with respect to Y_1 and its effect on the PRO feed osmotic pressure. It can clearly be seen that increasing the recovery of the first stage reduces the amount of the added seawater flow and decreases the osmotic pressure of the PRO entering feed solution due to the increase in the second stage retentate flow. At a recovery of $Y_1 = 77\%$, the osmotic pressure of the feed solution reaches its minimum, which corresponds to the osmotic pressure of the second stage retentate, where the addition of Q_{ad} is annulled. Consequently, at $Y_1 = 77\%$, the PRO specific energy production is the same for both SWRO-PRO configurations ($SE^2_{PRO} = SE^1_{PRO}$).

Under these conditions, the Specific Energy production can be written using the operational parameters of the SWRO as follows:

$$SE^{2}_{PRO} = \begin{cases} R_s \pi_{sw} \left(\frac{Y_1}{1-Y_1}\right)\left(\frac{1}{1-DF}\right)\left\{1 - \frac{(1-R_s)[Y_1 - Y_1Y_2(1-R_s)] + Y_1Y_2 - 2Y_1 + 1}{1 - Y_1(1-R_s)}\right\} & 0 < Y_1 \le 77\% \\ R_s \pi_{sw} \left(\frac{Y_1}{1-Y_1}\right)\left(\frac{r}{1-DF}\right)\left\{1 - (1-R_s)\left(\frac{Y_1}{r}\right)\left[\frac{1-Y_2(1-R_s)}{1-Y_1(1-R_s)}\right]\right\} & 77\% \le Y_1 < 100\% \end{cases} \quad (11)$$

Fig. 6 shows the model results for energy recovered by the PRO using the second configuration for different dilution factors and recoveries. As expected, the increase in the PRO membrane performance leads to a higher energy production. When the recovery of the first SWRO stage increases, the energy recovered also increases due to the increase in the osmotic pressure difference in the PRO module. Compared to the first configuration, the performance of the PRO is relatively better, thanks to the added seawater flow Q_{ad}. A comparison between the two configurations is discussed in the next section.

2.3.3. SWRO-PRO

The specific energy consumption of the thermodynamically reversible SWRO-PRO system, $SEC^{ideal}_{SWRO-PRO,}$ is obtained by combining the energy consumption of the SWRO sub-system and the specific energy production of the PRO process. Thus, $SEC^{ideal}_{SWRO-PRO}$, for both first and second configurations, is described as follows [31]:

$$SEC^{ideal}_{SWRO-PRO} = SEC_{SWRO} + SE_{PRO} \quad (12)$$

Fig. 7 shows the evolution of the ideal specific energy of the RO-PRO system as a function of PRO dilution for several RO_1 recoveries. As mentioned in the previous section, when the dilution factor increases, the PRO starts to produce energy and the SWRO-PRO system specific energy consumption decreases. For both configurations, positive values of $SEC^{ideal}_{SWRO-PRO}$ mean that the SWRO-PRO system consumes energy (EC system). In the opposite case, negative values mean that the SWRO-PRO system produces energy; in other words, the energy produced by the PRO overcomes the energy consumed by the SWRO (EP system). When the specific energy reaches zero, this point represents an ideal neutral energy system, where the energy consumed by the SWRO is compensated by the energy produced by the PRO. At low dilution, $SEC^{ideal}_{SWRO-PRO}$ is always positive for each configuration and recovery, which theoretically means that the exiting PRO draw solution flow is inferior to the SWRO feed solution flow. For the first configuration, no scenario corresponds to an EP system (e.g., $SEC_{RO} \le SE_{PRO}$), and all scenarios show EC systems, as shown in Fig. 7-A. Otherwise, the second configuration revealed three scenarios for theoretically possible EP systems (Fig. 7-B). Two operating parameters differentiate between the studied configurations: the PRO feed solution concentration and flow. The first configuration provides low a PRO feed concentration with a low feed flow, while the second one guarantees a high feed flow with a considerably high PRO feed concentration (at

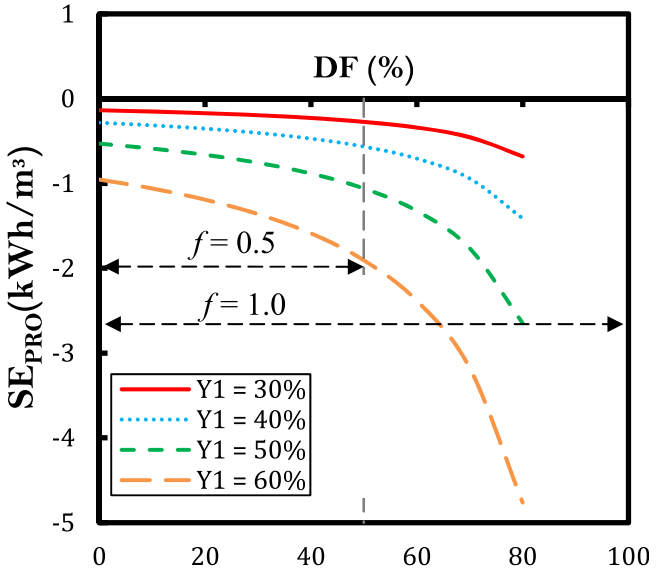

Fig. 6. Theoretical Specific Energy production of PRO for the second SWRO-PRO configuration under different dilution factors. The results are fitted for several recoveries of the first SWRO stage. T = 25 °C.The vertical dashed line indicates the limit of dilution for $f = 0.5$.

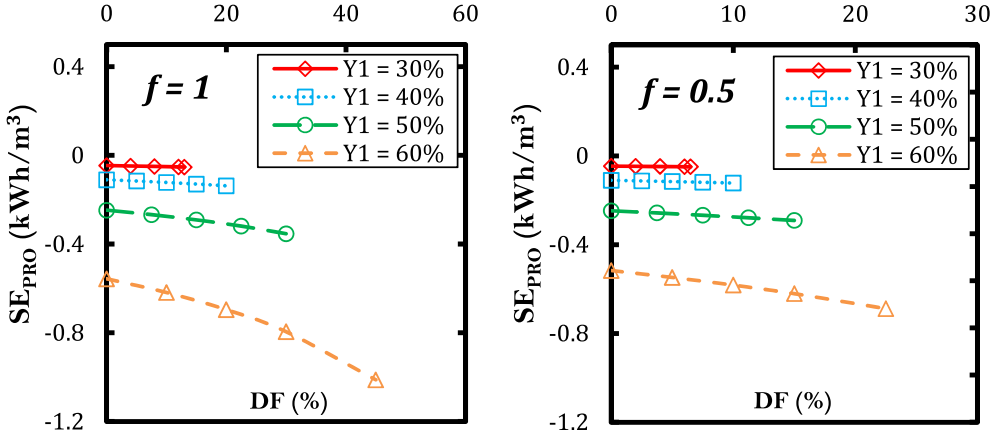

Fig. 5. Theoretical Specific Energy production of PRO for the first SWRO-PRO configuration under different dilution factors. The results are fitted for several recoveries of the first SWRO stage. T = 25 °C.

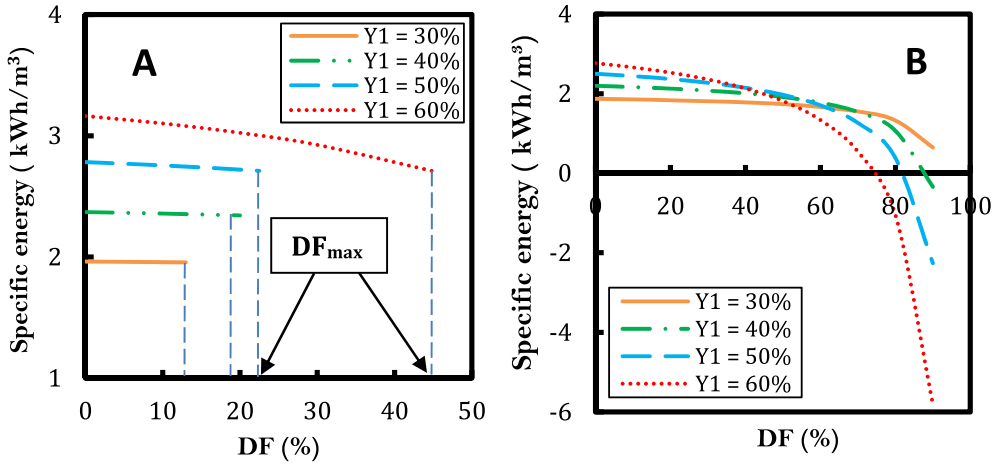

Fig. 7. Ideal specific energy consumption of SWRO-PRO system as a function of PRO dilution for several RO_1 recoveries. A- represents the model results for the SWRO-PRO system operating under the first configuration. B- represents the model results for the SWRO-PRO system operating under the second configuration.

$Y_1 < 60\%$). The model results show that the best performance was achieved when the feed flow is maintained equal to the draw solution flow. Therefore, the high osmotic pressure difference between the feed and draw solution is not the only key parameter that guarantees high energy recovery, but also the PRO entering flow ratio, named *r* here. In fact, when *r* increases, the SWRO-PRO energy consumption decreases. In addition, regardless of the configuration, it can be clearly seen that the best performance is achieved for high dilution factors, which reveals the strong relationship between the energy and membrane performance. Unfortunately, existing PRO full-scale membranes suffer from several drawbacks, such as concentration polarization, fouling, reverse salt diffusion, and pressure drops, which make, for instance, high dilution unreachable. Thus, in SWRO-PRO hybrid systems, three parameters should be properly controlled, namely: the recovery ratio, the dilution factor, and the PRO entering flow ratio.

2.4. Modeling the energy consumption of the SWRO-PRO system under realistic conditions

2.4.1. PRO model

Real life SWRO-PRO plants would be less energy efficient than theoretically calculated, due to electrical conversion losses and dissipation. The amount of additional energy required depends on the specific recovery strategy. In addition, the produced energy is proportional to the mixing volume. Consequently, dilution of the draw solution is inevitable. Therefore, the osmotic pressure difference decreases and reduces the performance of PRO. Besides that, previous works had shown that PRO membrane performance is limited by several limiting factors [23,26,27]. In fact, with a realistic membrane and imperfect hydrodynamics, three phenomena occur to reduce the *trans*-membrane water flux, as shown in Fig. S4. First, the porous support layer induces internal concentration polarization (ICP), which detrimentally enhances $\pi_{F,m}$by increasing the solute concentration at the feed-membrane interface, thus reducing the *trans*-membrane driving force. Second, without perfect hydrodynamics in the draw solution flow channel, dilutive external concentration polarization (ECP) develops, which lowers $\pi_{D,m}$and reduces the driving force. Lastly, because the membrane is no longer perfectly selective, reverse salt diffusion (RSD) takes place, resulting in uncontrolled mixing and, therefore, reduced energy extraction in the process. The water flux across the membrane, J_w, can be defined in terms of the membrane water permeability coefficient, *A*; the osmotic pressure at the draw side of the membrane active layer, $\pi_{D,m}$; the osmotic pressure at the feed side of the membrane active layer, π_{icp}; and the hydraulic pressure difference across the membrane:

$$J_w = A(\pi_{D,m} - \pi_{icp} - \Delta P) = A(\Delta\pi_m - \Delta P) \tag{13}$$

where $\Delta\pi_m$ is the osmotic pressure difference across the membrane active layer. Based on film theory, equations have been developed to determine the concentration on either side of the membrane with reverse salt flux and concentration polarization accounted for [25,26]:

$$C_{D,m} = \left(C_{D,b} + \frac{J_s}{J_w}\right)\exp\left(-\frac{J_w}{k_D}\right) - \frac{J_s}{J_w} \tag{14}$$

$$C_{F,m} = \left(C_{F,b} + \frac{J_s}{J_w}\right)\exp\left(\frac{J_w}{k_F}\right) - \frac{J_s}{J_w} \tag{15}$$

$$C_{icp} = \left(C_{F,b} + \frac{J_s}{J_w}\right)\exp\left(\frac{J_w}{k_F}\right)\exp(J_w K) - \frac{J_s}{J_w} \tag{16}$$

where $C_{D,b}$ is the bulk draw concentration, $C_{F,b}$ is the bulk feed concentration, and k_D and k_F are the mass transfer coefficient in the draw and feed sides, respectively. *K* is the solute diffusion coefficient. The water flux and the salt flux are related by the following relation [27]:

$$\frac{J_s}{J_w} = \frac{B}{A\beta RT}\left(1 + \frac{A\Delta P}{J_w}\right) \tag{17}$$

B is the salt permeability coefficient, and ΔP is the hydraulic pressure applied on the draw solution side. Assuming the van't Hoff relationship between osmotic pressure and concentration [25]:

$$\begin{aligned} J_w = A\Bigg\{&\left(\pi_{D,b} + \frac{B}{A}\left[1 + \frac{A\Delta P}{J_w}\right]\right)\exp\left(-\frac{J_w}{k_D}\right) \\ &- \left(\pi_{F,b} + \frac{B}{A}\left[1 + \frac{A\Delta P}{J_w}\right]\right)\exp(J_w K)\exp\left(\frac{J_w}{k_F}\right) - \Delta P\Bigg\} \end{aligned} \tag{18}$$

The variations along the membrane's length are often neglected in models designed to simulate bench scale systems because the effect is difficult to observe over very small membrane samples [26]. However, the passage of water through the membrane was followed by friction, which should cause some heating of solutions.

If the water flow had been created due to the pressure drop on either side of the membrane, this would have led to the loss of part of the energy released. These include flow rates, concentrations and hydraulic pressures, as well as all other variables that are dependent on them. Their local values should be considered for accurate modeling. These spatial variations can be accounted for either by taking an average of inlet and outlet variables, or by considering the membrane as a finite difference model [26–29]. To develop a model for full-scale PRO applications, the flat sheet membrane area is divided into segments perpendicular to the water flow, evaluating flow conditions at specific points along the membrane module. In this case, feed and draw solution flows are assumed to be in a co-current flow mode. Fig. S3 illustrates a single segment of a flat sheet PRO membrane. The permeate flow through the PRO membrane Q_w can significantly dilute the draw solution concentration C_D, which results in reduced flux performance compared to the small size test membrane. Such a dilution effect needs to be explicitly accounted for in a flat sheet module. Due to this variation, three main parameters are evaluated at each point along the membrane: the water flux, the pressure and the concentrations. The model development steps are presented in the Supplementary material.

2.4.2. SWRO model

The energy consumption of each RO stage in a two-stage RO plant, at the limit of the thermodynamic restriction and in the absence of energy recovery, is developed in Ref. [21]:

$$SEC_{RO_1} = \frac{R_s \pi_{sw}}{\eta_{P_1} Y_1 (1 - Y_1)} \tag{19}$$

$$SEC_{RO_2} = \frac{R_s \pi_p}{\eta_{P_2} Y_2 (1 - Y_2)} \tag{20}$$

R_s is the salt rejection, and η_P is the pump conversion. The specific energy cost for RO, in the presence of an energy recovery device (ERD), operating at the limit of the thermodynamic restriction, is:

$$SEC_{RO_1}^{ERD} = R_s \pi_{sw} \left(\frac{1 - \eta_{ERD}[1 - Y_1]}{\eta_P Y_1 [1 - Y_1]} \right) \tag{21}$$

where η_{ERD} is the efficiency of the energy recovery device.

2.4.3. ERD energy recovery

The recovery of energy from SWRO systems has been a major factor in the reduction of the cost of desalinated seawater, to a point where it is beginning to offer a challenge to conventional sources. In our case, an ERD is placed after the first RO stage to recover energy from the rejected brine. As mentioned previously, the ERD reduces the pressure of the brine to a suitable value for PRO operational applied pressure ($\Delta P \approx \frac{\Delta \pi_m}{2}$). This condition is a key parameter for the optimum performance of the PRO process. In the second configuration, the osmotic pressure of the PRO feed solution is relatively high at low RO_1 recoveries, which is not the case for the first configuration. Therefore, the energy recovered using ERD depends on the osmotic pressure that enters the PRO module. As π_F changes with the recovery, the contribution of ERD in the second configuration also varies regarding the osmotic pressure of the PRO feed solution. Then, the energy recovered by ERD in the second configuration will be much lower than in the first one. Subtracting Eq. (21) from Eq. (19), the energy recovered by the ERD at the thermodynamic restriction is expressed as follows:

$$SE_{ERD}^1 = -R_s \pi_{sw} \left(\frac{\eta_{ERD}[1 - Y_1]}{\eta_P Y_1 [1 - Y_1]} \right) \tag{22}$$

$$SE_{ERD}^2 = -R_s [\pi_{sw} - \pi_F] \left(\frac{\eta_{ERD}[1 - Y_1]}{\eta_P Y_1 [1 - Y_1]} \right) \tag{23}$$

The subscripts 1 and 2 refer to the first and second configuration, respectively. The osmotic pressure π_F in Eq. (23) highlights the effect of the PRO feed osmotic pressure. As can be seen in Fig. S5, the contribution of ERD to the energy recovery is much higher in the first configuration. In fact, in usual RO recovery ($40\% \leq Y_1 \leq 60\%$), the ERD energy recovery is between 1.32 and 2 kWh/m^3. Thus, the ERD effectively reduces the SEC by almost 50%. This result is well-known in the literature [21]. Using the second configuration, the ERD contribution is not significant due to the high pressure required for the PRO process. At high recovery, the ERD energy becomes slightly significant due to the dilution of the added seawater by the rejected water of the second RO stage.

3. Results and discussion

3.1. Modeling parameters

The simulations in this study are based on the characteristics of a cellulose acetate flat-sheet membrane used in our previous work, where a power density of 6.2 W/m^2 at 13 bar has been obtained in lab-scale tests using 1.026 M NaCl solution as the draw solution and 8.55 mM NaCl solution as the feed solution [25]. The characteristics of the membrane and the hypothetical module parameters are summarized in Table S1. The initial seawater flow was chosen arbitrarily to be 256 m^3/h, which is the real amount of treated water in the SETA-SWRO plant studied here. The sweater concentration is chosen to be 0.6 M (35 g/L). The added flow rate Q_{ad} is considered to be pre-treated before being involved in the process. It should be noted that the effect of organic fouling is not considered in this study, so the energy produced may be lower in the presence of feed water charged with natural organic matter (NOM).

3.2. PRO model results

The SE_{PRO} model was investigated by studying the response of the PRO sub-system after the variation in the effect of the operating conditions (draw and feed solution concentrations). As can be seen in Fig. 8, the increase in the draw solution concentration leads to an increase in the energy recovery by the sub-system. On the other hand, the increase in the feed solution concentration is followed by a decrease in the energy. Lastly, the increase in the draw solution temperature improves the performance of the PRO due to the improvement in the effective osmotic pressure and also the intrinsic membrane parameters, such as the water permeability coefficient. These results are in agreement with the model behavior using a lab-scale PRO membrane. Fig. 9 illustrates the SE_{PRO} in Eq. (S1), corresponding to the PRO model results for the proposed configurations when diluting RO_1 brine back to the sea, as a function of the SWRO recovery using the cellulose acetate flat-sheet membrane with the characteristics presented in Table S1. When recovery increases, the draw solution concentration increases, and the SE_{PRO} also increases. The minimum SE_{PRO} recoveries are 0 kWh/m^3 for both configurations. This magnitude increases with RO_1 recovery to reach an SE_{PRO} production of 0.702 kWh/m^3 at 77% of recovery. Compared to the theoretical SE_{PRO} production (Fig. 5), the model produces a specific energy noticeably far from the ideal case.

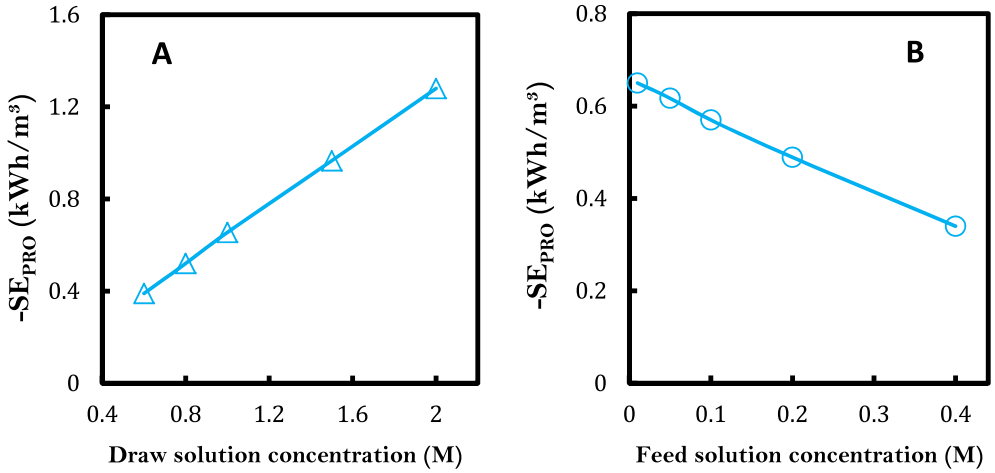

Fig. 8. PRO specific energy production (SE_{PRO}) modeled as a function of feed and draw solution concentrations under optimum PRO hydraulic pressure. Feed and draw solution flows are considered equal. For (A): the feed solution concentration is 8.55 mM. For (B): the draw solution is 1.026 M. T = 25 °C.

3.3. SWRO-PRO model results

The total energy consumption of the SWRO-PRO system for both configurations is studied here. As mentioned previously, the study only takes into account the effect of the recovery ratio of the first RO stage, so that of the second stage is considered constant (Y_2 = 70%). According to Figs. 10 and 11, the $SE_{SWRO-PRO}$ consumption is much lower for the ideal case than for the model results for both configurations. This behavior is due to the fact that the ideal SE_{PRO} production is noticeably higher than the model SE_{PRO} production. Because of the higher starting value of the model $SE_{SWRO-PRO}$ and the lower rate at which the model SE_{RO-PRO} consumption decreases, the model of the SWRO-PRO system is not able to reach energy neutrality ($SE_{SWRO-PRO} = 0$). Fig. 10 shows the variation of the modeled energy consumption $SEC_{SWRO-PRO}$ with the applied pressure ΔP under two RO_1 recovery ratios without using an ERD. It can be seen that $SEC_{SWRO-PRO,}$ when Y_1 = 40%, is higher than the case when Y_1 = 50% for both configurations. Moreover, at a low recovery ratio, the performance of the second configuration is better than the first one in terms of energy generation and low applied pressure. When the recovery ratio increases, the second configuration shows a better performance than the first, due to the decrease in the PRO feed solution concentration. As a comparison, for (A), the maximum energy recovery is 2.45% and 4% when Y_1 = 40% and 50%, respectively. For (B), the energy recovery is 6% and 8% when Y_1 = 40% and 50%, respectively. Fig. 11 shows a comparison between the total energy consumption of the SWRO plant with the presence of PRO and ERD. It can be seen that the maximum $SE_{SWRO-PRO}$ consumption point for each RO recovery is the point at which there is no PRO sub-system contribution (DF = 0). In other words, this is the maximum SE_{RO} consumption for each RO recovery. For configuration (A), the contribution of the PRO sub-system is very limited at a low RO_1 recovery ratio (Y_1 < 30%), where more than 96% of the energy recovery is accomplished by ERD. This is due to the low amount of rejected water coming from the second RO stage, which constitutes the feed solution for the PRO sub-system. This result corresponds, theoretically, to less than 20% of dilution. In addition, the high concentration of the draw solution may induce severe concentration polarization, which reduces the performance of the membrane. Contrary to configuration (A), the contribution of PRO is considerable at a low recovery ratio because the amount of PRO feed solution is provided directly from the pre-treated seawater and remains nearly constant at this range of RO_1 recovery ratio (Y_1 < 20%). The contribution of the PRO in the total energy recovered is around 45%. This high value is because of the limited contribution of ERD in this case due to the high PRO feed solution concentration. Also, when the PRO feed flow ratio was maintained equal to unity, the experimental dilution factor increased. For example, when Y_1 = 40%, the energy recovered corresponds to DF = 40%, which is double the dilution in the first configuration case. This result clearly shows the strong relationship between the feed flow ratio and the dilution factor in the PRO process. To summarize, the notable difference between the ideal case and the model case is related to the membrane performance. In fact, to reach high values of dilution, an improvement in the water permeability across the membrane is fundamental. Moreover, avoiding the reverse salt diffusion by reducing the salt permeability of the active layer material enhances the dilution factor. Lastly, improving the inner structure of the PRO membrane support layer, to reduce the effect of the internal concentration

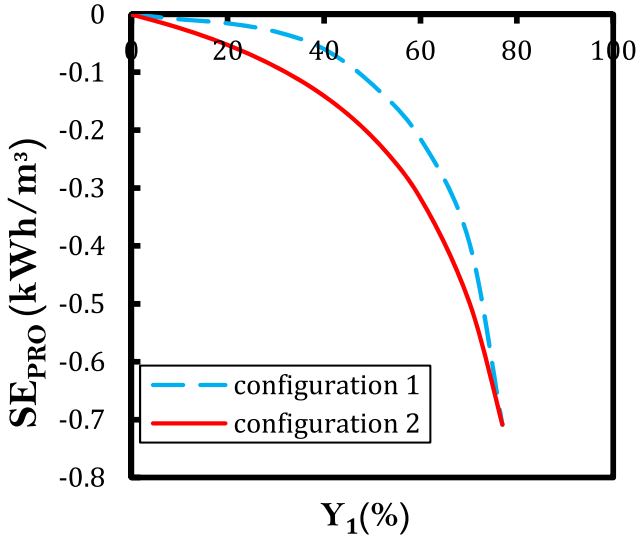

Fig. 9. PRO specific energy production (SE_{PRO}) modeled as a function of RO_1 recovery for a cellulose acetate flat-sheet membrane under optimal ΔP for both proposed configurations.

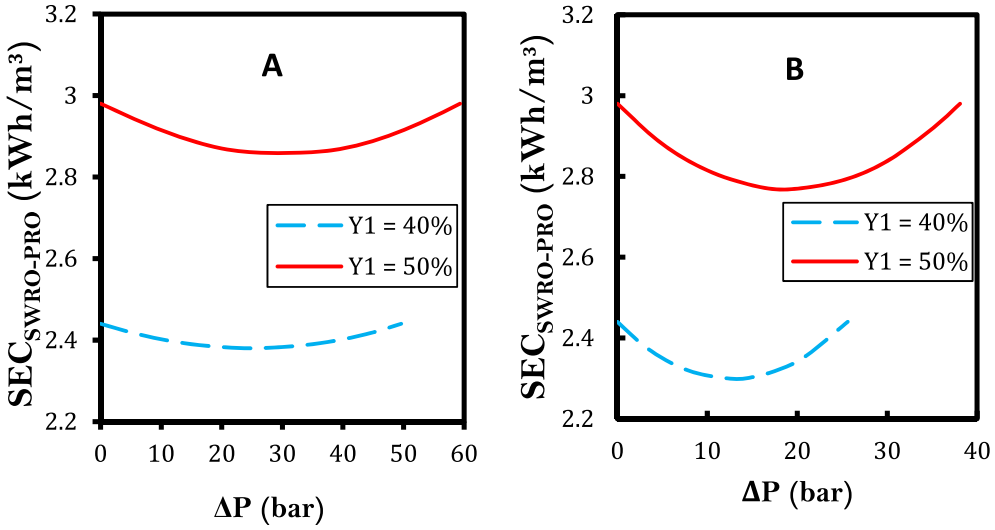

Fig. 10. SWRO-PRO specific energy without using ERD, as a function of the applied pressure Δ*P* for different RO recoveries for the model case. (A) represents the result for the first configuration and (B) for the second configuration.

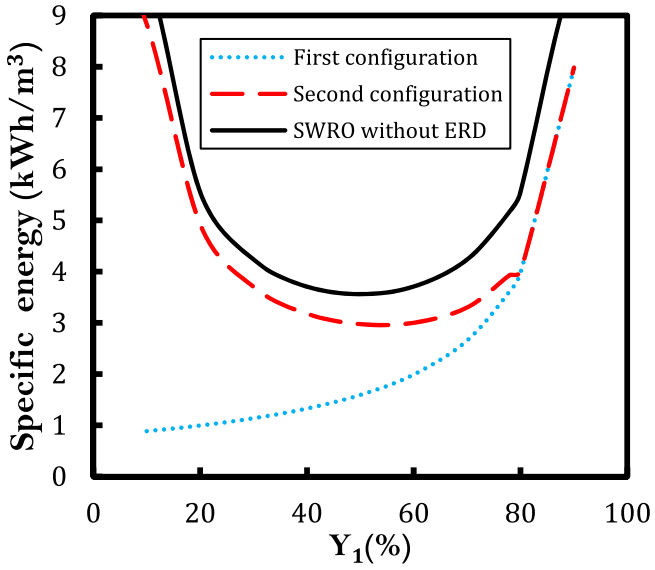

Fig. 11. SWRO-PRO specific energy consumption as a function of the RO_1 recovery for the proposed configurations. Pump efficiency, membrane salt rejection, and ERD efficiency were taken as 90%, 98%, and 95%, respectively.

polarization and optimize the operating conditions in order to minimize the external concentration polarization, is a challenge that can guarantee a better PRO dilution and therefore more recovered energy.

4. Dilution factor in realistic conditions

The dilution factor reflects the amount of feed water that is mixed with the draw water to produce energy. This parameter is strongly dependent on the membrane performance and the driving force, Δπ. In other words, increasing the water flux across the membrane leads to the increase in the dilution. In the ideal case with a perfect membrane, the water flux depends only on the osmotic pressure difference. Then, to achieve high dilutions, the concentrations of feed and draw solutions should be optimized. In realistic conditions, the maximum dilution is not reachable because of several limiting factors, such as the concentration polarization (CP) and reverse salt diffusion (RSD), which reduce the performance of the membrane. The realistic dilution factor is investigated in the current section.

The maximum amount of feed flow that crosses the membrane to be mixed with the draw solution, ΔQ_{max}, can be calculated using the following equation [32]:

$$\Delta Q_{max} = \frac{\sqrt{C_{D,b}} - \sqrt{C_{F,b}}}{\sqrt{C_{D,b}} + \frac{\varnothing}{1-\varnothing}\sqrt{C_{F,b}}} Q_F \tag{24}$$

Eq. (24) is applicable only for an ideal membrane with perfect hydrodynamics. The rearrangement of Eq. (24) using Eqs.(5) and (6) gives the maximum dilution factor:

$$DF_{max} = r\frac{\sqrt{C_D} - \sqrt{C_F}}{\sqrt{C_D} + \frac{1}{r}\sqrt{C_F}} \tag{25}$$

where C_D and C_F are the draw and feed solution concentrations. To introduce the impact of detrimental effects, Eq. (25) is modified by substituting C_D and C_F by Eqs. (14)–(16) according to the variation of the effective feed and draw concentrations described in Fig. S4 (Supplementary material). Table S2 summarizes the different equations of DF for each case studied. The realistic dilution factor can be determined using the parameters described in Table S1 and the modeling results of section 3.2. To investigate the effect of each detrimental effect, DF_{max} is modeled under several operating conditions. In fact, the draw solution is assimilated to the seawater RO brine concentration (1.2 M of NaCl) and the feed solution is modified for each studied case from freshwater to river water concentration. The modeling results are presented in Fig. 12. The maximum dilution is obtained using an ideal membrane with no reverse salt diffusion J_S (RSD), concentration polarization, and an advanced state-of-the-art membrane with perfect hydrodynamics. In this case, the water flux J_w is directly proportional to the osmotic pressure difference $= \pi_{D,b} - \pi_{F,b}$. The maximum dilution achievable in this case is 92%. When considering only the effect of the external concentration polarization, which is caused by non ideal hydrodynamics in the draw solution flow channel, which induces the dilutive External Concentration Polarization (dilutive ECP) at the draw side and the concentrative External

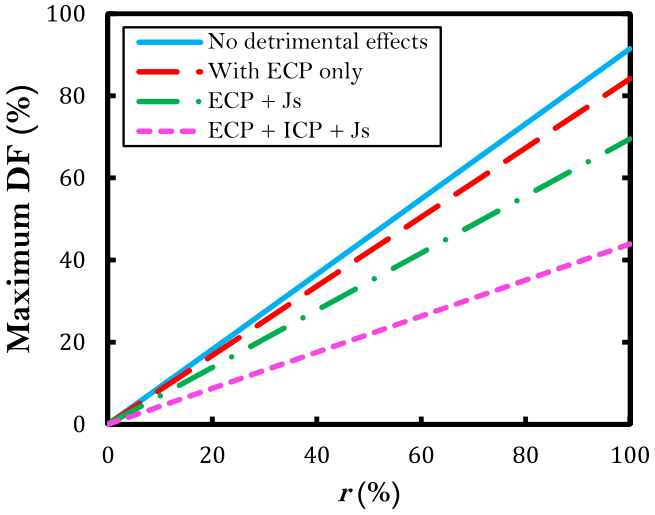

Fig. 12. Modeled dilution factor under different operating conditions and detrimental effects as a function of the feed flow ratio. Dilution factor for ideal membrane with the absence of detrimental effects (solid blue line). Membrane with concentrative External Concentration Polarization (dashed red line). Membrane with salt diffusion and External Concentration Polarization (green dashed line). Membrane with salt diffusion, Internal Concentration Polarization and External Concentration Polarization (purple dashed line). The draw solution concentration is 0.6 M and the applied pressure ΔP is 14.5 bar. T = 20 °C. The characteristics of the membrane are presented in Table S1. (For interpretation of the references to colour in this figure legend, the reader is referred to the web version of this article.)

Concentration Polarization (concentrative ECP) at the feed side, the values of the dilution factor decrease by almost 8% from the ideal case. This behavior is caused by the decrease in the effective osmotic pressure difference from $\Delta\pi$ to $\Delta\pi_{ECP} = \pi_{D,m} - \pi_{F,m}$ (see Fig. S4). With the existence of RSD, the decrease in the DF is around 24% from the ideal case. In fact, RSD causes the drop in the driving force due to the penetration of salt from the draw to the feed side, which induces a decrease of J_w. To emphasize the effect of the concentration polarization and internal concentration, the concentration of river water (0.015 M) is considered. Under these conditions, the decrease in the DF reaches 52%. As can be clearly seen, most of the DF reduction is due to the internal concentration polarization with a contribution of 28%. ICP, caused by the accumulation of salt at the active layer/support layer boundary, decreases the driving force from $\Delta\pi$ to $\Delta\pi_m = \pi_{D,m} - \pi_i$. Consequently, a severe drop occurs in J_w; therefore, DF decreases drastically. As the energy is directly proportional to the dilution, the DF loss from the realistic PRO operation may have a significant impact on the net specific energy recovered from the process. The optimization of the membrane performance is a critical operation to guarantee high energy recovery. It should be pointed out that this study does not consider the effect of organic fouling. In fact, it was shown in a previous study that fouling severely reduces the water flux and therefore the dilution. This energy loss caused by membrane limitations, in conjunction with the pre-treatment energy requirements, pumping energy costs, inefficiencies in the hydro-turbine and pressure exchanger, may limit the amount of energy harvested from the PRO process. Of course, the increase in the concentration difference between the feed and draw solution concentrations may provide a sizable amount of energy using the PRO process. Nevertheless, the increase in the PRO entering solution concentration should be well chosen and treated to avoid the accentuation of the concentration polarization and the reverse salt diffusion, which lead to the decrease in the driving force; the osmotic pressure difference.

5. Conclusion

In the current investigation, two configurations of SWRO-PRO were proposed for energy recovery. The first configuration considers that the brine of the second stage is the PRO feed solution and the brine of the first stage represents the PRO draw solution. For the second configuration, the PRO feed solution is a mixture of the second stage brine and pre-treated seawater. For this, a model describing the evolution of the energy recovery with the SWRO operating conditions was developed and compared to the ideal case model. The results showed that the performance of the PRO was better for the second configuration due to the optimized initial flow ratio. However, for the whole system, the energy recovered from the first configuration was remarkably better for an extended interval of RO recovery, because of the contribution of the energy recovery device. The second part of this investigation deals with the relation between the initial flow ratio (r) and the dilution factor (DF). It was found that the increase in r increases the DF. Then, the DF was modeled for realistic conditions. It was found that the internal concentration polarization is the factor that contributes most to dilution reduction. Consequently, well treated solutions and optimized membrane performance are strongly recommended to achieve a sizable amount of energy from the PRO process. The current work revealed that the energy recovery from the SWRO process using PRO may be optimized not only by the mitigation of the limiting factors (CP, Js, pressure drop, etc …), but also by the well chosen location of PRO integration in the process. This, in the end, depends on the SWRO design, the number of stages, and the characteristics of the output waters. Thus, further work will focus on the integration of multistage PRO in one-stage and multi-stage SWRO processes for water and clean energy production.

Acknowledgements

This work was funded by MICINN DPI2014-54530-R and FP7 H2OCean (Grant 288145).

List of symbols

A	Water permeability coefficient. ($m.s^{-1}.Pa^{-1}$)
A_m	Membrane surface. (m^2)
B	Salt permeability coefficient. ($m.s^{-1}$)
$C_{D,m}$	Salt concentration of the membrane surface at the draw solution side. ($mol.l^{-1}$)
$C_{F,m}$	Salt concentration on the support layer surface at the side of the feed. ($mol.l^{-1}$)
$C_{D,b}$	Salt concentration of the draw solution bulk. ($mol.l^{-1}$)
$C_{F,b}$	Salt concentration on the feed solution bulk. ($mol.l^{-1}$)
C_{icp}	Salt concentration on the membrane surface at the boundary active layer-support layer ($mol.l^{-1}$)
d	Diameter of the pipe. (m)
d_h	Hydraulic diameter of the flow channel. (m)
D_D	Diffusion coefficient of the draw solution. ($m^2.s^{-1}$)
D_f	Diffusion coefficient of the feed solution. ($m^2.s^{-1}$)
DF	Dilution factor. (−)
J_w	Water flux that crosses the membrane. ($m.s^{-1}$)
J_s	Salt flux that crosses the membrane. ($mol.m^{-2}.s^{-1}$)
k	Mass transfer coefficient. ($m.s^{-1}$)
K	Solute resistivity. ($s.m^{-1}$)
L	Length of the channel. (m)
N	Number of segments. (−)
ΔP	*Trans*-membrane Pressure. (Pa)
$\Delta\pi$	Difference of osmotic pressure between the draw solution and the feed solution. (Pa)
R	Gas constant. ($J.mol^{-1}\ K^{-1}$)

r	Feed flow ratio. (–)
Re	Reynolds number. (–)
s	Structure parameter of the support layer. (m)
Sc	Schmidt number. (–)
Sh	Sherwood number. (–)
T	Temperature of the bulk. (°C)
u	Cross-flow velocity. ($m.s^{-1}$)
w	Width of the channel. (m)
η	Dynamic viscosity of the solution. (Pa.s)
$\pi_{D,m}$	Osmotic pressure at the surface of the active layer. (Pa)
$\pi_{F,m}$	Osmotic pressure at the surface of the support layer. (Pa)
$\pi_{D,b}$	Osmotic pressure of the draw solution bulk. (Pa)
$\pi_{F,b}$	Osmotic pressure of the feed solution bulk. (Pa)
π_{icp}	Osmotic pressure at the limit surface between the active layer and the support layer. (Pa)
t_s	Length of the support layer. (m)
τ	Tortuosity of the membrane. (–)
ε	Porosity of the membrane. (–)
β	van't Hoff coefficient. (–)
δ_D	Thickness of the boundary layer at the draw solution side. (m)
δ_F	Thickness of the boundary layer at the feed solution side. (m)
μ	Water kinematic viscosity. ($m^2.s^{-1}$)
φ	Initial feed flow rate fraction. (–)

Appendix A. Supplementary data

Supplementary data related to this article can be found at http://dx.doi.org/10.1016/j.renene.2016.12.030.

References

[1] D. Zhou, L. Zhu, Y. Fu, M. Zhu, L. Xue, Development of lower cost seawater desalination processes using nanofiltration technologies — a review, Desalination 376 (2015) 109–116.

[2] Y. Hun Jung, Y. HoonJeong, J.F. Choi, A. Wibisono, J.I. Lee, H. Cheon No, Feasibility study of a small-sized nuclear heat-only plant dedicated to desalination in the UAE, Desalination 337 (2014) 83–97.

[3] N. Ghaffour, S. Lattemann, T. Missimer, K. Choon Ng, S. Sinha, G. Amy, Renewable energy-driven innovative energy-efficient desalination technologies, Appl. Energy 136 (2014) 1155–1165.

[4] I. Ersever, V. Ravindran, H.-H. Tsai, M. Pirbazari, Modeling and design of anaerobic fluidized bed reactor with recycling for denitrification of reverse osmosis concentrates, Chem. Eng. Sci. 108 (2014) 111–122.

[5] J.L. Fuentes-Bargues, Analysis of the process of environmental impact assessment for seawater desalination plants in Spain, Desalination 347 (2014) 166–174.

[6] M. Li, Reducing specific energy consumption in Reverse Osmosis (RO) water desalination: an analysis from first principles, Desalination 276 (2011) 128–135.

[7] S.A. Avlonitis, K. Kouroumbas, N. Vlachakis, Energy consumption and membrane replacement cost for seawater RO desalination plants, Desalination 157 (2003) 151–158.

[8] A. Altaee, Forward osmosis, potential use in desalination and water reuse, J. Membr. Sep. Technol. 1 (2012) 79–93.

[9] A. Altaee, A. Sharif, Pressure retarded osmosis: advancement in the process applications for power generation and desalination, Desalination 356 (2015) 31–46.

[10] K. Touati, A. de la Calle, F. Tadeo, L. Roca, T. Schiestel, D.C. Alarcón-Padilla, Energy recovery using salinity differences in a multi-effect distillation system, Desalin. Water Treat. (2014) 1–8.

[11] W. He, Y. Wang, M.H. Shaheed, Maximum power point tracking (MPPT) of a scale-up pressure retarded osmosis (PRO) osmotic power plant, Appl. Energy 136 (2014) 1155–1165.

[12] W. He, Y. Wang, V. Elyasigomari, M.H. Shaheed, Evaluation of the detrimental effects in osmotic power assisted reverse osmosis (RO) desalination, Renew. Energy 93 (2016) 608–619.

[13] K. Touati, F. Tadeo, Green energy generation by Pressure Retarded Osmosis: state of the art and technical advancement -review, Int. J. Green Energy (2016), http://dx.doi.org/10.1080/15435075.2016.1255633.

[14] K. Saito, M. Irie, S. Zaitsu, H. Sakai, H. Hayashi, A. Tanioka, Power generation with salinity gradient by pressure retarded osmosis using concentrated brine from SWRO system and treated sewage as pure water, Desalin. Water Treat. 41 (2012) 114–121.

[15] A. Achilli, J.L. Prante, N.T. Hancock, E.B. Maxwell, A.E. Childress, Experimental results from RO-PRO: a next generation system for low-energy desalination, Environ. Sci. Technol. 48 (11) (2014) 6437–6443.

[16] J.L. Prante, J.A. Ruskowitz, A.E. Childress, A. Achilli, RO-PRO, desalination: an integrated low-energy approach to seawater desalination, Appl. Energy 120 (2014) 104–114.

[17] L.G. Palacin, F. Tadeo, C. De Prada, K. Touati, Evaluation of the recovery of osmotic energy in desalination plants by using pressure retarded osmosis, Desalin. Water Treat. 51 (1–3) (2013) 360–365.

[18] C.F. Wan, T.-S. Chung, Osmotic power generation by pressure retarded osmosis using seawater brine as the draw solution and wastewater retentate as the feed, J. Memb. Sci. 479 (2015) 148–158.

[19] C.F. Wan, T.-S. Chung, Maximize the operating profit of a SWRO-PRO integrated process for optimal water production and energy recovery, Renew. Energy 94 (2016) 304–313.

[20] J.O. Jaber, S.D. Probert, O. Badr, Water scarcity: a fundamental crisis for Jordan, Appl. Energy 57 (2–3) (1997) 103–127.

[21] A. Zhu, P.D. Christofides, Y. Cohen, Minimization of energy consumption for a two-pass membrane desalination: effect of energy recovery, membrane rejection and retentate recycling, J. Memb. Sci. 339 (2009) 126–137.

[22] www.h2ocean-project.eu.

[23] P. Straub A, S. Lin, M. Elimelech, Module-scale analysis of Pressure Retarded Osmosis: performance limitations and implications for full-scale operation, Environ. Sci. Technol. 48 (2014) 12435–12444.

[24] E.M.V. Hoek, J. Allred, T. Knoell, B.H. Jeong, Modeling the effects of fouling on full-scale reverse osmosis processes, J. Memb. Sci. 314 (2008) 33–49.

[25] K. Touati, C. Hänel, F. Tadeo, T. Schiestel, Effect of the feed and draw solution temperatures on PRO performance: theoretical and experimental study, Desalination 365 (2015) 182–195.

[26] K. Touati, F. Tadeo, Study of the Reverse Salt Diffusion in pressure retarded osmosis: influence on concentration polarization and effect of the operating conditions, Desalination 389 (2016) 171–186.

[27] Tadeo F. TouatiK, C. Hänel, T. Schiestel, Effect of the operating temperature on hydrodynamics and membrane parameters in pressure retarded osmosis, Desalin. Water Treat. (2015) 1–13, http://dx.doi.org/10.1080/19443994.2015.1039600.

[28] M.F. Naguib, J. Maisonneuve, C.B. Laflamme, P. Pillay, Modeling pressure-retarded osmotic power in commercial length membranes, Renew. Energy 76 (2015) 619–627.

[29] J. Maisonneuve, P. Pillay, C.B. Laflamme, Pressure-retarded osmotic power system model considering non-ideal effects, Renew. Energy 75 (2015) 416–424.

[30] A.P. Straub, A. Deshmukha, M. Elimelech, Pressure-retarded osmosis for power generation from salinity gradients: is it viable? Energy Environ. Sci. 9 (2016) 31–48.

[31] B.J. Feinberg, G. Ramon, E.M.V. Hoek, Thermodynamic analysis of osmotic energy recovery at a reverse osmosis desalination plant, Environ. Sci. Technol. 47 (2013) 2982–2989.

[32] N.Y. Yip, M. Elimelech, Thermodynamic and energy efficiency analysis of power generation from natural salinity gradients by pressure retarded osmosis, Environ. Sci. Technol. 46 (2012) 5230–5239.